

DTIC FILE COPY

AD-A202 705



DTIC
ELECTE

JAN 18 1980

S D

H



DEPARTMENT OF THE AIR FORCE
AIR UNIVERSITY

AIR FORCE INSTITUTE OF TECHNOLOGY

Wright-Patterson Air Force Base, Ohio

DISTRIBUTION STATEMENT A

Approved for public release;
Distribution Unlimited

89

1 17 032

AFIT/GAE/AA/88D-28

INVESTIGATION OF FAILURE MODES
IN FIBER REINFORCED CERAMIC
MATRIX COMPOSITES

THESIS

Joseph W. Moschler, Jr.
Captain, USAF

AFIT/GAE/AA/88D-28

DTIC
ELECTE
S JAN 18 1989 D
H

Approved for public release; distribution unlimited

AFIT/GAE/AA/88D-28

INVESTIGATION OF FAILURE MODES IN
FIBER REINFORCED CERAMIC MATRIX COMPOSITES

THESIS

Presented to the Faculty of the School of Engineering
of the Air Force Institute of Technology

Air University

In Partial Fulfillment of the
Requirements for the Degree of
Master of Science in Aeronautical Engineering

Joseph W. Moschler, Jr., B. S.

Captain, USAF

December 1988

Approved for public release; distribution unlimited

Preface

The purpose of this study was to investigate the damage progression in fiber reinforced ceramic-glass matrix composites. Four composite material systems were fabricated using four different borosilicate glasses with silicon carbide monofilament fibers. Each glass had a different coefficient of thermal expansion so that the residual stresses at the fiber-matrix interface in each system could be varied. The composites were tested in tension to determine the mechanical properties and failure characteristics. Three analytical model predictions of matrix cracking stress were compared to experimental results.

I would like to acknowledge the help of those I received in the experimentation and writing of this thesis. I am very grateful to Dr. Amit Chatterjee of Adtech Systems Research, Inc. Without his patience and guidance, I would not have completed this work. I also wish to thank Dr. Shankar Mall, my faculty advisor. His continual guidance and assistance throughout my graduate work are deeply appreciated. Finally, I thank my wife Paula and daughter Sarah Ann who have been so understanding for the past eighteen months. I love them both very much.

Joseph W. Moschler, Jr.

For



| | |
|--------------------|---------|
| Availability Codes | |
| Avail and/or | |
| Dist | Special |
| A-1 | |

Table of Contents

| | Page |
|---|------|
| Preface..... | ii |
| List of Figures..... | iv |
| List of Tables..... | vii |
| List of Symbols..... | viii |
| Abstract..... | x |
| I. Introduction..... | 1 |
| II. Background..... | 8 |
| Theoretical Models..... | 8 |
| Material Selection..... | 20 |
| III. Experimental Procedure..... | 25 |
| Sample Fabrication..... | 25 |
| Sample Preparation..... | 29 |
| Test Procedures..... | 31 |
| IV. Results and Discussion..... | 38 |
| Mechanical Properties from MTS Tests..... | 41 |
| Damage Formation and Progression..... | 54 |
| Theoretical Models..... | 84 |
| V. Conclusions..... | 103 |
| VI. Recommendations..... | 107 |
| Bibliography..... | 109 |
| Appendix: Stress-strain curves..... | 111 |
| Vita..... | 119 |

List of Figures

| Figure | Page |
|--|------|
| 1. Fiber-matrix Shear Lag Model..... | 9 |
| 2. Steady-state Matrix Crack in a Composite..... | 13 |
| 3. Matrix Cracking Stress for Frictionally Constrained Fibers..... | 16 |
| 4. AVCO SCS-6 Fiber Core and Coatings..... | 23 |
| 5. Fiber Layer Sequence for Fabrication..... | 26 |
| 6. Sample Loaded in Graphite Die for Hot Pressing.... | 26 |
| 7. Glass-transition Temperature..... | 28 |
| 8. Tabbed Specimen for Testing..... | 30 |
| 9. Constant Load Straining Fixture..... | 32 |
| 10. Straining Fixture with Composite Sample Loaded.... | 33 |
| 11. Olympus Inverted Metallurgical Microscope and Camera Used for Damage Observation..... | 35 |
| 12. Elastic Modulus Values for Glass/AVCO Composites.. | 44 |
| 13. Transverse Elastic Modulus Values for Glass/AVCO Composites..... | 45 |
| 14. Ultimate Tensile Strength Values for Glass/AVCO Composites..... | 48 |
| 15. Transverse Ultimate Tensile Strength Values for Glass/AVCO Composites..... | 47 |
| 16. Stress-Strain Curve for AVCO/7761 Sample 28-Z..... | 51 |
| 17. Stress-Strain Curve for AVCO/7052 Sample 39-B..... | 52 |
| 18. Residual Stresses at Fiber-matrix Interface for 7761/AVCO System..... | 56 |
| 19. Matrix Cracking in 7761/AVCO Composite at .08 Percent Strain..... | 57 |
| 20. Fiber Cracks in 7761/AVCO Composite at .14 Percent Strain..... | 59 |

List of Figures (cont.)

| | | |
|-----|---|----|
| 21. | Fiber and Matrix Cracks in 7761/AVCO Composite at .04 Percent Strain..... | 60 |
| 22. | Fiber and Matrix Cracks in 7761/AVCO Composite at .05 Percent Strain..... | 60 |
| 23. | Fiber-matrix Debonding in 7761/AVCO Composite at .13 Percent Strain | 61 |
| 24. | Fiber Core Pullout in 7761/AVCO Composite at .13 Percent Strain..... | 62 |
| 25. | Extensive Matrix Shattering in 7761/AVCO Composites Prior to Failure..... | 63 |
| 26. | SEM Photographs of Fiber-matrix Interface in 7761/AVCO Composite After Fabrication..... | 66 |
| 27. | 7761/AVCO Composite Sample at .14 Percent Strain.. | 69 |
| 28. | Residual Stresses at Fiber-matrix Interface for 7052/AVCO and 9741/AVCO Systems..... | 71 |
| 29. | Fabricated Plate of 7052/AVCO Composite Showing Matrix Cracking..... | 72 |
| 30. | Matrix Cracking in 7052/AVCO Composite from CTE Mismatch Between Fiber and Matrix..... | 73 |
| 31. | Multiple Matrix Cracks in 7052/AVCO Samples Prior to Testing..... | 75 |
| 32. | Fiber Cracks Close to Existing Matrix Cracks in 7052/AVCO Composite at .06 Percent Strain..... | 76 |
| 33. | Matrix Cracks Prior to Testing and Fiber Cracks at .06 Percent Strain in 7052/AVCO Samples..... | 79 |
| 34. | Multiple Matrix Cracking in 7740/AVCO Composite at .08 Percent Strain..... | 80 |
| 35. | Fiber Crack in 7740/AVCO Composite at .06 Percent Strain..... | 80 |
| 36. | Extensive Matrix Cracking Under Strain Gage in a 7740/AVCO Composite Sample..... | 82 |
| 37. | Matrix Cracking Stress Vs. Interfacial Shear Stress for 7761/AVCO Composite..... | 91 |

List of Figures (cont.)

| | | |
|-----|---|-----|
| 38. | Matrix Cracking Stress Vs. Interfacial Shear Stress for 7740/AVCO Composite..... | 92 |
| 39. | Matrix Cracking Stress Vs. Interfacial Shear Stress for 9741/AVCO Composite..... | 93 |
| 40. | Matrix Cracking Stress Vs. Interfacial Shear Stress for 7052/AVCO Composite..... | 94 |
| 41. | Matrix Cracking Stress Vs. Volume Fraction of Fibers for 7761/AVCO Composite..... | 95 |
| 42. | Matrix Cracking Stress Vs. Volume Fraction of Fibers for 7740/AVCO Composite..... | 96 |
| 43. | Matrix Cracking Stress Vs. Volume Fraction of Fibers for 9741/AVCO Composite..... | 97 |
| 44. | Matrix Cracking Stress Vs. Volume Fraction of Fibers for 7052/AVCO Composite..... | 98 |
| 45. | Thermal Expansion Vs. Temperature for Glass..... | 100 |
| 46. | Stress-Strain Curve for AVCO/7761 Sample 28-X..... | 112 |
| 47. | Stress-Strain Curve for AVCO/7761 Sample 24-B..... | 113 |
| 48. | Stress-Strain Curve for AVCO/7761 Sample 27-C (Transverse)..... | 114 |
| 49. | Stress-Strain Curve for AVCO/7740 Sample 32-A..... | 115 |
| 50. | Stress-Strain Curve for AVCO/7052 Sample 39-C..... | 116 |
| 51. | Stress-Strain Curve for AVCO/7052 Sample 40-B (Transverse)..... | 117 |
| 52. | Stress-Strain Curve for AVCO/9741 Sample 42-C..... | 118 |

List of Tables

| Table | Page |
|---|------|
| I. Properties of the AVCO SCS-6 Fiber..... | 23 |
| II. Properties of Selected Glasses..... | 24 |
| III. Percent Composition of Selected Glasses..... | 24 |
| IV. Sample Fiber Volume Fraction Measurements..... | 37 |
| V. Mechanical Properties of Glass/AVCO Composites.. | 43 |
| VI. Average Mechanical Properties..... | 48 |
| VII. Comparison of Composite Elastic Moduli..... | 48 |
| VIII. Comparison of Interfacial Shear Stress..... | 86 |
| IX. Theoretical Model Comparisons..... | 89 |

List of Symbols

| | |
|-----------|--|
| c | Crack length |
| c_0 | Characteristic crack length associated with MCE model |
| E | Elastic modulus |
| K | Critical Mode I stress intensity factor |
| n_j | Unit outward normal vector |
| P^* | Inverse of volume fraction of fibers associated with Oel and Frechette model ($1/V_f$) |
| r | Radius |
| T_g | Glass-transition temperature |
| T_i | Components of traction vector associated with NDSANDS model |
| T_m | Glass melting temperature |
| u | Crack opening distance |
| U_i | Components of boundary displacement vector associated with NDSANDS model |
| u_0 | Equilibrium crack opening distance associated with MCE model |
| V | Volume fraction |
| x | Matrix crack spacing |
| x_j | Cartesian coordinates associated with NDSANDS model |
| α | Coefficient of thermal expansion |
| β | E_m/E_f associated with Oel and Frechette model |
| β_1 | Parameter used in matrix cracking stress formulation in BHE model |
| β_2 | Parameter used in matrix cracking stress formulation in BHE model |
| Γ | $E_f V_f / E_m V_m$ associated with MCE model |

List of Symbols (cont.)

- ϵ_{mu} Matrix cracking strain associated with ACK model
- ϵ_{o13} Average strain over a volume element associated with NDSANDS model
- μ Poisson's ratio
- σ_{or} Matrix cracking stress associated with BHE model
- σ_1 Matrix cracking stress for case of slipping fibers associated with BHE model
- σ^I Initial matrix stresses due to fabrication associated with BHE model
- σ_{mu} Matrix cracking stress associated with ACK model
- σ_o Matrix cracking stress for case of no slip of fibers associated with BHE model;
- Matrix cracking stress associated with MCE model
- σ_{o13} Average stress over a volume element associated with NDSANDS model
- σ_r Radial stress
- σ_θ Tangential stress
- σ_z Axial stress
- τ Interfacial shear stress
- Ω Strain mismatch resulting from fabrication associated with BHE model

Subscripts

- c composite
- f fiber
- m matrix

Abstract

Fiber reinforced ceramic matrix composite materials are receiving a great deal of consideration for use in high temperature structural applications. But much remains to be learned about the failure characteristics of these materials. By understanding the failure mechanisms, the performance of the materials can be more accurately predicted. This experimental study was conducted to investigate the damage progression in fiber reinforced ceramic matrix composites under tensile loading. As part of this study, the effect of the residual stresses at the fiber-matrix interface on the damage progression was evaluated.

The composites tested in this work were fabricated from silicon carbide fibers and glass matrices in a vacuum hot press. The monofilament fibers were manufactured by AVCO Specialty Materials, a division of Textron, Inc. Four different borosilicate glasses manufactured by Corning Glass Works served as the matrices in the composites. Each glass has a different coefficient of thermal expansion than the fiber and through the variation of this mismatch, the residual stresses at the fiber-matrix interface were varied which resulted in different bonding conditions at the fiber-matrix interface. The testing of the samples consisted of three main steps. The mechanical properties of the composites were measured using a servo-hydraulic mechanical testing machine. Then tensile tests were

conducted using a constant load straining device. Failure mechanisms were observed using an optical microscope. Lastly, the experimental stresses when matrix cracks first occurred were compared to predicted stress values from analytical models. During the mechanical property tests, transverse strain reversal was observed which is believed to be caused by axial matrix cracks and fiber-matrix debonding. Matrix cracking occurred in the composites tested before the onset of nonlinearity in the stress-strain curves. The residual stress state at the fiber-matrix interface showed a significant role in the damage progression in the systems tested. Composite samples with tensile radial stresses at the interface failed by random fiber and matrix cracks under tensile loading and in some cases fiber-matrix debonding was observed. At high stresses, extensive matrix damage took place. Samples tested with compressive radial stresses at the fiber-matrix interface did not exhibit random cracking or heavy matrix damage even at high stresses. Large thermal coefficient of expansion mismatch between fiber and matrix caused residual stresses high enough to produce matrix cracking in the composites. Specifically, samples with axial tensile stresses at the fiber-matrix interface had transverse matrix cracks that formed during fabrication. The existing analytical models were found to vastly overestimate the stresses at which matrix cracking would occur in these composites.

Investigation of Failure Modes in Fiber Reinforced Ceramic Matrix Composites

I. Introduction

Materials engineers have long sought materials with high strength and stability at elevated temperatures. The demand for such high performance materials is increasing rapidly with the push for hypersonic flight and other advanced aerospace applications. Many ceramics and glasses possess the high strength and stability at high temperatures, but have low fracture toughness prohibiting their use in high stress applications. However the recent development of fiber reinforced ceramic matrix composites has generated much interest among materials scientists. Fiber reinforcement offers tougher materials and increased strain at fracture. Composite materials normally consist of strong fibers surrounded by a weaker matrix to protect the fibers and bind the fibers together. Composite materials are no longer isotropic as most conventional materials and thus the mechanical property assessment of composites is much more complicated. But without a better understanding of the failure mechanisms in ceramic composites, their use in critical structural elements is not possible. The failure of fiber reinforced ceramic composites is a complex process occurring in several stages. During tensile loading, failure may involve multiple matrix

cracking, fiber-matrix debonding, fiber pullout and fiber fracture. The initiation of damage in the composites is not well understood. Presently, the indication of matrix cracking is assumed to be the point at which the stress-strain curve becomes nonlinear. This assumption is prevalent in many theoretical modeling efforts today. The failure mode of fiber-reinforced materials is governed in part by the transfer of stress between the fiber and matrix according to Cooper and Kelly (4). This transfer takes place at the fiber-matrix interface and therefore the properties of the interface will affect the properties of the composite. An important interfacial property is the difference in coefficient of thermal expansion of the fiber and the matrix. This parameter determines the residual stress-strain distribution after fabrication and can have significant effects on the resultant composite mechanical properties (6:954).

With these needs in mind, this study was undertaken to further understand the failure mechanisms in fiber reinforced glass matrix composites under tensile loading and to provide evidence regarding the present assumptions of the initial damage mode. Also the effect of thermal coefficient of expansion mismatch between fiber and matrix is investigated.

A. Background

The general theory of fiber reinforcement suggests that significant strengthening will only occur if the elastic modulus of the fibers is greater than that of the matrix, and if tensile stresses can be transmitted to the fiber (6:950). For fibers with a lower modulus than the matrix, the failure stress of the composite will be reduced because the matrix will carry a greater proportion of the applied load. The high strength and large failure strain of high modulus fibers would be most readily exploited by incorporation into a ductile and protecting matrix (6:951). Stresses would be transmitted to the fiber by plastic or elastic deformation of the matrix. It would appear that using high modulus fibers to strengthen brittle ceramics which do not exhibit plastic flow or high elastic deformation would not significantly add to the ceramic's strength. However, it can be shown theoretically that the failure strain of the brittle matrices is increased by the high modulus fibers (6:951). Currently several techniques are available for predicting the onset of matrix cracking in fiber reinforced ceramics. Three of these methods are presented in greater detail in chapter II, but will be discussed briefly in the following section.

Aveston, Cooper, and Kelly (2) discussed the multiple fracture of brittle matrices reinforced with fibers having a larger failure strain than that of the matrix. For

composites, tensile testing results in progressive damage of the matrix. Aveston et al developed a relation that predicts a matrix cracking strain based on the crack spacing in the matrix using an energy balance analysis. The authors found good agreement between the theoretical results and experimental tests with glass in plaster, glass in cement, and carbon fibers in glass.

Marshall, Cox, and Evans (13) addressed matrix fracture in brittle matrix composites and calculated the stress for matrix cracking using a stress intensity approach. Their expression for the matrix cracking stress is virtually the same as that derived by Aveston et al but is developed in terms of incremental crack extension. The energy balance analysis used by Aveston et al was based on a comparison of energies before and after cracking of the matrix.

Budiansky, Hutchinson, and Evans (3) introduced another variation of the Aveston, Cooper, and Kelly theory considering two situations at the fiber-matrix interface. For the first case, unbonded fibers held in the matrix by thermal or strain mismatches, but susceptible to frictional slip were analyzed. For this case, the prediction is the same as that by Aveston et al. The second case looked at fibers that initially are weakly bonded to the matrix, but may be debonded by the stresses near the tip of an advancing matrix crack. Additionally, Budiansky et al

included the state of residual stress in the matrix in their prediction for matrix cracking stress.

Besides the three models that predict matrix cracking stress mentioned above, two models should be briefly discussed which predict the stress distribution at the fiber-matrix interface of a composite system. Pagano and Tandon (15) developed a three-phase concentric cylinder model for analyzing multidirectional coated continuous fiber composites. Their model assumes the fiber, coating, and matrix to be linearly elastic, homogeneous, and perfectly bonded. In a similar approach to determine the stress distribution in multiphase systems, Oel and Frechette (14) developed a plane stress formulation for thin cylindrical disks. Their model predicts radial and circumferential stresses at the fiber-matrix interface.

B. Purpose of This Study

This thesis has the primary purpose of supporting the efforts to better understand failure characteristics of fiber reinforced ceramic composites. Specifically, this thesis involves: (1) studying the damage progression in unidirectional glass matrix composites under tensile loads; (2) varying the state of residual stress at the fiber-matrix interface and observing its effect on damage progression in the composite; and (3) measuring the

mechanical properties of the composite systems and comparing the results to predicted values.

C. Approach

For this study, fiber reinforced glass matrix composites were fabricated and tested under tension to analyze damage progression. The experiments were conducted at the USAF Materials Laboratory, Wright-Patterson Air Force Base, Ohio. The composites tested were unidirectional laminates of AVCO SCS-6 fibers made by Textron and four glasses manufactured by Corning Glass Works (Codes 7761, 7740, 7052, and 9741). The AVCO fiber is a continuous monofilament fiber consisting of a graphite core coated with silicon carbide by chemical vapor deposition (CVD). The fiber is then further coated with several layers of carbon to seal the fiber and reduce stress concentrations. The coefficient of thermal expansion (CTE) of the AVCO SCS-6 fiber is $3.6 \times 10^{-6}/^{\circ}\text{C}$. The matrices in the composite are borosilicate glasses and are commercially available with the exception of the Code 7761 glass. The CTE's of the glasses covered a broad range to allow variation of the residual stresses at the fiber matrix interface of the composites and are as follows:

| <u>Glass Code</u> | <u>CTE ($\times 10^{-6}/^{\circ}\text{C}$)</u> |
|-------------------|---|
| 7761 | 2.6 |
| 7740 | 3.5 |
| 7052 | 5.2 |
| 9741 | 4.9 |

The composites were fabricated in the form of two inch (5.1 cm) square plates made up of 12 unidirectional layers of fibers using a vacuum hot press. The processed composite plates were cut into 0.2 inch (.51 cm) wide and two inch (5.1 cm) long samples and polished to reduce surface scratches and flaws.

Tensile tests on the composites were carried out at room temperature using a constant load straining fixture. Failure modes involving matrix cracks, fiber-matrix debonding, and fiber cracks were observed using an optical metallurgical microscope. Mechanical properties of the composites were measured for both the longitudinal and transverse direction using a servo-hydraulic mechanical testing machine (MTS). Finally, the results of the experimental tests are compared to predicted values from three theoretical models.

II. Background

Fiber reinforced glass-ceramic matrix composites are classified as brittle matrix composites (BMC). They are characterized by matrices which are stiff compared to the fibers and exhibit relatively low strain to failure (9:1). Because of the low strain capability of the matrix in these composites, matrix damage is usually present well before final failure of the composite.

A. Theoretical Models

Several analytical models exist that attempt to predict the damage process in brittle matrix composites. In these models, the composites are assumed to fail by either single fracture or multiple fracture of the matrix because of the larger failure strain of the fibers than that of the matrix. Single fracture will occur when the fibers are unable to sustain the additional load they receive when the matrix fails. The transition from single fracture to multiple fracture of the matrix occurs at a critical value of volume fiber fraction determined by the properties of the fiber and matrix. Aveston, Cooper, and Kelly (2) discussed the condition of multiple matrix fracture for composite materials stressed in tension parallel with the fibers. They assumed that if one of the two constituents of a composite breaks at a lower strain

than the other, the more brittle phase will continue to show multiple fracture until final failure. This also assumes that the non-broken constituent is able to bear the load after the more brittle phase initially breaks. The matrix will break into lengths between x and $2x$ (Figure 1) which are determined by the rate of stress transfer between the fiber and matrix. This rate of transfer is determined by the maximum shear stress τ the interface can sustain (2:16). From a force balance on a segment of fragmented fiber and matrix shown in Figure 1,

$$\sigma_{mu}[\pi(r_m^2 - r_f^2)] = \tau 2\pi r_f x \quad (1)$$

where σ_{mu} is the breaking stress of the matrix, r is radius, and the subscripts f and m refer to fiber and matrix respectively.

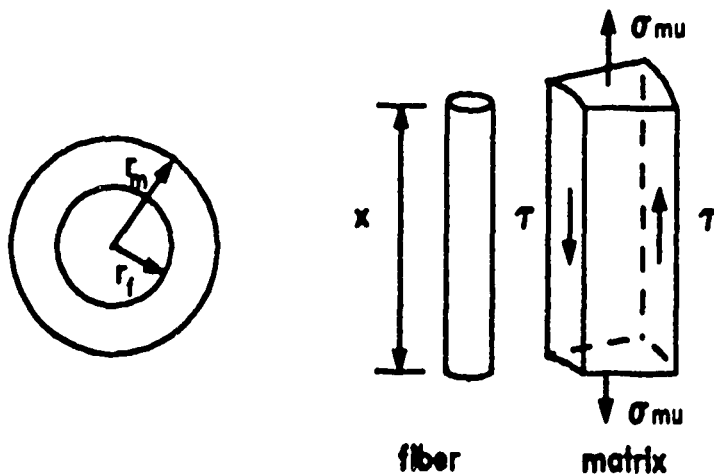


Figure 1. Fiber-matrix Shear Lag Model (3)

Then letting $V_f = \pi r_f^2 x$ and $V_m = \pi(r_m^2 - r_f^2)x$, and rearranging yields $V_m/V_f = (r_m^2 - r_f^2)/r_f^2$. By using this expression for V_m/V_f in equation 1 and solving for the crack spacing x , the following relation can be obtained:

$$x = (\sigma_{mu}/2\tau)(V_m/V_f)r_f \quad (2)$$

From energy absorption during multiple fracture, Aveston et al developed an expression relating material and composite parameters for the strain at which a crack forms in the matrix.

$$\epsilon_{mu} = \{12\tau K_m^2(1-\mu^2)E_f V_f^2/E_o E_m^3 r_f V_m\}^{1/3} \quad (3)$$

where K_m is the fracture toughness of the matrix and μ is the Poisson's ratio of the matrix. E_o is the composite modulus and given by the rule of mixtures:

$$E_o = E_f V_f + E_m V_m \quad (4)$$

By substituting $E_m \epsilon_{mu}$ for σ_{mu} in equation 2, the crack spacing x can be expressed in terms of the composite and material parameters:

$$x = \{.75 r_f^2 V_m^2 E_f K_m^2 (1-\mu^2)/\tau^2 V_f E_o\}^{1/3} \quad (5)$$

Kimber and Keer (10:354) show statistically that $x = x'/1.34$ where x' is the average crack spacing. Equation 5 can then be rearranged to obtain an expression for shear stress τ .

$$\tau = \{.75(1-\mu^2)K_m^2 V_m^2 r_f^2 E_f / E_c V_f(x)^3\}^{1/2} \quad (6)$$

Marshall, Cox, and Evans (13) analyzed brittle matrix composites with only frictional bonding between fiber and matrix and built on the efforts of Aveston, Cooper, and Kelly. In their work, Marshall et al used a stress intensity approach for determining crack growth and showed their result to be equivalent to the energy balance method that Aveston et al (2) used. However in their energy balance solution, Marshall et al examined the energy change for incremental crack extension while Aveston et al compared energies before and after cracking of the matrix. Marshall et al also addressed the presence of strength controlling defects in the matrix. Aveston, Cooper, and Kelly (2) assumed the matrix possessed a characteristic strength independent of these defects (13:2014). Marshall, Cox, and Evans derived an expression for matrix cracking stress σ_o :

$$\sigma_o = \{6(1-\mu^2)K_m^2 \tau E_f V_f^2 V_m (1+l)^2 / E_m r_f\}^{1/3} \quad (7)$$

where $\Gamma = E_f V_f / E_m V_m$. This expression for σ_0 can be derived identically from an energy balance and stress intensity analysis. They also concluded that for large crack lengths the matrix cracking stress is independent of crack size. Large crack lengths are defined as having a crack opening u which asymptotically approaches the equilibrium separation u_0 of the failed matrix (13:2014). This separation is present at a distance c_0 from the crack tip as shown in Figure 2. The crack tip stress concentration is induced only over the length c_0 and thus the stress needed to extend the crack is independent of crack length (13:2014). Crack growth in this region is called steady-state crack growth. Because of the crack-size independence of the matrix cracking stress, Marshall et al (13) defined matrix cracking stress (for large cracks) as an intrinsic property of the composite which takes into account the reinforcing effect of the fibers. They stated that for composites with a higher fiber modulus than the matrix modulus, the matrix cracking stress of the composite is higher than the strength of the unreinforced matrix for a given crack length (13:2019).

Budiansky, Hutchinson, and Evans (3) also considered the matrix cracking in fiber-reinforced ceramic composites. They looked at two different fiber-interface conditions in the system. The first one was the same as considered by

Marshall et al (13) where the fiber and matrix are bonded only by thermal or strain mismatches and the sliding of the fibers in the matrix is resisted by frictional forces only. The second case is where the fibers are initially weakly bonded to the fibers but readily debond due to the stresses

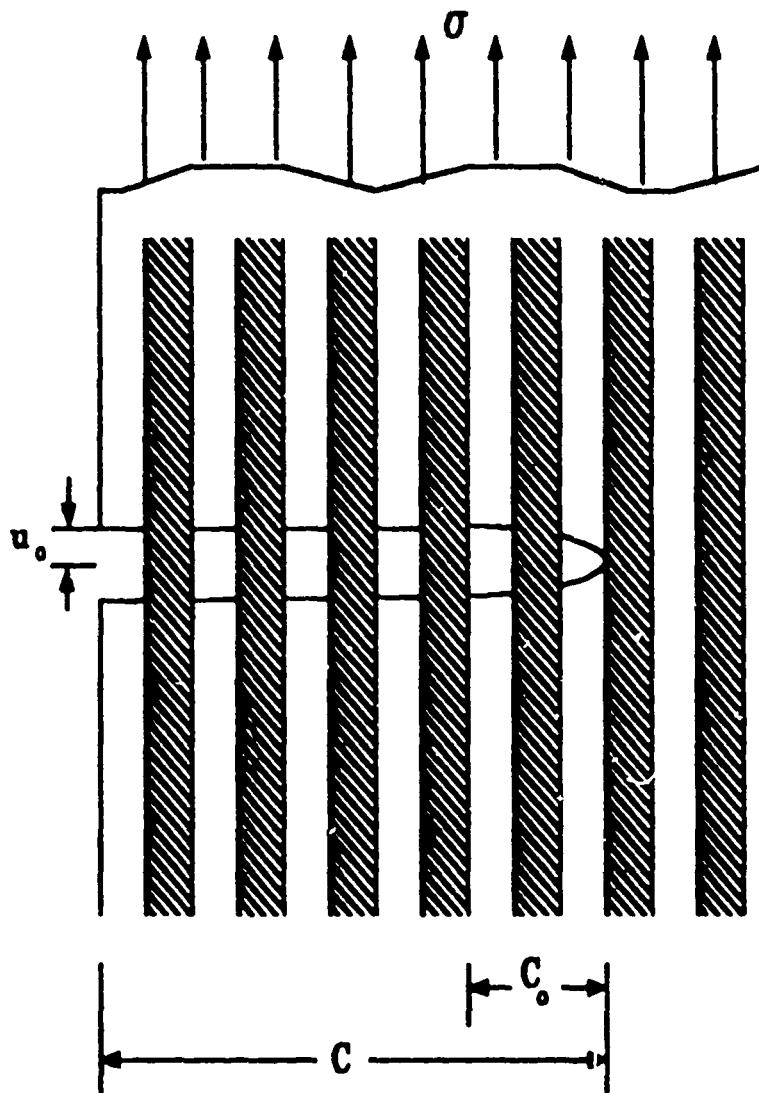


Figure 2. Steady-state Matrix Cracking in a Composite (13)

near the advancing matrix crack. For the frictional bonding case, the result generalizes that of the ACK model and is based on the analysis of steady state crack growth in the matrix (3:168). They assumed that a planar crack would propagate across the composite under an applied stress that becomes constant as soon as the crack passes two to three fibers. This steady state cracking stress is the same as the cracking stress of the ACK model. For the case of the weakly bonded fibers, the matrix cracking stress will depend on the debonding toughness of the interface (3:169). Only the unbonded fiber model is considered here. The theoretical prediction for cracking stress developed by Budiansky et al is given by

$$\sigma_{or} = \sigma_1 - (E/E_m)\sigma^I \quad (8)$$

and is valid for unbonded fibers where frictional sliding between fiber and matrix is allowed. In this expression σ_1 is given by

$$\sigma_1/E_o = 1/E_m\{6V_f^2 E_f \tau K_m^2 (1-\mu^2)/r_f E_m E_o V_m\}^{1/3} \quad (9)$$

and is equivalent to the ACK relation for matrix cracking stress. The term σ^I represents the initial matrix stresses that occur during fabrication due to cooling, plasticity,

creep, or phase transformation (3:179). These stresses are given as

$$\sigma^I/E_m = \beta_2/\beta_1[E_f/E][V_f/1-\mu]\Omega \quad (10)$$

where $\Omega = (\epsilon_f - \epsilon_m)$ is the strain mismatch between fiber and matrix. β_1 and β_2 are functions of V_f , E_f/E_m , μ_f , and μ_m and assuming that $\mu_f = \mu_m = \mu$, then they become

$$\beta_1 = 1 - \frac{1}{2}(1 - 2\mu/1 - \mu)(1 - E/E_f) \quad \text{and} \quad \beta_2 = \frac{1}{2}(1 + E/E_f) \quad (11).$$

Budiansky et al also considered the case of unbonded fibers but for no slip matrix cracking. The relation for this case is similar to equation 8 but with σ_1 replaced by σ_o where

$$\sigma_o/E_o = B[6V_f^2 E_f/V_m^2 E_o(1+\mu)]^{1/4}[K_m^2(1-\mu^2)/r_f E_m^2]^{1/2} \quad (12)$$

and $B = [2V_m^3/-6\log V_f - 3V_m(3-V_f)]^{1/4}$.

Budiansky et al obtained the relation $\{\sigma_{or} + (E/E_m)\sigma^I\}/\sigma_o$ as a function of (σ_1/σ_o) as shown in Figure 3 where the linear portion of the curve is the region of large slip and equation 8 is applicable. In the no slip region, equation 8 still applies, with σ_1 replaced by σ_o from equation 12.

The transfer of stress between the fiber and matrix partially governs the mechanical behavior of reinforced

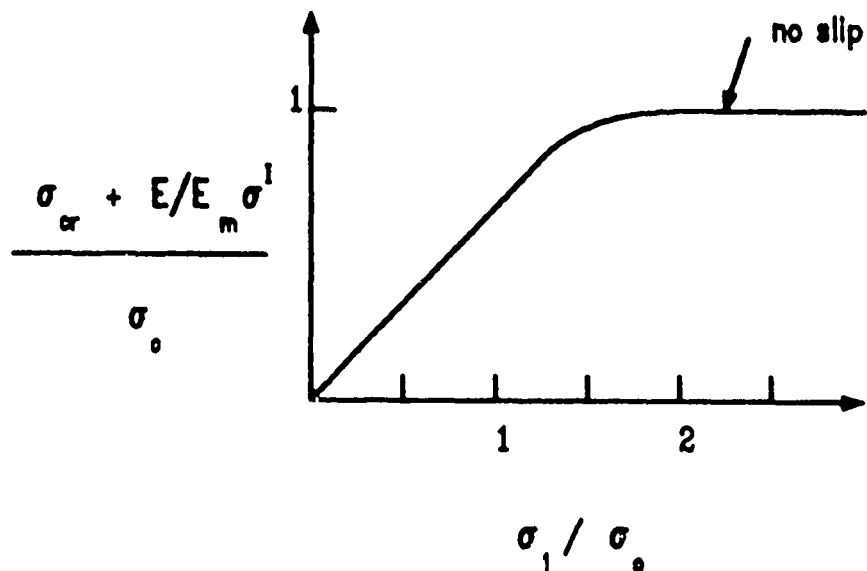


Figure 3. Matrix Cracking Stress for Frictionally Constrained Fibers (3)

material. By tailoring the interfacial properties, desirable composite properties can be achieved. Coatings of different materials and varying thicknesses can be used to modify the composite behavior. In order to determine how coatings applied to a fiber can alter the state of stress at the fiber-matrix interface, Pagano and Tandon developed a model which approximates the elastic response of a composite reinforced by coated fibers oriented in various directions (15). They analyzed a multidirectional coated continuous fiber composite using a three-phase concentric cylinder model. Using the model, the effective

thermoelastic properties and the stress distribution inside the fiber, and the matrix can be determined. The model assumptions are that the fiber, coating, and the matrix are linearly elastic, homogeneous, and perfectly bonded. The coated fiber reinforced composite is modeled by a representative volume element composed of concentric, circular cylinder elements. The innermost cylinder is the fiber, the next ring is the coating, and the outer ring is the matrix (15). Additionally, the displacements and tractions acting on the composite cylinder elements are assumed to be continuous. In determination of the stress field, a given set of boundary conditions of the form

$$U_i(s) = \epsilon_{ij}x_j \quad \text{or} \quad T_i(s) = \sigma_{ij}n_j \quad (13)$$

is applied to the composite material volume, where s is the boundary surface, x_j are the Cartesian coordinates of the surface, n_j is the unit outward normal vector on the surface, ϵ_{ij} and σ_{ij} are constants and U_i and T_i represent components of the boundary displacement and traction vector respectively (15:277). For the boundary conditions given, it can be shown that

$$\epsilon_{ij} = \epsilon^0_{ij} = \text{constant} \quad \text{or} \quad \sigma_{ij} = \sigma^0_{ij} = \text{constant} \quad (14)$$

where the "o" superscript denotes the average value over the whole volume. For prescribed displacements the average strains are known and using Hooke's law, the stresses can be determined. For prescribed tractions the average stresses are known and the strains can be determined. In order to analyze composites with their model, Pagano and Tandon incorporated it into a computer code known as NDSANDS. Thus a practical tool is available to evaluate composites of different materials and arbitrary fiber orientations (15:292).

Oel and Frechette (14) investigated the stress distribution of composites with curved interfaces such as fiber reinforced materials. Their study involved measuring the stress distribution in thin cylindrical glass disks and comparing the measured values to calculated stresses. The test specimens were prepared by sealing a disk of one optical glass in another having a higher thermal expansion (14:343). The stress formulations were developed by modifying the stress distribution for a cylindrical system given by the theory of elasticity. The disks were considered thin and the axial stresses (σ_z) were assumed to be zero. The resultant equation for the radial stress at the fiber-matrix interface is

$$\sigma_r = -\Delta\alpha\Delta TE_m\{P^2-1\}/\{[\beta(1-\mu_f) + (1+\mu_m)]P^2 + (1-\mu_m) - \beta(1-\mu_f)\} \quad (15)$$

and the tangential stress is given by

$$\sigma_{\theta} = \Delta\alpha\Delta TE_m\{P^2+1\}/\{[\beta(1-\mu_f) + (1+\mu_m)]P^2 + (1-\mu_m) - \beta(1-\mu_f)\} \quad (16)$$

where $\Delta\alpha = \alpha_m - \alpha_f$, $\Delta T =$ cooling range, $P^2 = 1/V_f$, μ_m and μ_f are the Poisson's ratios of the matrix and fiber respectively, and $\beta = E_m/E_f$. The formulations given by Oel and Frechette are very similar to those by Pagano and Tandon except that Oel and Frechette assume plane stress for the thin disks.

In summary, the models developed by Aveston, Cooper, and Kelly (ACK); Marshall, Cox, and Evans (MCE); and Budiansky, Hutchinson, and Evans (BHE) all predict the matrix cracking stress for fiber reinforced brittle matrix composites. The predicted matrix cracking stress predicted by each is the same for a given system, however the formulation and assumptions of the three models are different. Additionally, the BHE model includes the initial matrix stresses due to strain mismatch between the fiber and matrix that occur during fabrication. The NDSANDS model developed by Pagano and Tandon determines the stress distribution in composites reinforced by coated fibers in various orientations. Oel and Frechette evaluated the stress distribution in thin composite disks using a similar formulation to that of Pagano and Tandon but with the

assumption that for the thin disks the axial stresses are zero.

B. Material Selection

In this section the fiber and matrices used in this research are discussed as well as the reasons for their selection. The main objective of this study was to investigate the effect of the fiber-matrix interface on damage progression in a fiber-reinforced glass matrix composite under tensile loading. Ceramic materials have long been prized for their high temperature capabilities, oxidation resistance, chemical durability, and low density relative to metals (1:624). But their brittle behavior prevents their use in highly stressed structures such as engines and aerospace vehicles. Fiber-reinforcement has been used to improve the strength and toughness of brittle ceramics. This strengthening will occur when the elastic modulus of the fibers is greater than that of the matrix, and if tensile stresses can be transmitted to the fibers (6:950). Ideally a ductile and protecting matrix to bind the fibers and inhibit crack propagation would take advantage of the high strength, high modulus fibers. In the case of low modulus ceramic matrices it appears their low failure strains would limit their ability to be strengthened by fiber-reinforcement. However, the actual failure strain of brittle matrices should be theoretically

increased by the addition of higher modulus fibers (6:951). Thus the fibers to be used in reinforcement of brittle ceramic matrices should have high strength, high modulus, high temperature capability, and chemical stability. The important characteristics of the matrix to consider are compatibility with the fibers, fabricability, and refractoriness. The matrix and fiber should be chemically compatible such that both phases remain stable during processing. Good fabricability will allow more samples to be produced with fewer defects and thus allow more effort to be devoted to the study of damage progression. Both the fiber and matrix material used should retain their strength and stability at elevated temperatures. For this study it is desirable for the matrix to be optically transparent to observe damage initiation and progression. Transparent matrices will allow direct observation of damage at the fiber-matrix interface. Also because the effect of residual stress at the fiber-matrix interface on failure mechanisms is to be investigated, there must be some means to vary these stresses. Matrices with different coefficients of thermal expansion (CTE) will change the CTE mismatch between the fiber and matrix which result in different states of stress at the fiber-matrix interface. For this, composite systems with glass matrices have the greatest potential because of their ease of fabrication,

chemical stability, transparency, and variable coefficients of thermal expansion.

The fiber selected for use in this composite is a continuous monofilament fiber produced by AVCO Specialty Materials (a division of Textron, Inc.) in Lowell, Massachusetts. The fiber is produced by coating a 37 micron carbon core with Beta silicon carbide using chemical vapor deposition (CVD). The fiber is then coated with various layers of carbon and carbon-silicon carbide to seal the fiber. According to Prewc and Jarmon (16) the outer coatings placed on the basic fiber (carbon coated with SiC) nearly double the strength of the fiber by reducing notches and stress concentrations. Also the coatings make the fiber more environmentally stable. Figure 4 depicts the overall make-up of the AVCO SCS-8 fiber and the properties of the fiber are listed in Table I.

The glasses chosen to be used for this study were all made by Corning Glass Works and all except one are commercially available. The glasses are borosilicate glasses and were chosen because of their potential for transparency and their broad range of thermal coefficients of expansion. The properties and composition of these glasses are shown in Table II and Table III respectively.

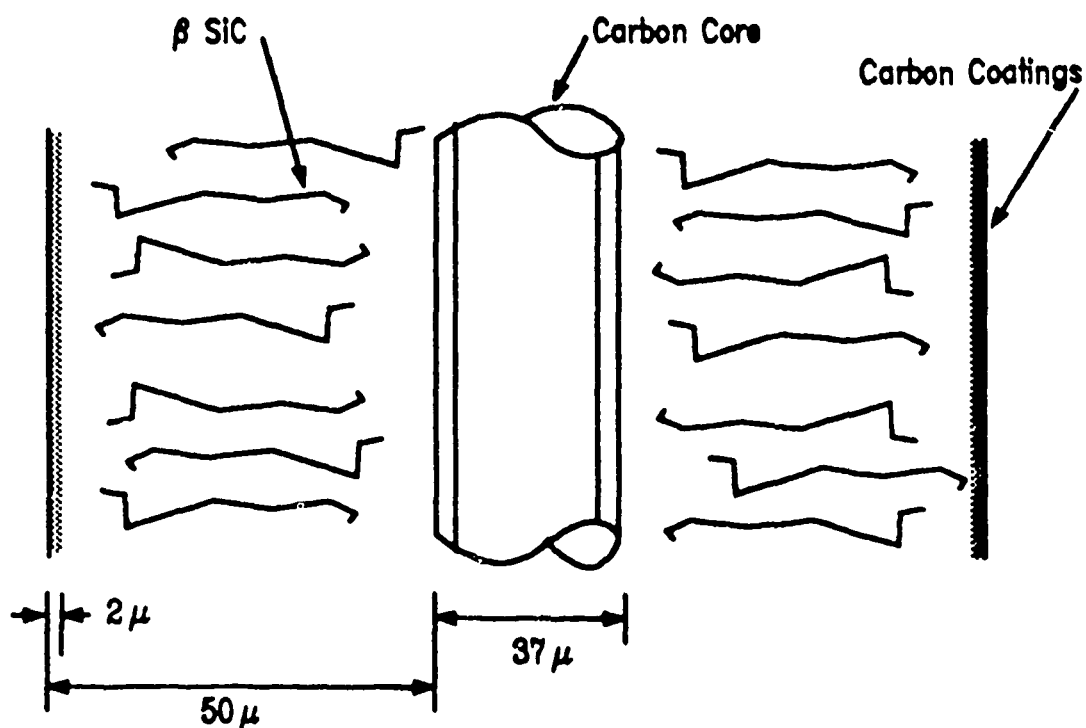


Figure 4. AVCO SCS-6 Fiber Core and Coatings (17)

Table I. Properties of the AVCO SCS-6 Fiber (17)

| | |
|--|------|
| Fiber diameter (x10 ⁻⁶ m) | 144 |
| Density (g/cc) | 3.1 |
| Tensile Strength (MPa) | 3450 |
| Elastic Modulus (GPa) | 415 |
| Thermal Expansion Coeff. (x10 ⁻⁶ /°C) (22-500°C) | 3.6* |

*from Thermo Mechanical Analyzer, Dupont Model 8900

Table II. Properties of Selected Glasses (12)

| PROPERTY | MFG. CODE | | | |
|---|-----------|------|------|-------|
| | 7052 | 9741 | 7740 | 7761* |
| THERMAL EXP. COEFFICIENT ($\times 10^{-6}/^{\circ}\text{C}$) 22-500 $^{\circ}\text{C}$ | 5.2 | 4.9 | 3.5 | 2.6 |
| VISCOSITY - TEMPERATURE ($^{\circ}\text{C}$) | | | | |
| STRAIN PT. | 436 | 421 | 515 | 515 |
| ANNEALING PT. | 480 | 465 | 565 | 565 |
| SOFTENING PT. | 712 | 714 | 820 | 820 |
| WORKING PT. | 1128 | 1161 | 1252 | 1252 |
| DENSITY (g/cc) | 2.27 | 2.18 | 2.23 | 2.23 |
| YOUNG'S MODULUS (GPa) | 56.5 | 49.6 | 62.7 | 62.7 |
| POISSON'S RATIO | 0.22 | 0.23 | 0.20 | 0.20 |

* The 7761 glass is an experimental glass and except for the coefficient of thermal expansion the mechanical properties are not available, but are similar to those of 7740.

Table III. Percent Composition of Selected Glasses (12)

| Code | SiO ₂ | B ₂ O ₃ | Al ₂ O ₃ | K ₂ O | Na ₂ O | PbO |
|------|------------------|-------------------------------|--------------------------------|------------------|-------------------|-----|
| 7761 | 82.0 | 16.0 | | 2.0 | | |
| 7740 | 80.3 | 9.0 | 6.4 | | 4.0 | |
| 9741 | 66.5 | 23.7 | 5.6 | 0.8 | 2.2 | |
| 7052 | 65.3 | 17.8 | 7.4 | | 3.8 | 5.7 |

III. Experimental Procedure

A. Sample Fabrication

The composite specimens tested were all fabricated using a vacuum hot press. The AVCO fibers came in six inch (15.3 cm) wide rolls backed with aluminum. From this roll, two inch (5.1 cm) squares of the fibers were cut with the edges taped so that the aluminum backing could be removed. Next the squares were painted with glass slurry composed of glass powder, polyvinyl acetate, and acetone. The polyvinyl acetate serves as a binder for the fibers until hot pressing. The aluminum backing was removed from the squares and both sides were painted with the slurry. After the slurry dried, 12 squares were stacked unidirectionally to form a sample. Between each layer of fibers, two fibers were layed transversely across the fibers (one at each end) to improve the distribution of matrix between the fiber layers as shown in Figure 5. The 12 layer stack of plies was then heated to a temperature between 700-750°C to burn off the binder and partially sinter the glass. The sample was then loaded in a graphite die for hot pressing. The die was lined with molybdenum sheet on the four interior sides to prevent the glass from reacting with the graphite die parts. Ten grams of glass powder were packed above and below the stack of fiber layers and molybdenum sheets were again used to prevent reaction of glass with the graphite rams within the die

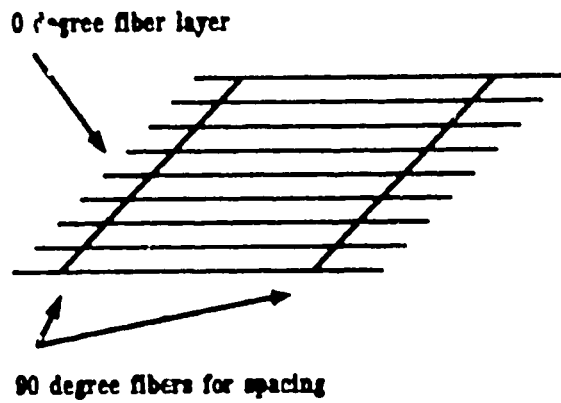


Figure 5. Fiber Layer Sequence for Fabrication

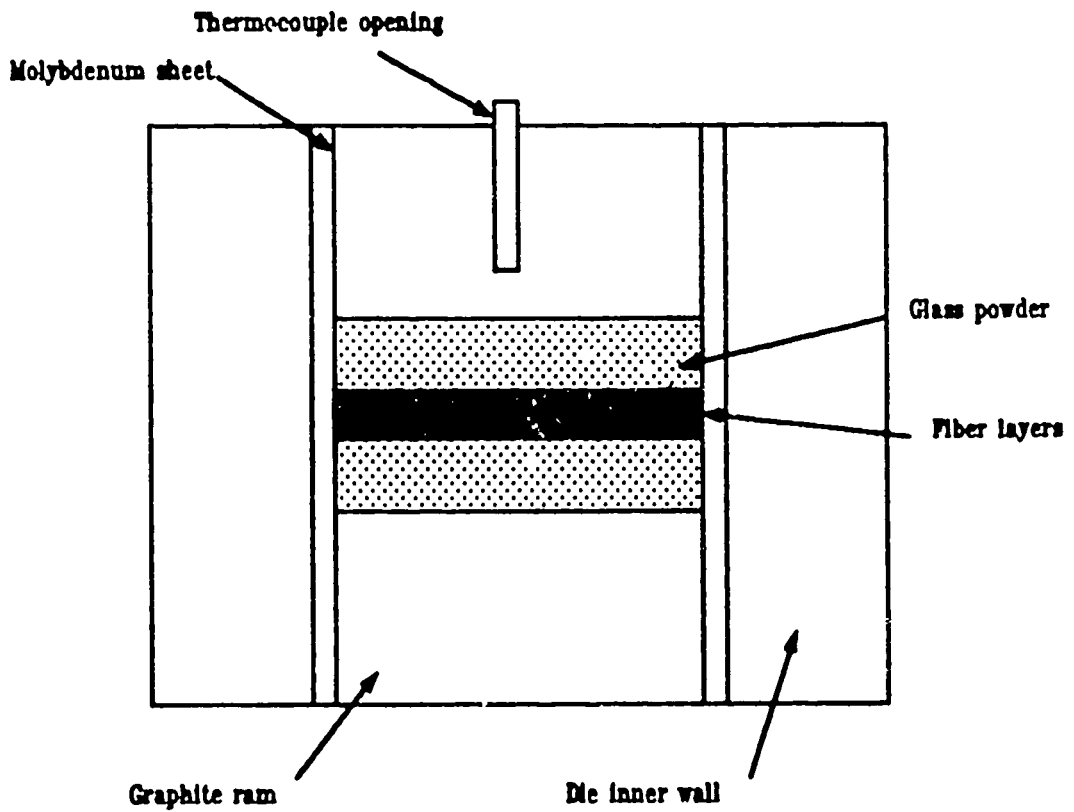


Figure 6. Sample Loaded in the Graphite Die

(Figure 6). The sample was heated by induction under vacuum until the glass powder slumped freely. This temperature was approximately 50°C to 100°C above the glass annealing point. The glass annealing point is defined as the temperature at which glass under tensile stress viscously elongates at specified rates and equates to a viscosity of 10^{13} poises (12:323). This temperature corresponded to a temperature of 850°C to 1150°C on the thermocouple inserted into the die. At the processing temperature, argon was added to the hot-press chamber and the ram pressure on the sample was increased to approximately 1000 psi (6.895 MPa). The sample was held in these conditions between 25 to 30 minutes.

The fabrication conditions were critical in the processing of samples, primarily because of the glass matrices used. To understand the effects of temperature and pressure on the fabrication process, some discussion of glass is helpful. Glass is an example of an amorphous material, or a non-crystalline elastic solid (14:134). More specifically, at the atomic level glasses do not have long-range order, but only short-range order. Glasses become viscous liquids at elevated temperatures. When the glass cools, there is no sharp freezing point as there is in crystalline solids (7:260). The glass simply becomes more viscous and then becomes rigid. This takes place at the glass-transition temperature (T_g) which distinguishes

between a glass and a supercooled liquid as seen in Figure 7. Just above the glass transition temperature the supercooled, highly viscous liquid is semirigid, but it progressively reduces its viscosity and becomes a more fluid liquid as the temperature is raised. Below this temperature, the glass is a rigid solid (18:122).

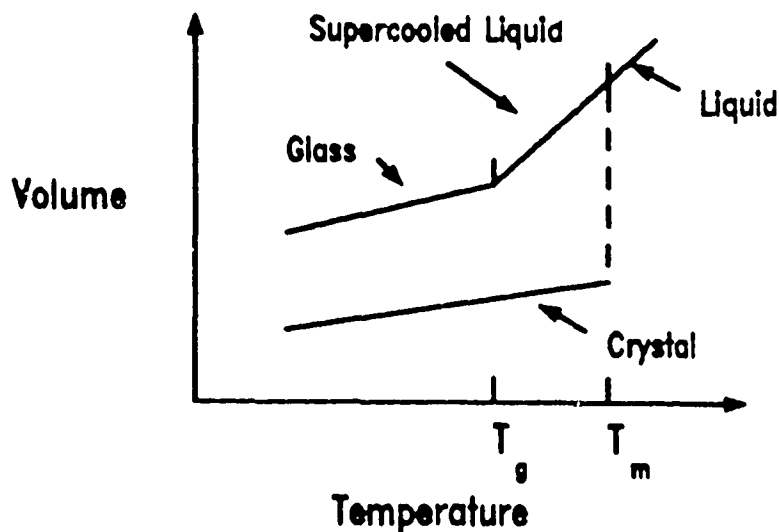


Figure 7. Glass-transition Temperature (18)

However, the glass liquid does have a freezing temperature below which a more stable crystalline structure can form. The activation energy necessary for structural rearrangement to the more stable crystalline structure is sufficiently high, and the heat of fusion which is released is sufficiently low, so that the crystallization process occurs slowly at the freezing temperature. At room temperature, negligibl, few of the atoms will have the

necessary energy to break the existing bonds for rearrangement (18:121). Normally then, during fusion of the glass, very little crystallization takes place. If however during hot pressing the freezing temperature was exceeded and held for a sufficient time, crystallization of the glass constituents could occur. This was a danger in fabrication when too high a temperature was used. Another problem existed in that high temperatures decreased the viscosity of the glass, allowing it leak out between the rams and inner walls of the die. Also the denser fibers would settle to the bottom of the sample and excess glass would form above the top layer of fibers. Applying pressure helps in densification of the glass and increases flow throughout the fiber layers. Additionally, the pressure prevents the nucleation and growth of bubbles. However, too high a pressure would force out the glass along the die inner walls and the molybdenum sheets. Too low a pressure would allow residual bubbles to form. The argon was introduced to suppress the formation of bubbles in the glass and provide an inert atmosphere.

B. Sample Preparation

After hot pressing, the two inch (5.1 cm) square samples were cut into 0.2 inch (0.51 cm) wide strips using a low speed diamond saw to minimize cutting edge damage. The cut samples were then mounted on thick steel disks with thermoplastic cement and polished progressively on the top

and bottom to remove the excess glass covering the fiber layers. The first step of polishing was done with a 75 micron diamond wheel. Then successively smaller sized diamond pastes (15, 6, 1, and .25 micron) impregnated on a cloth-covered wheel were used to further polish out surface scratches and imperfections. For final polishing the samples were placed in 0.05 micron alumina in a Vibronet machine. End tabs made of 0/90° fiberglass/epoxy were bonded to the samples using epoxy cement for gripping during testing. The tabs were placed on the samples such that a 0.75 inch (1.91 cm) length was exposed for damage detection and strain gage attachment as shown in Figure 8. The surface opposite that with the strain gage was observed during testing with the straining fixture. The samples tested in the straining fixture and those tested on the MTS machine were prepared in the same manner.

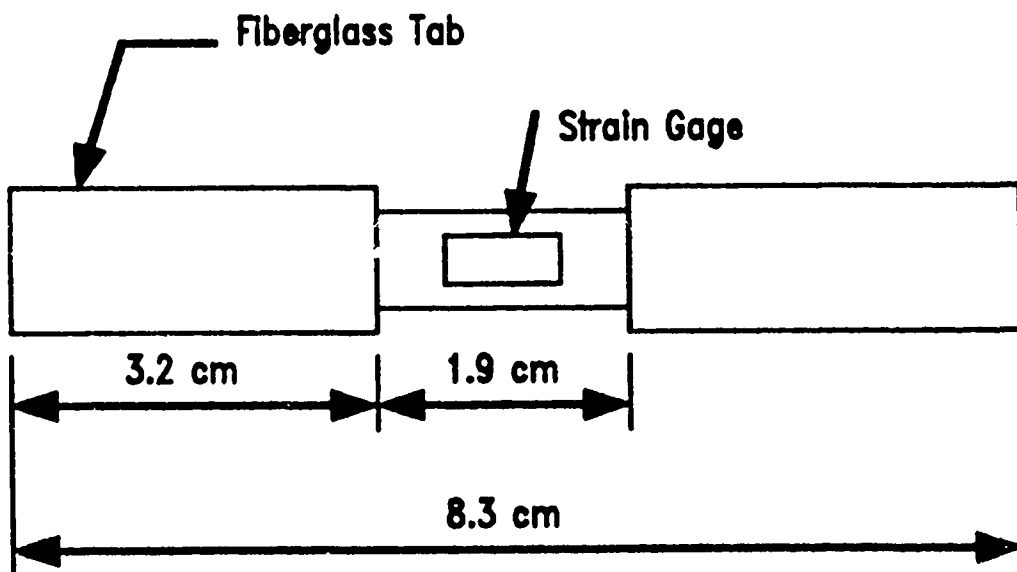
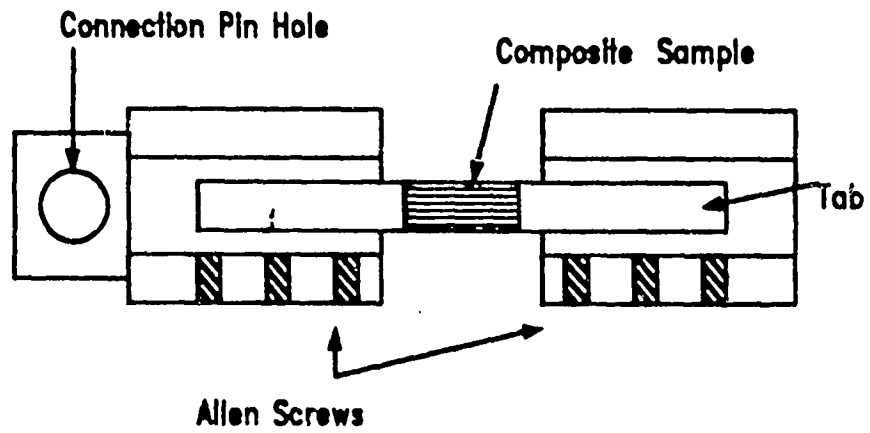


Figure 8. Tabbed Specimen for Testing

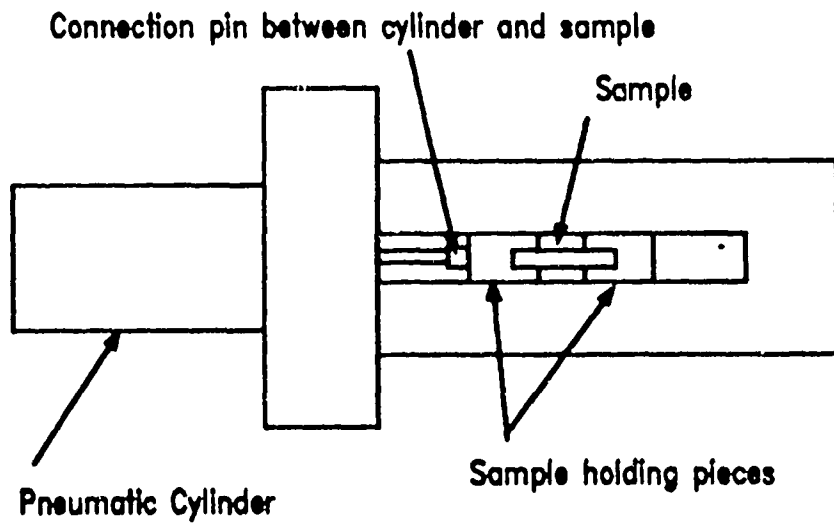
Each sample's thickness and width were carefully measured using a micrometer to determine the cross-sectional area. Then a 350 ohm strain gage (Type CEA-06-062VW-350) was attached longitudinally to one side of the sample to be tested in the straining stage. For the longitudinal samples tested on the MTS machine for mechanical properties, a stacked 0/90° strain gage (Type CEA-06-062WT-350) was used.

C. Test Procedures

In order to observe damage formation and progression in the samples, a specially devised straining fixture was used which was developed by Dr. Ran Y. Kim of the University of Dayton Research Institute. The apparatus consists of a stainless steel pneumatic cylinder, a grooved steel block, two pieces that grip the specimen, and a strain indicator. The holding pieces grip the sides of the specimens with allen screws. A tensile or a compressive load may be applied to the specimen via a gas bottle through the pneumatic cylinder. Figure 9 illustrates the straining fixture schematically and Figures 10a and 10b are photographs of the apparatus. The device applies a constant load to the specimen controlled by the pressure regulator on the gas bottle. One psi of pressure on the bottle pressure indicator corresponds to a 2.65 lb load on

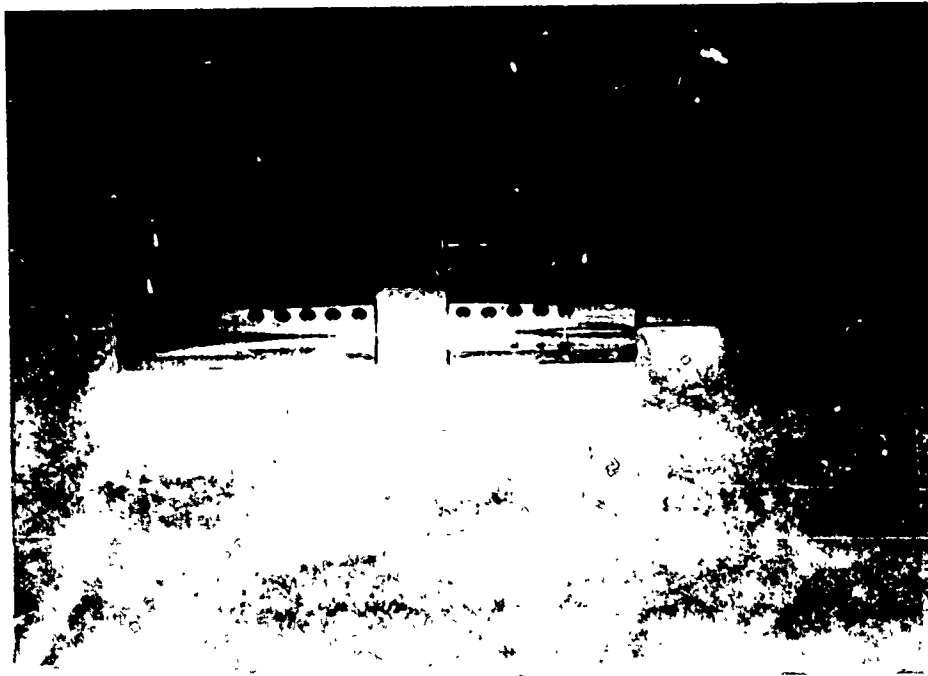


a. Sample holding pieces

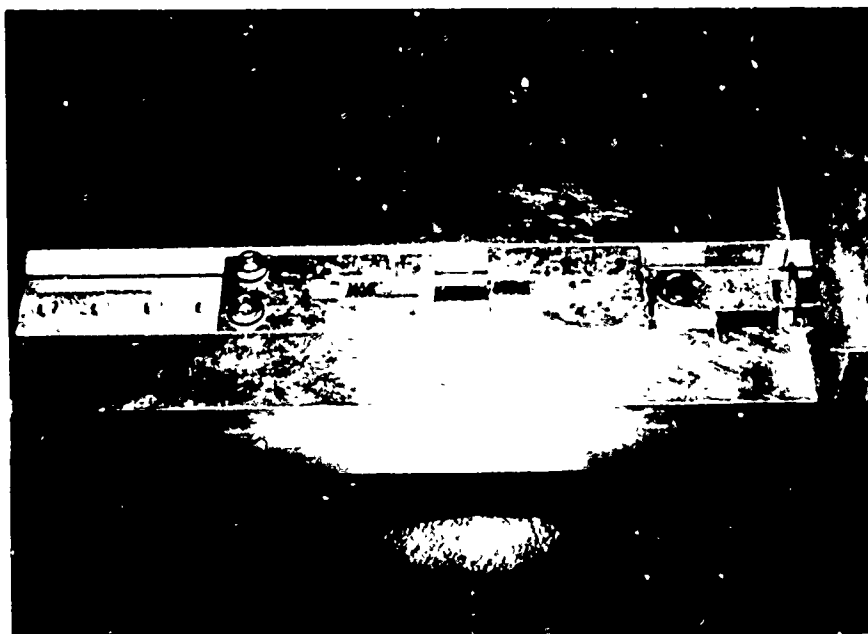


b. Schematic of components of straining fixture

Figure 9. Straining Fixture



a. Composite sample gripped in holding pieces

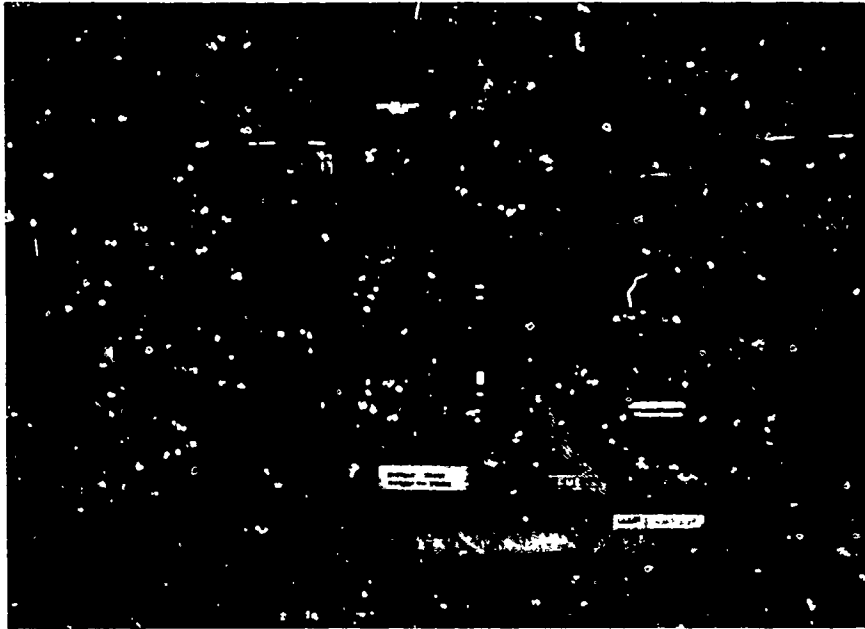


b. Composite sample loaded in straining fixture

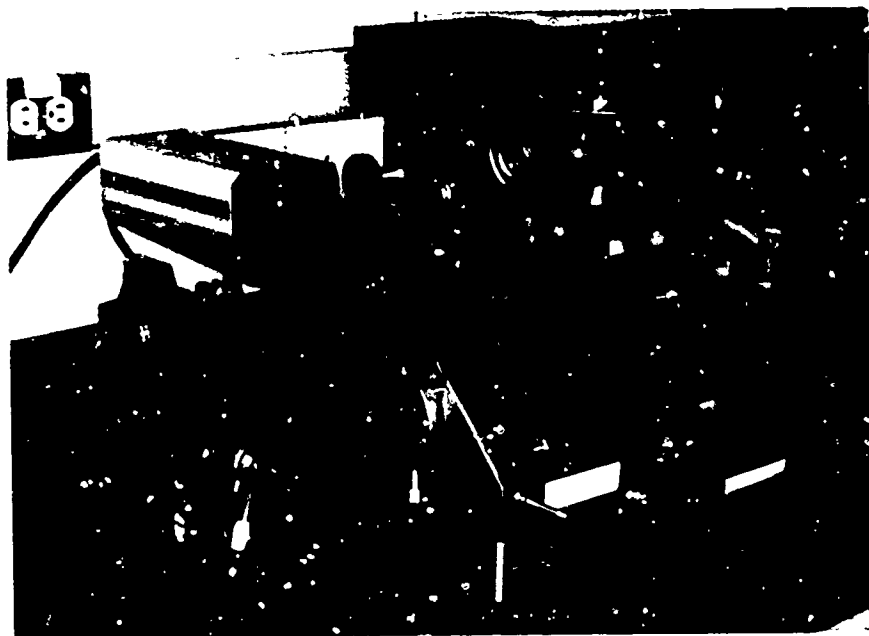
Figure 10. Straining fixture components

the specimen. This relation was determined by calibrating the straining fixture using a sample of aluminum with a known elastic modulus. The aluminum sample was strain gaged and loaded in tension. Knowing the modulus and strain value, the stress applied was determined. From the applied stress, the load was calculated using the cross-sectional area of the specimen. Finally the relation between the load on the specimen and the pressure delivered by the pressure regulator was determined. To observe and record the formation and progression of damage in the samples, an Olympus inverted metallurgical microscope with a Polaroid camera attached was used and is shown in Figures 11a and 11b. The magnification power of the microscope ranged from 50X to 1000X.

For the straining stage tests, the strain-gaged sample was gripped in the device and any pre-strain noted. The sample side visible on the microscope was observed for any pre-existing cracks or noticeable defects. A tensile load was then applied to the sample to produce approximately 100 micro strain. The sample surface was then studied for new cracks or damage. Any significant change was photographed. The strain was increased in increments of 100 micro strain until the sample failed. To obtain the mechanical properties of the composite systems, samples of each glass and fiber were tested on a MTS Model 800 machine. Tensile tests were performed on samples cut both longitudinally



a. Metallurgical microscope



b. Polaroid camera attachment

Figure 11. Olympus inverted metallurgical microscope and camera used for damage observation

and transversely. The samples were prepared as discussed in Section B of this chapter and had dimensions as previously shown in Figure 8. The 0/90° stacked strain gages were mounted on some of the longitudinal samples to record both longitudinal and transverse displacement. The longitudinal samples were tested at a constant load rate of 2.5 lb/in and a grip pressure of 800 psi. The transverse samples were tested at load rate of 1.25 lb/in and a grip pressure of 400 psi.

The fiber volume fraction (V_f) was determined for each sample by using hydrofluoric acid to leach out the glass matrix. A piece of each sample tested was weighed and placed in a solution of hydrofluoric acid to leach out the glass. The remaining fibers were dried in a quartz crucible and reweighed to determine the weight fraction of fibers. The volume fraction of fibers was then calculated for each. Table IV summarizes the fiber volume fractions for the samples tested. The desired V_f for the composites fabricated was approximately 0.4. As Table IV indicates, the V_f 's obtained varied from 0.225 to 0.469. This variation resulted primarily from the hot pressing conditions used in fabrication. As mentioned in Section A earlier in this chapter, at higher temperatures the viscosity of the glass decreases resulting in glass leaking from the sample along the die walls during hot pressing. The loss of glass from the composite caused higher volume

fractions than desired. This was the case in the samples made with the 7740 glass as in Sample 32. In fabrication extra glass powder was added when loading the fiber layers and glass because of the high probability that some glass would leak out at elevated temperatures during processing. If the graphite die parts fit tightly and the glass did not require a very high temperature for sintering ($\approx 850^{\circ}\text{C}$) as in the case for the 7052 and 9741 glasses, there was little leakage of the glass. The resultant composites then had lower volume fraction of fibers than desired as in Samples 27, 40, and 42.

Table IV. Sample Fiber Volume Fraction Measurements

| <u>Sample</u> | <u>Glass</u> | <u>Fiber Volume Fraction</u> |
|---------------|--------------|------------------------------|
| 24 | 7761 | .397 |
| 27 | 7761 | .225 |
| 28 | 7761 | .404 |
| 32 | 7740 | .469 |
| 39 | 7052 | .327 |
| 40 | 7052 | .285 |
| 41 | 9741 | .304 |
| 42 | 9741 | .231 |

IV Results and Discussion

During recent years, there has been an increasing demand for high-performance materials for use in advanced engine and aerospace applications. Of particular interest are those materials for use at elevated temperatures. Many ceramics and glasses exhibit relatively high strength and stability at high temperatures, combined with low density and chemical inertness (6:849). However these materials are notch-sensitive and brittle. They have low fracture toughness. Fiber reinforcement offers improvements in strength and toughness in ceramics such that they may be used in highly stressed, high temperature applications. Before fiber reinforced ceramics can be used in these critical applications, the factors affecting their strength and failure mechanisms must be better understood. For instance, fiber reinforced ceramics show a tendency toward matrix-microcracking at stress levels below the ultimate composite strength and the problems associated with this phenomena are not well known. Additionally, designers must be able to predict the strength of fiber reinforced systems to ensure structural integrity and cost effectiveness. Several failure prediction techniques for these brittle-matrix composites exist (2,3,13), but little has been done to verify their predictions with experimental data. In this study, the initiation of damage formation and growth in unidirectional fiber reinforced glass composites was

investigated experimentally. This may depend on interface conditions of the fiber and matrix, and hence the effect of the residual state of stress at the interface on damage progression was investigated. Also, some of the fracture prediction models for brittle-matrix composites were evaluated and compared to the experimental data of the present study.

Four composite systems were fabricated and tested. In the first composite, which was made of Code 7761 glass and AVCO fibers, the fiber-matrix interface was under tensile stresses in the radial direction. The second system (Code 7740 glass and AVCO fibers) theoretically had very little residual stress at the fiber-matrix interface. In the last two composites tested, (7052/AVCO and 9714/AVCO) the interface residual stresses were compressive in the radial direction. The residual stresses in the 7052/AVCO system were higher than the 9714/AVCO system because of the greater coefficient of thermal expansion mismatch between the fiber and matrix.

Before the test results are discussed, a brief summary of the fabrication conditions and problems for each composite is given here. As explained in Section A of Chapter III, the fabrication conditions vary for each glass dependent upon the glass composition. The proper fabrication conditions were essential for producing suitable samples. Unfortunately, the correct conditions were not

known beforehand and had to be determined by trial and error for each glass. The fabrication of 7761/AVCO samples was accomplished without much difficulty once the proper processing temperature was determined. For these samples, a thermocouple temperature of approximately 1050°C was required. The pressure applied during hot pressing did not appear to affect the samples greatly, but pressures in the range of 750 psi (5.17 MPa) proved to be optimum.

The 7052/AVCO and 9741/AVCO composites were fabricated easily primarily because the processing temperature required was relatively low (approximately 850°C). This lower temperature kept the glass viscosity high enough that leakage from the die was minimal. The viscous glass allowed higher pressure to be applied during hot pressing so that the samples had low porosity. However, as discussed in more detail later in this chapter, the high coefficient of thermal expansion mismatch between the fiber and glass in these systems (7052/AVCO and 9741/AVCO) caused high residual stresses. The high tensile residual stress at the fiber-matrix interface in the axial direction caused evenly spaced transverse cracks in the matrix. These cracks resulted solely from the residual tensile stress in the composite from fabrication.

The proper fabrication conditions for the 7740/AVCO composites proved difficult to find and even more difficult to achieve in the hot press. The hot pressing temperature

required was very high (1150°C) to ensure complete sintering and prevent crystallization of the glass. At this high temperature, the viscosity of the glass was low, causing excessive leakage of the glass from the die and poor fiber alignment in the samples. Also high pressure was required to densify the samples and prevent bubbles from forming in the glass. The high pressure further aggravated the leakage problem, squeezing the glass out between the die walls. This system required both high pressure and high temperature for processing which were difficult to obtain without excessive glass leakage. As a result of these processing problems, no 7740/AVCO samples were produced that did not have defects such as poor fiber alignment, high porosity, or high volume fraction of fibers.

A. Mechanical Properties from MTS Tests

Samples made from each of the four glasses with AVCO fibers were tested under tensile loading using a MTS machine. Tests were performed on both longitudinally cut and transversely cut samples as discussed in Chapter III. Table V lists the samples tested and the measured properties. Additionally, this table lists specific comments on sample defects and testing problems. Figures 12 thru 15 depict graphically the variation in data

obtained for the composite mechanical properties: elastic modulus, transverse elastic modulus, ultimate tensile strength, and transverse ultimate tensile strength. Table VI shows the average values of the mechanical properties measured from the MTS tests. For some glasses, the sample data was widely scattered. In the case where a test gave vastly different values of a specific property, this test result was not included in the averages shown in Table VI. For example in the 7740/AVCO system, three longitudinal samples were tested on the MTS machine. The values of composite modulus (E_c) measured were 173.5 GPa, 169.5 GPa, and 269.4 GPa. The E_c of 269.4 GPa was not included in the average modulus for the 7740/AVCO composite. For the 7740/AVCO system no transverse samples were available for determining E_2 because of the problems with fabrication using this glass. During the test of a 9741/AVCO transverse sample, the strain gage debonded from the sample surface. A second sample to be tested was broken during preparation for the test. Thus no valid E_2 was obtained for this system.

Table VII compares the predicted elastic moduli for the composites by the rule of mixtures to the moduli measured during testing. In looking at Table VII, the longitudinal moduli determined experimentally from the MTS data was generally lower than the predicted values from rule of mixtures for the 7761/AVCO and 7740/AVCO

Table V. Mechanical Properties of Glass/AVCO Composites

| Sample | Type* | V _f | X-Section Area(in ²) | E(GPa) | UTS(MPa) | Comments |
|------------------------------|-------|----------------|----------------------------------|--------|----------|----------|
| <u>Glass 7761</u> | | | | | | |
| 24B | L | .397 | .0115 | 200.4 | 438.8 | |
| 28X | L | .404 | .0118 | 146.6 | 436.8 | |
| 28Y | L | .404 | .0126 | 182.9 | 274.4 | |
| 28Z | L | .404 | .0128 | 199.7 | 425.9 | |
| 27A | T | .225 | .0123 | 17.2 | 8.7 | |
| 27B | T | .225 | .0157 | 23.8 | 12.1 | |
| 27C | T | .225 | .0140 | 49.4 | 17.3 | |
| <u>Glass 7740</u> | | | | | | |
| 32A | L | .469 | .0160 | 169.5 | 275.0 | 2,3 |
| 32B | L | .469 | .0141 | 269.3 | 306.9 | 2,3 |
| 32C | L | .469 | .0166 | 173.5 | 312.4 | 2,3,6 |
| No transverse samples tested | | | | | | |
| <u>Glass 7052</u> | | | | | | |
| 39B | L | .327 | .0213 | 127.1 | 262.5 | 5 |
| 39C | L | .327 | .0196 | 146.7 | 206.9 | 5 |
| 39D | L | .327 | .0219 | 117.9 | 200.5 | 5,6 |
| 40A | T | .285 | .0214 | 90.5 | 7.4 | 5 |
| 40B | T | .285 | .0203 | 40.8 | 4.3 | 5 |
| <u>Glass 9741</u> | | | | | | |
| 42B | L | .231 | .0237 | 242.0 | - - | 5,6 |
| 42C | L | .231 | .0250 | 127.6 | 293.3 | 5,6 |
| 42D | L | .231 | .0235 | 183.8 | 110.3 | 5 |
| 41B | T | .304 | .0219 | - - | 3.9 | 1,7 |

*Type: L indicates longitudinally cut sample
T indicates transversely cut sample

Comments:

- | | |
|-----------------------------------|-----------------------|
| 1. Strain gage debonded | 5. Pre-cracked matrix |
| 2. High volume fraction of fibers | 6. Pulled out of tabs |
| 3. Poor fiber alignment | |
| 4. High porosity | |

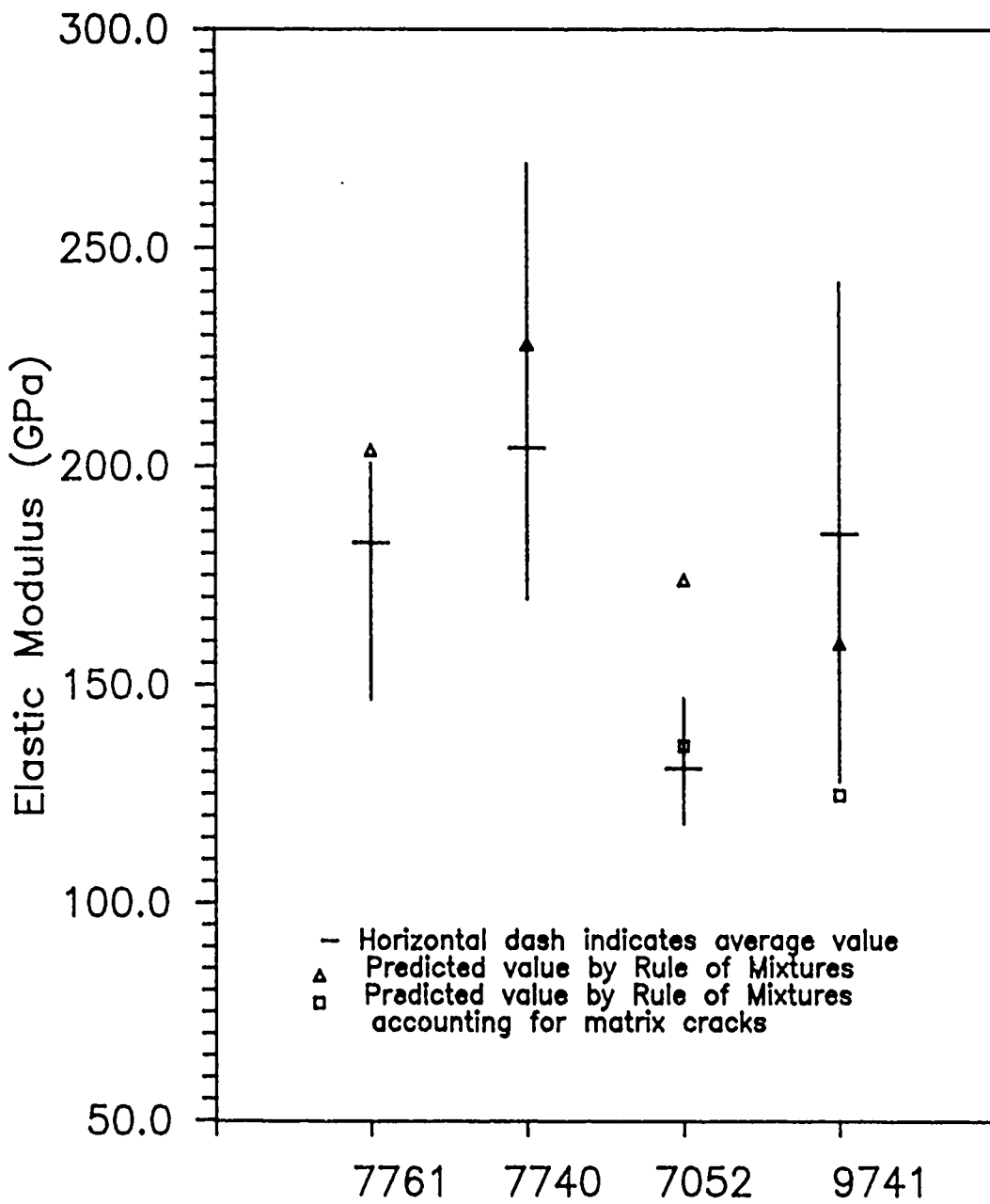


Figure 12. Elastic Modulus Values for Glass/AVCO Composites

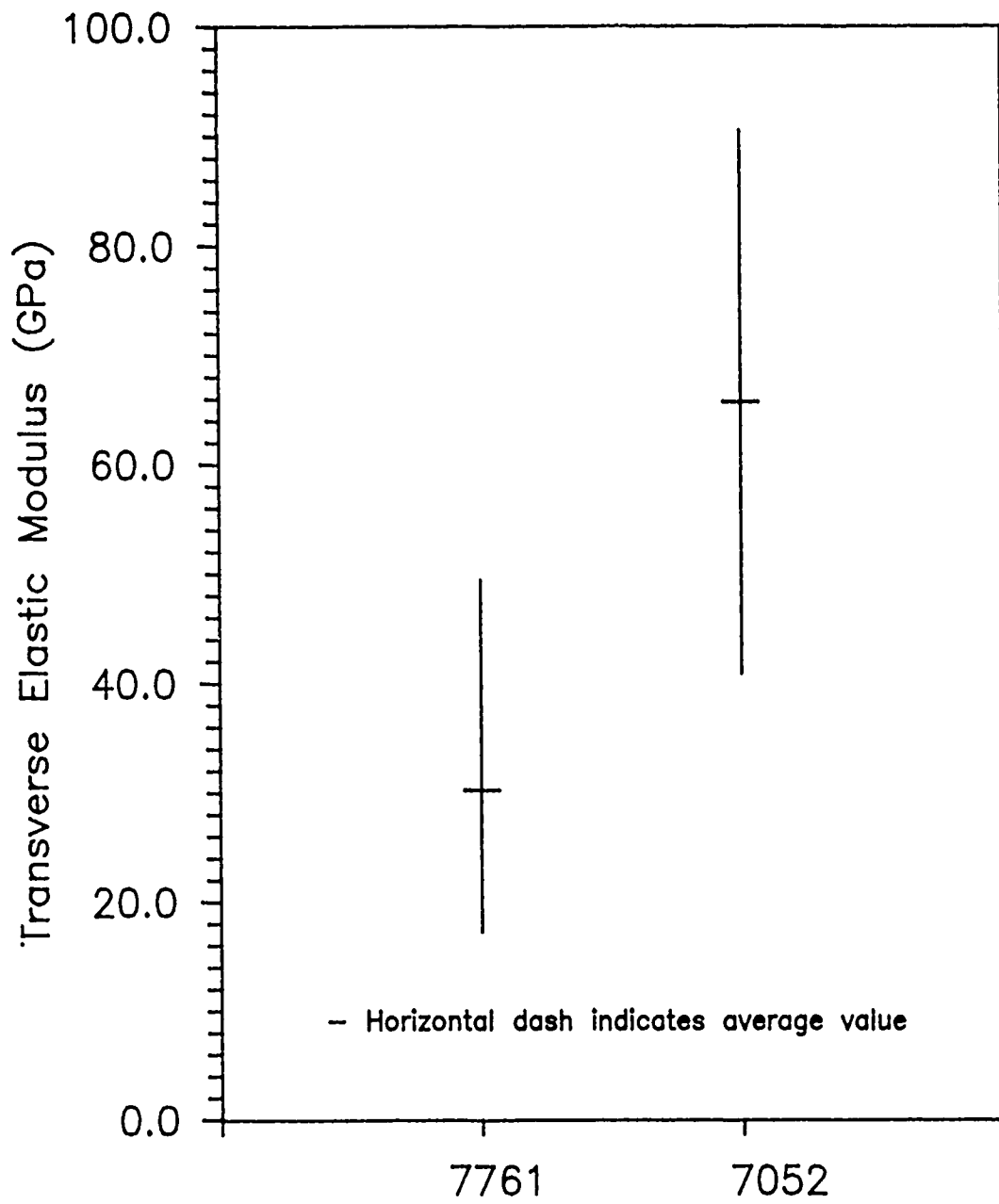


Figure 13. Transverse Elastic Modulus Values for Glass/AVCO Composites

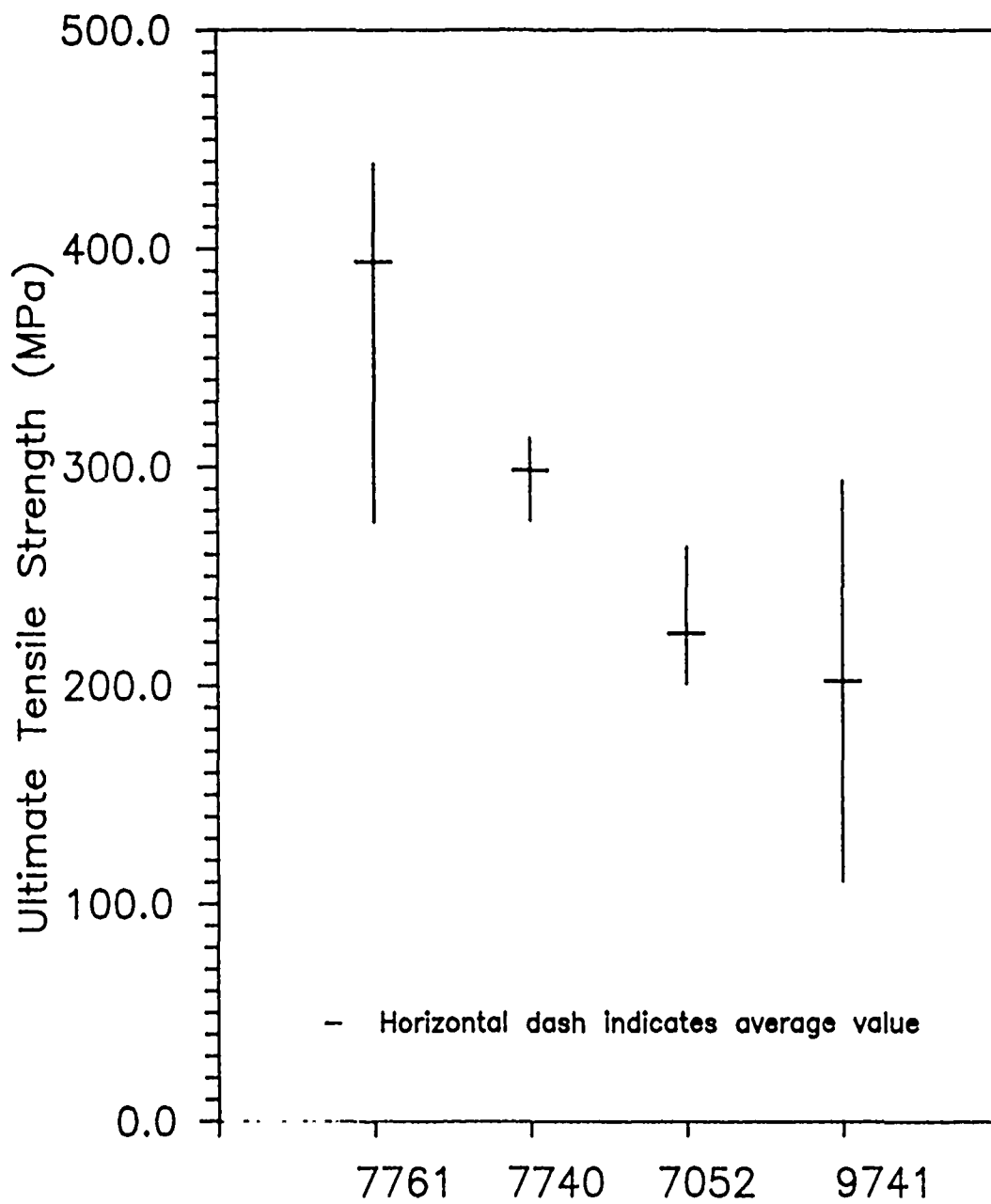


Figure 14. Ultimate Strength Values for Glass/AVCO Composites

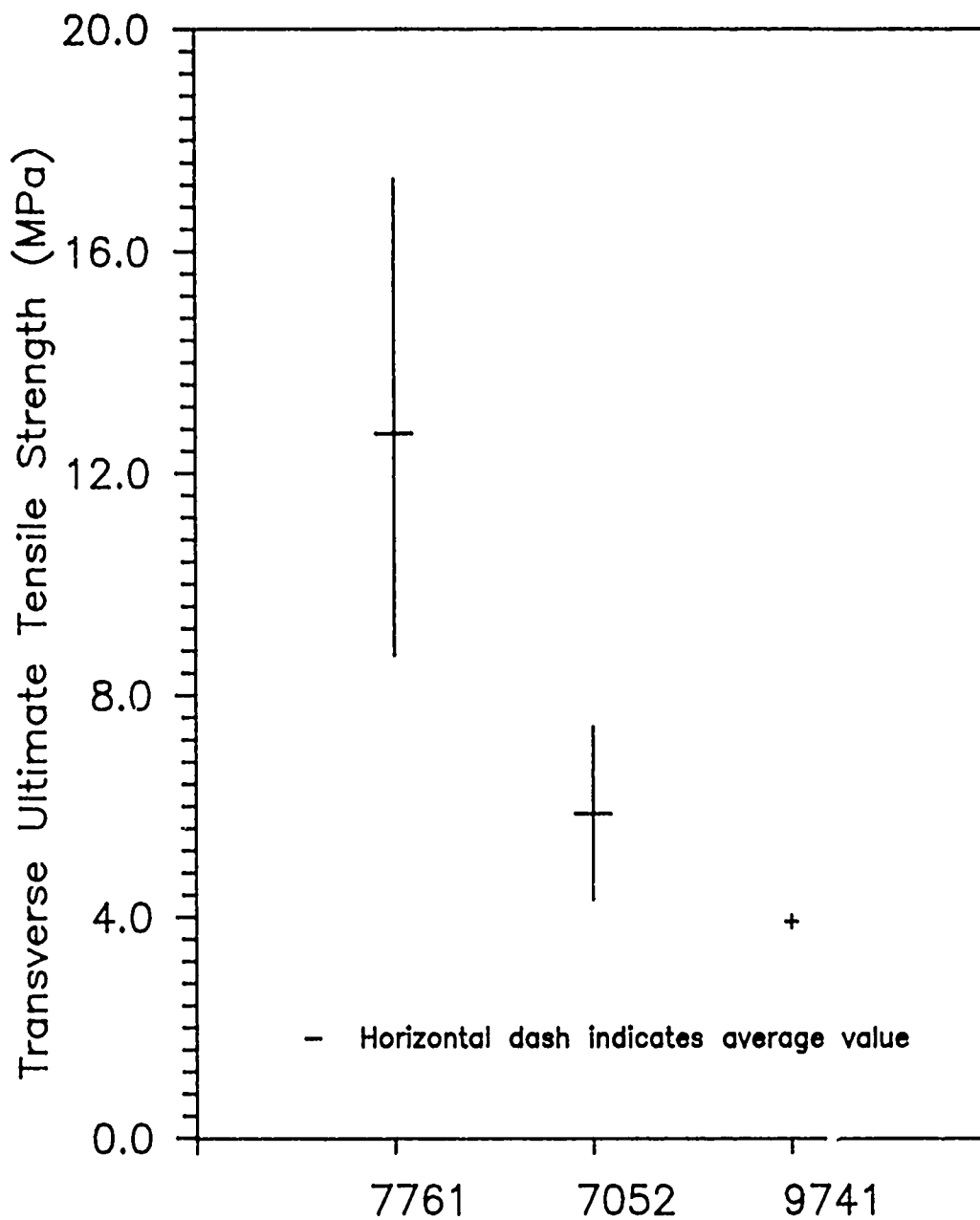


Figure 15. Transverse Ultimate Strength Values for Glass/AVCO Composites

Table VI. Average Mechanical Properties

| <u>Glass</u> | <u>E(GPa)</u> | <u>UTS(MPa)</u> | <u>Trans. E(GPa)</u> | <u>Trans. UTS(MPa)</u> |
|--------------|---------------|-----------------|----------------------|------------------------|
| 7761 | 182.9 | 394.0 | 36.6 | 12.7 |
| 7740* | 171.5 | 293.0 | - | - |
| 7052 | 130.6 | 223.3 | 65.6 | 5.8 |
| 9741** | 155.7 | 293.3 | - | 3.9 |

* Sample 32B was excluded in calculations

** Sample 42B was excluded in calculations

Table VII. Comparison of Composite Elastic Moduli

| | <u>7761</u> | <u>7740</u> | <u>7052</u> | <u>9741</u> |
|--|-------------|-------------|--------------------|--------------------|
| Predicted E_c by Rule of Mixtures (GPa) | 203.6 | 227.9 | 173.7 | 159.2 |
| | | | 135.7 ¹ | 124.5 ¹ |
| Average E_c from MTS Tests (GPa) | 182.9 | 171.5 | 130.6 | 155.7 |

¹Based on calculation which included matrix cracks-see text

composites. The rule of mixtures predicts the elastic modulus of the composite (E_c) to be 203.6 GPa for the 7761/AVCO system ($V_f = .4$). From Table VII, the average E_c is 182.9 GPa for this system. In the case of the 7740/AVCO composite, the predicted E_c is 227.9 GPa ($V_f = .469$) while the measured E_c is 171.5 GPa. The samples tested from the 7052 and 9741 glasses were already cracked transversely during processing due to the CTE mismatch between the fiber and matrix. Therefore the predicted E_c was calculated for two cases for these systems. First it was assumed that the matrix was free of any cracks and the rule of mixtures was applied normally to determine E_c . In the second case the cracks were considered for the calculation of E_c . To account for these cracks, the contribution of the matrix to the composite strength can be neglected in the rule of mixtures or $E_c = E_f V_f$. In the 7052/AVCO system, the average measured E_c of 130.6 GPa was very close to the value predicted by the rule of mixtures which accounted for the matrix cracking (135.7 GPa). For the 9741/AVCO system, the opposite was true. The average measured value of E_c was 155.7 GPa which was very close to the rule of mixtures prediction that assumed no matrix cracking existed (159.2 GPa). The 7052/AVCO composite had more closely spaced matrix cracks than the 9741/AVCO system and overall was more extensively cracked prior to testing. This may explain why the 7052/AVCO system measured values of E_c were

closer to the composite modulus predicted by the rule of mixtures that accounted for the matrix cracks or $E_c = E_f V_f$. Figure 12 also shows the composite modulus predicted by the rule of mixtures compared to the experimental values.

Looking again at Table VI, the tensile strength in the transverse direction of these unidirectional composites is much less than the longitudinal tensile strength. The samples proved very fragile in the transverse direction and could be broken simply by rough handling.

From the load-displacement curves produced by the MTS testing, apparent stress-strain curves were calculated using the initial cross-sectional area of the samples. Two examples of the stress-strain curves are shown in Figures 16 and 17. The curves for the other samples tested are shown in the Appendix in Figures 46 thru 52. An interesting aspect noted in the curve for the 7761/AVCO longitudinal specimen (Figure 16) is the reversal of transverse strain. This phenomena was first reported by Kim and Katz (9) in their study of failure processes of fiber reinforced ceramic matrix composites. In the stress-strain curves obtained from the tensile tests, both the axial and transverse stress-strain curves exhibit a proportional limit. The transverse stress-strain curve became nonlinear at .013 percent strain as indicated by Point A on Figure 16. The axial curve became nonlinear at .072 percent strain as shown by Point B in Figure 16.

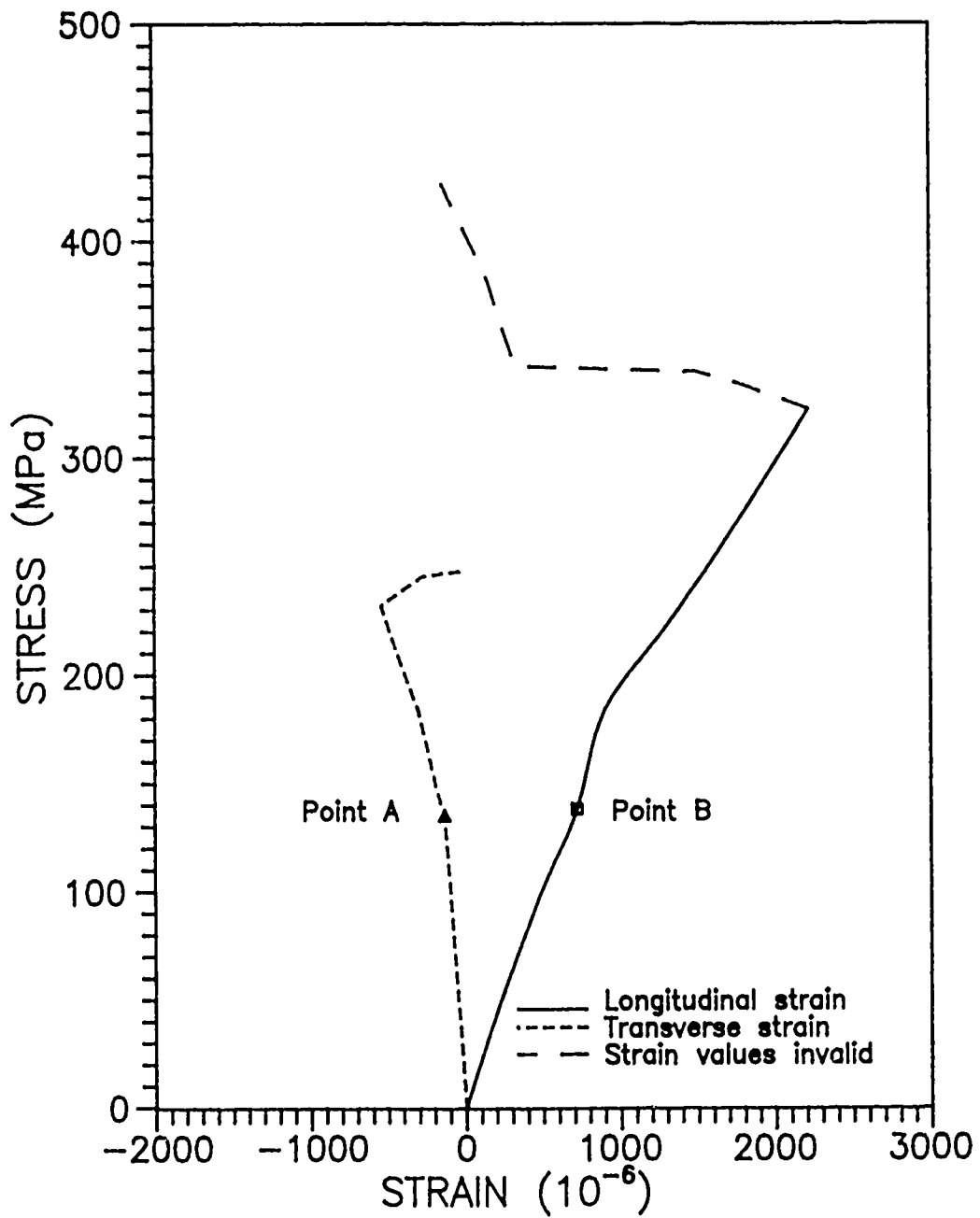


Figure 16. Stress-Strain Curve for AVCO/7761
Sample 28-Z

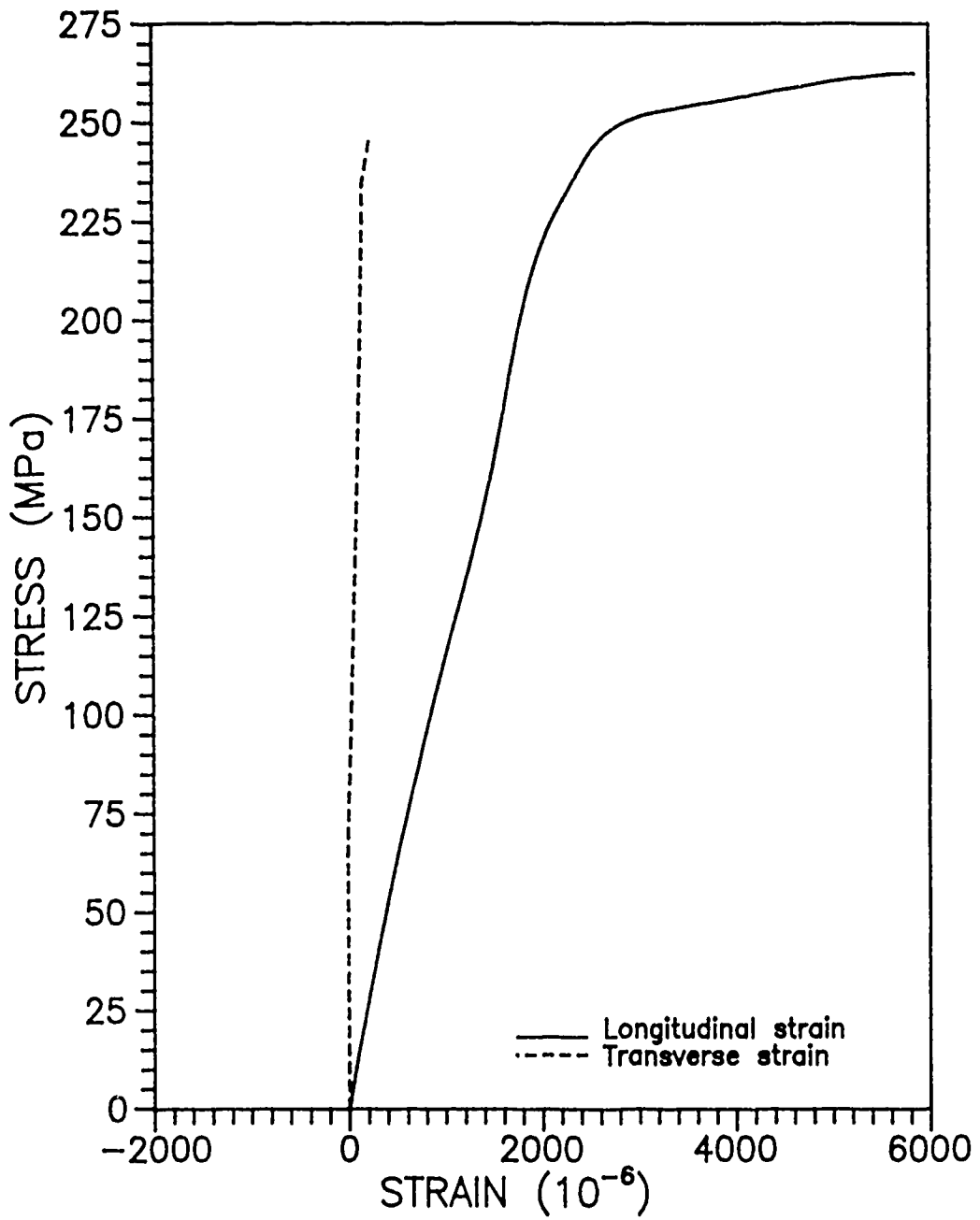


Figure 17. Stress-Strain Curve for AVCO/7052
Sample 39-B

Beyond their respective proportional limit, the curves behave nonlinearly. In this nonlinear region, the axial or longitudinal strain continues to increase while the transverse strain decreases. The transverse strain actually changes its direction. Physically this means that the composite stops contracting in the lateral direction and begins expanding. This transverse strain reversal is not well understood, but is believed to be caused by the formation of axial matrix cracks and to fiber-matrix debonding (9:1). Another observation during these tensile tests is that transverse matrix cracks appeared on the surface of some of the longitudinal specimens well before the onset of nonlinearity in the stress-strain curves. This was determined by noting the strain at which the first crack appeared on the sample surface and comparing this to the strain at which the stress-strain curve became nonlinear. For example, during the test of Sample 28-Z, a 7761/AVCO system sample, matrix cracking was observed at an axial strain of .05 percent while the onset of nonlinearity occurred at .072 percent strain (Point B on Figure 16). The number of cracks increased with increasing stress and are assumed to be partially responsible for the nonlinearity of the stress-strain curve. But because some cracks did appear before the proportional limit, it can be said that the onset of nonlinearity in the stress-strain curve is not a reliable indication of the initiation of

matrix cracking in this composite system. This assumption that the initiation of matrix cracking causes the stress-strain curve to become nonlinear is prevalent in literature (1,3). As discussed earlier concerning the 7052/AVCO system, the assumption that the pre-cracked matrix does not contribute to the composite strength is also supported by the transverse strain curves of these samples shown in Figure 17 and Figure 50 of the Appendix. The transverse strains for these samples were very small and did not exhibit the linear decrease or reversal as the 7761/AVCO samples did. A possible explanation for this behavior is that the cracked matrix is simply attached to the fibers in segments and not supporting any stress. Hence the matrix does not strain in the lateral direction.

B. Damage Formation and Progression

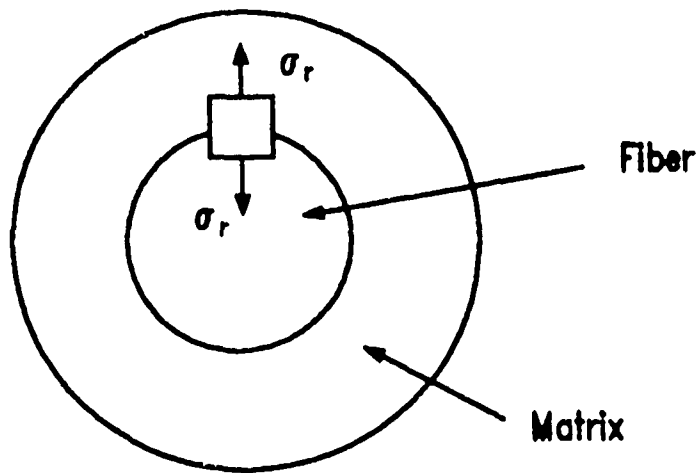
Case I: Corning 7761 Glass with AVCO SCS-6 Fibers

In this composite system, the coefficient of thermal expansion of the fiber ($\alpha_f = 3.6 \times 10^{-6}/^{\circ}\text{C}$) is greater than that of the 7761 glass ($\alpha_m = 2.6 \times 10^{-6}/^{\circ}\text{C}$). Because of this CTE mismatch, the resultant residual stresses are as follows:

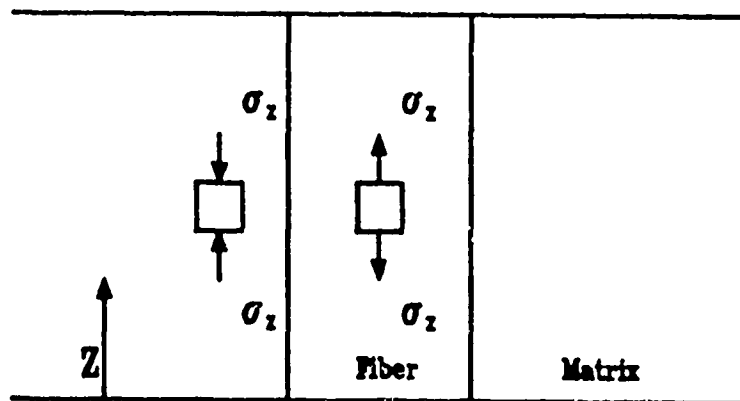
1. Along the radial direction, the stresses on the fiber-matrix interface are of tensile nature, as shown in Figure

18a. This stress if strong enough may result in the fiber and matrix debonding at the interface.

2. In the axial direction, the fibers will place the matrix in compression while the fibers themselves are in tension (Figure 18b). This matrix pre-stressing will increase the overall strain required to initiate failure and thus increase the overall strength of the composite. However this pre-stressing assumes the fiber and matrix are strongly bonded. If the interface cannot support the induced stresses, little or no matrix pre-stressing will occur (6:954). To obtain quantitative values for these stresses, the NDSANDS model developed by Pagano and Tandon (16) was used. This model assumes the fiber and matrix to be linearly elastic, homogeneous, and perfectly bonded. The predicted state of stress at the fiber-matrix interface for the composite systems tested is presented in Table IX and will be discussed later in this chapter. For the AVCO/7761 system, three samples were tested on the straining stage. The first sample tested exhibited matrix cracking at strains of .08 percent as shown in Figures 19a and 19b. In these figures, the gray area is the glass matrix and the white bands are fibers. In Figure 19a, the fibers are below the glass and appear as light colored horizontal bars. In Figure 19b two fibers are seen at the surface of the sample. In both figures the cracks run transversely across the sample width and appear as dark



a. Radial stresses at fiber-matrix interface (tension-tension)



b. Axial stresses at fiber-matrix interface (matrix in compression, fibers in tension)

Figure 18. Stresses at fiber-matrix interface
7761/AVCO system



a. (100X)



b. (50X)

Figure 19. Matrix cracking in 7761/AVCO composite at .08 percent strain

vertical lines. The first cracks in the fibers were noted at a strain of .14 percent as seen in Figure 20. In this figure a great deal of matrix cracking is present along with the crack in the center fiber at the surface. Both fiber and matrix cracking were random in this sample. The next two samples behaved somewhat differently in that both matrix and fiber cracks appeared at approximately .05 percent strain as seen in Figures 21 and 22. These figures show cracks in both the fiber and matrix that appeared simultaneously. Again the formation of cracks appeared randomly. Both fiber and matrix cracking continued as the stress was increased. Some debonding at the fiber-matrix interface was observed in these samples at approximately .14 percent strain as shown in Figure 23. The dark ragged areas along the fibers are the regions where the fiber and matrix are debonded. In one sample of the 7761/AVCO system, several fiber cores pulled out of the fiber at a strain value of .13 percent. Figure 24a shows two broken AVCO fibers in which the carbon core has pulled out. The dark thin protrusions from the fiber ends are the pulled out carbon cores. Figure 24b shows the area surrounding the two fibers seen in Figure 24a. At high stress levels (corresponding to strains of .15 percent) extensive matrix shattering was exhibited which can be seen in Figures 25a and 25b. At high stresses the matrix in the samples made

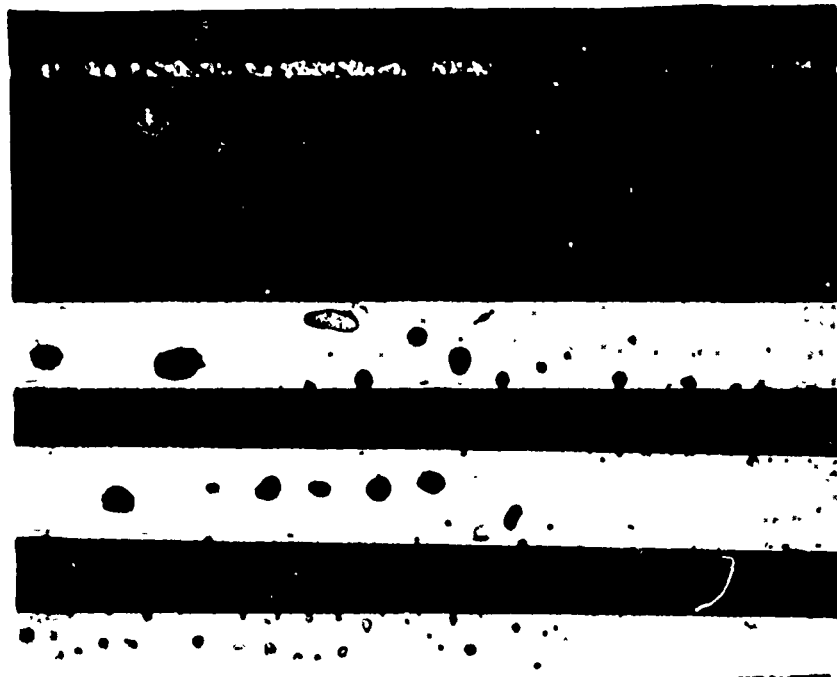


Figure 20. Fiber cracks in 7761/AVCO composite at .14 percent strain (100X)



Figure 21. Fiber and matrix cracks in 7761/AVCO composite at .04 percent strain (100X)



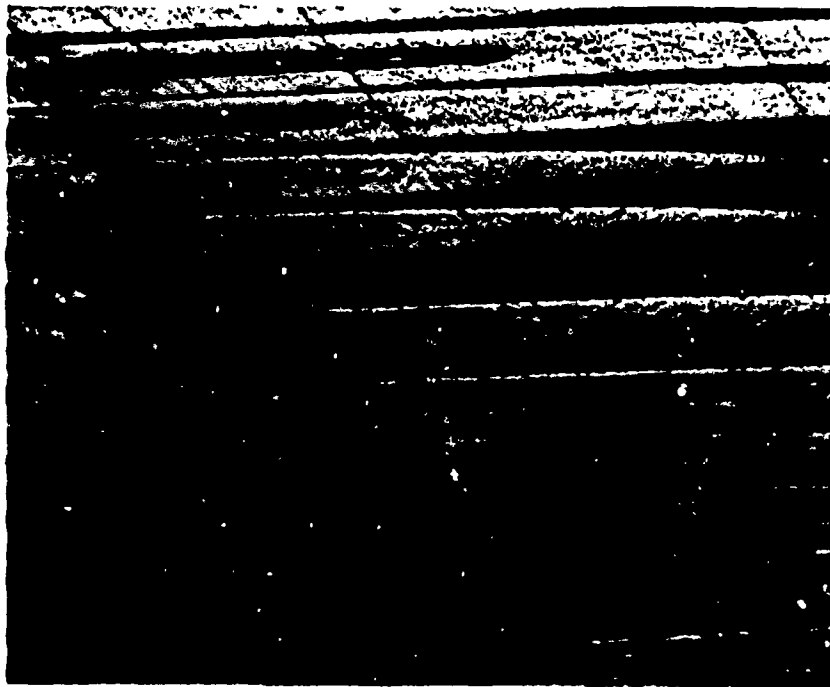
Figure 22. Fiber and matrix cracks in 7761/AVCO composite at .05 percent strain (100X)



Figure 23. Fiber-matrix debonding in 7761/AVCO composite at .13 percent strain



a. (200X)



b. (50X)

Figure 24. Fiber core pullout in 7761/AVCO composite at .13 percent strain



a. 7761/AVCO sample at .16 percent strain



b. 7761/AVCO sample at .15 percent strain

Figure 25. Extensive matrix shattering in 7761/AVCO composite samples prior to failure

from 7761 glass became heavily cracked and literally fell off of the fibers.

One particular puzzling aspect of the tests on this system was the premature cracking of fibers on the surface of the samples. The AVCO SCS-6 fiber has a tensile strength of 3450 MPa and an elastic modulus of 415 GPa. This corresponds to a failure strain of approximately .83 percent while fibers in the straining stage were cracking at strains as low as .05 percent. One possible explanation of this occurrence is that during the polishing of the samples the surface fibers are being damaged. Stress concentrations and defects are being formed on the fiber coatings and core reducing the strength of the fibers. AVCO has reported that the uncoated fibers are half as strong as those with coatings (17:5). An argument against this rationale is that the composites tested in tension on the MTS machine failed at a much lower stress than that of the fibers, indicating that fibers throughout the sample may be cracking prematurely as well (Table VI). One other explanation to explain the fiber cracks at low stresses is that there may be partial debonding between the fibers and matrix. Several factors are in support of this :

1. As discussed earlier in this section, the CTE mismatch of the 7761/AVCO system ($\alpha_f > \alpha_m$) causes a residual tensile stress at the fiber-matrix interface. If these stresses

are strong enough, debonding may occur even before any load is applied.

2. Scanning electron microscope (SEM) microphotography indicates possible partial debonding of fiber and matrix in a sample of the 7761/AVCO composite. Figure 26a shows a transverse slice of a 7761/AVCO sample in a scanning electron microscope at 500X. The large circular areas are the fibers and the carbon core and the outer carbon coatings can be clearly seen. The area between the fibers is the matrix. The sample had not undergone any loading prior to being examined with the SEM. Figure 26b is the same area of the sample seen in Figure 26a at a magnification of 5000X. The thick black band and the lighter colored band adjacent to it in the left third of the photograph are the carbon and the silicon carbide coatings on the outer diameter of the fiber. The thin dark strip in the center of the photo dividing the fiber and the matrix appears to be a gap or void. This gap may be the result of debonding between the fiber and matrix in the composite.

3. The measured longitudinal modulus of the composites from MTS testing is lower than that predicted by the rule of mixtures. The average longitudinal modulus measured for the 7761/AVCO system was 182.3 GPa (see Table VI) while the predicted modulus from the rule of mixtures is 203.6 GPa. This lower modulus may be a result of debonding between the



a. (500X)



b. (5000X)

Figure 26. SEM photos of fiber-matrix interface in 7761/AVCO composite after fabrication

fibers and matrix. The load is not transferred through the matrix to the fibers, hence less stress can be carried by the system and the resulting composite modulus is lower.

4. The NDSANDS model predicts the effective elastic properties of the composite system assuming the fiber and matrix are perfectly bonded. However by replacing the fibers in the matrix with cylindrical holes, the properties for the composite are calculated as if the fiber and matrix are completely debonded. By using this approach, NDSANDS predicts the transverse modulus E_2 as 131 GPa for the perfectly bonded fiber and matrix and 23.8 GPa for the unbonded case. From MTS tensile tests on 7781/AVCO transverse samples, the average value of E_2 is 36.6 GPa as shown in Table VI. This experimental value falls between the transverse moduli for the cases of the perfectly bonded fiber and the unbonded fiber, indicating possible partial debonding between fiber and matrix. Although the factors listed here seem to support the idea of partial debonding between the fiber and matrix, it cannot be concluded that in fact debonding is taking place. Each observation discussed may be caused by reasons unrelated to debonding. At this point neither the explanation that the surface fibers are weakened by polishing nor the case for debonding offers a satisfactory answer to the question concerning premature surface fiber cracks. The occurrence of fiber cracks at low stresses in the 7781/AVCO composites needs

further study to determine the actual cause. One strategy that should be pursued is determining whether the fibers throughout the sample thickness are cracking prematurely along with those at the surface.

In summary, for the 7761/AVCO system (where $\alpha_f > \alpha_m$) the straining fixture tests resulted in random fiber and matrix cracking. The fiber cracks appeared at strains well below the strain to failure of the fiber. At high stresses the matrix cracked extensively and broke away from the fibers. Figure 27 is a schematic view of a 7761/AVCO sample after testing showing the randomness of fiber and matrix cracks at a strain of .14 percent in the 7761/AVCO composite system.

Case II: Corning 7052 Glass with AVCO SCS-6 Fibers
Corning 9741 Glass with AVCO SCS-6 Fibers

The thermal expansion coefficient of these two glasses is greater than that of the AVCO SCS-6 fiber. Composites were fabricated using two different glasses for this case. Samples made from the 7052 glass had matrix cracks from the high residual stresses resulting from the large CTE mismatch between the fiber and matrix. To try and prevent these cracks, a glass (9741) was tried with a CTE closer to that of the fiber to reduce the CTE mismatch and hence reduce the residual stress in the system.

First to be discussed is the 7052/AVCO system where the CTE of the 7052 glass is $5.2 \times 10^{-6}/^{\circ}\text{C}$ compared to the

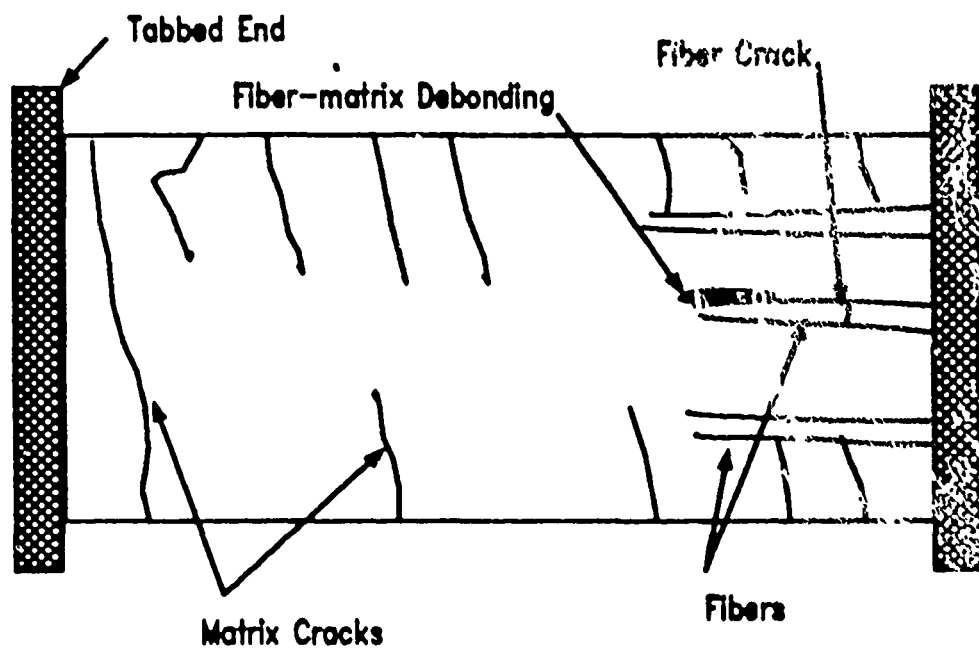
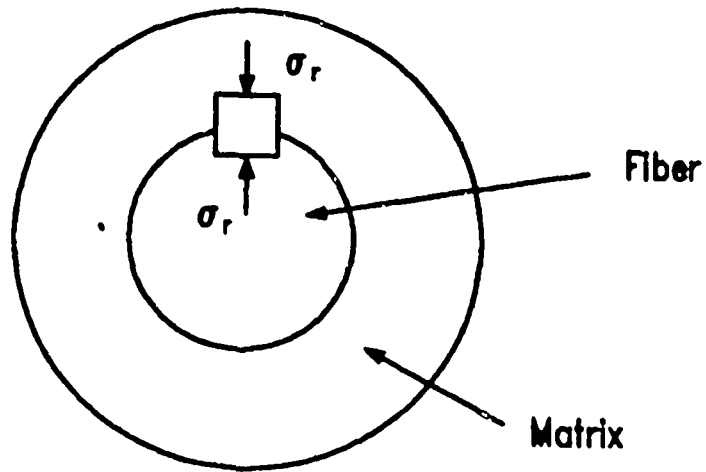


Figure 27. Schematic diagram of damage in 7761/AVCO sample at .14 percent strain

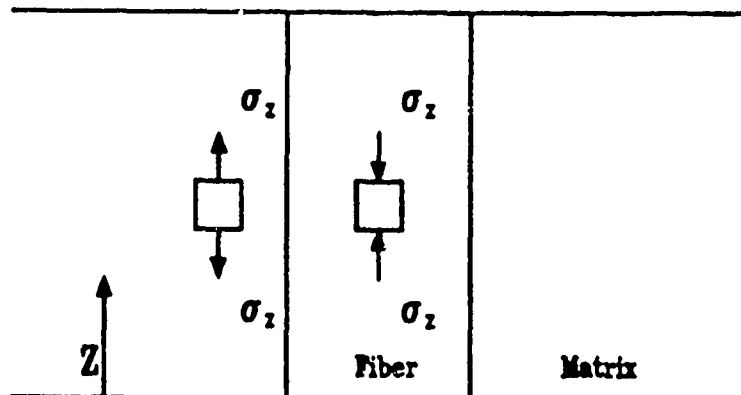
$3.6 \times 10^{-6}/^{\circ}\text{C}$ CTE of the fiber ($\alpha_m > \alpha_f$) The resultant residual stresses are:

1. Along the radial direction, the fiber-matrix interface is in compression, increasing the frictional fiber-matrix bond (Figure 28a).

2. Along the axial direction, the fibers will place the matrix in tension (Figure 28b). If the differential in CTE is large enough, the failure strain of the matrix may be exceeded and a network of microcracks may develop perpendicular to the fiber axis (6:954). As mentioned previously in the discussion of residual stress, when $\alpha_m > \alpha_f$, the matrix is in tension while the fibers are in compression. When the CTE mismatch is great enough, the residual tensile stress placed on the matrix may exceed the strength of the matrix. This proved to be the case for the 7052/AVCO system. All samples fabricated from this system exhibited uniformly spaced matrix cracking transverse to the fiber direction after processing. Figure 28 shows a schematic of the cracks in a 2 inch (5.1 cm) square plate. Two samples of the 7052/AVCO composite with the matrix cracking are shown in Figures 30a and 30b. To ensure the cracks were not a result of processing, the temperature and ram pressure applied during hot pressing were varied. Additionally, the samples were annealed to relieve any residual stresses. The cracks remained in all fabricated samples indicating the cracks were indeed a result of CTE



a. Radial stresses at fiber-matrix interface (compression, compression)



b. Axial stresses at fiber-matrix interface (matrix in tension, fiber in compression)

Figure 28. Stresses at fiber-matrix interface for 7052/AVCO and 9741/AVCO systems

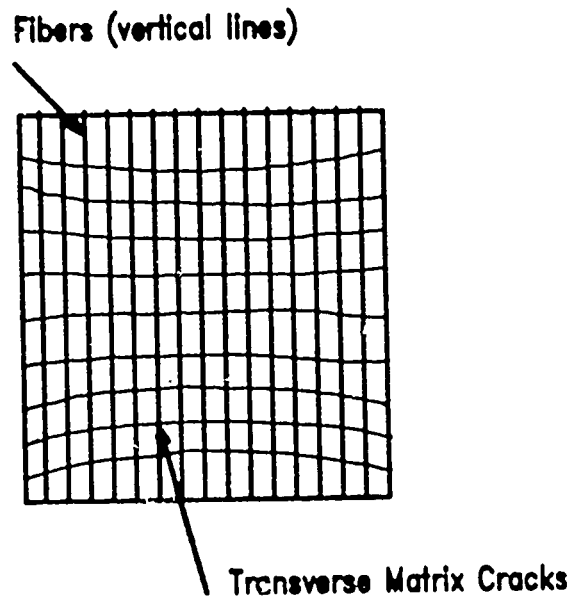
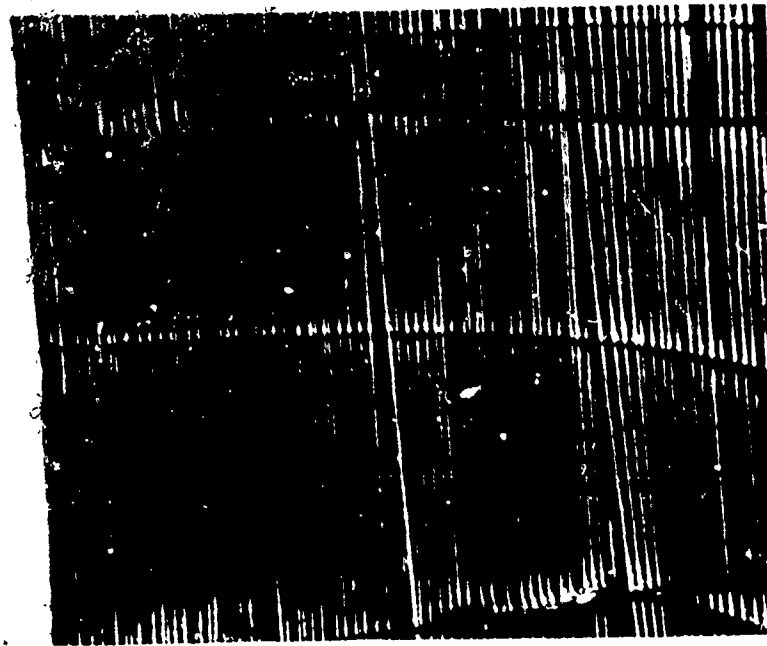
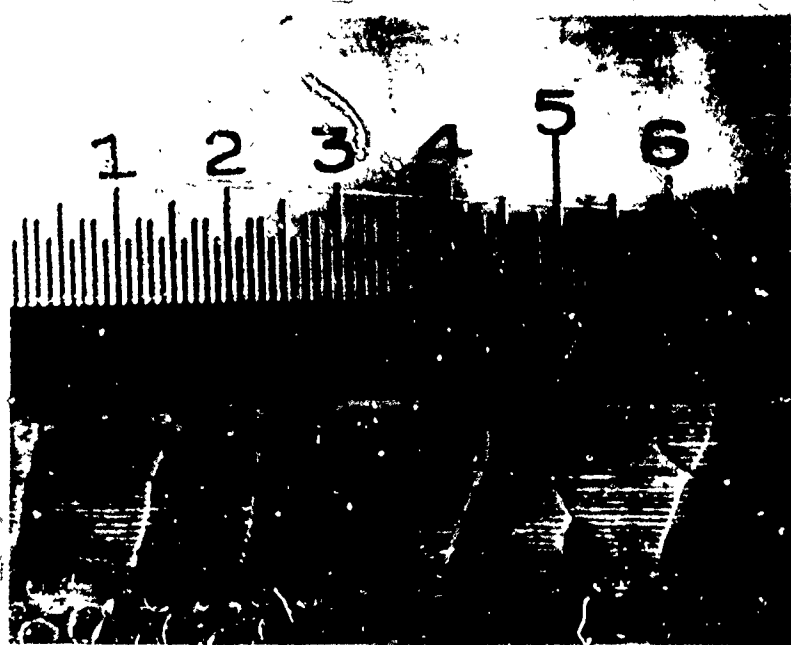


Figure 29. Matrix cracks in a 7052/AVCO composite plate after fabrication

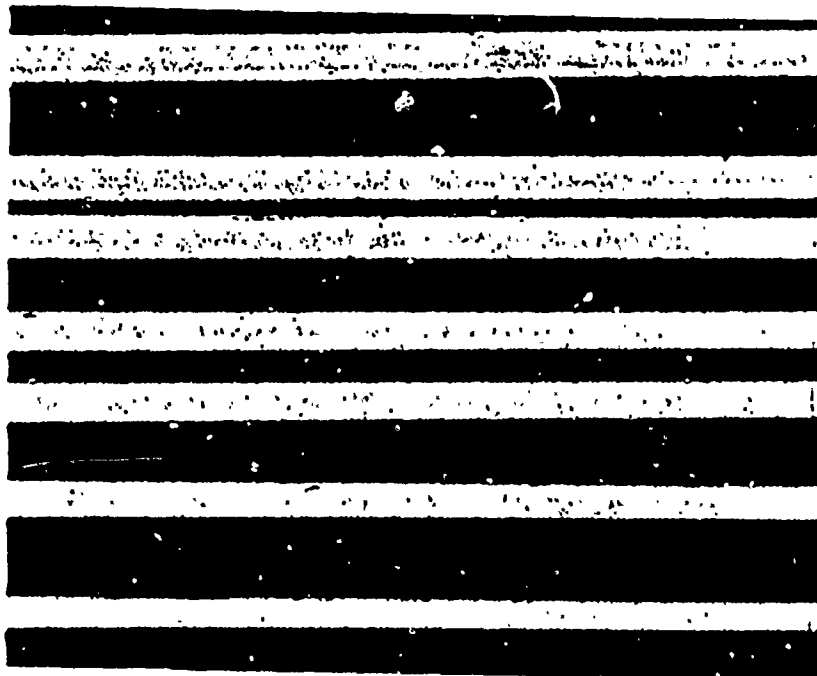


a. Matrix cracks in 7052/AVCO composite plate after processing



b. Edge of 7052/AVCO composite plate with matrix cracks

Figure 30. Matrix cracking in 7052/AVCO composite from CTE mismatch in fiber and matrix

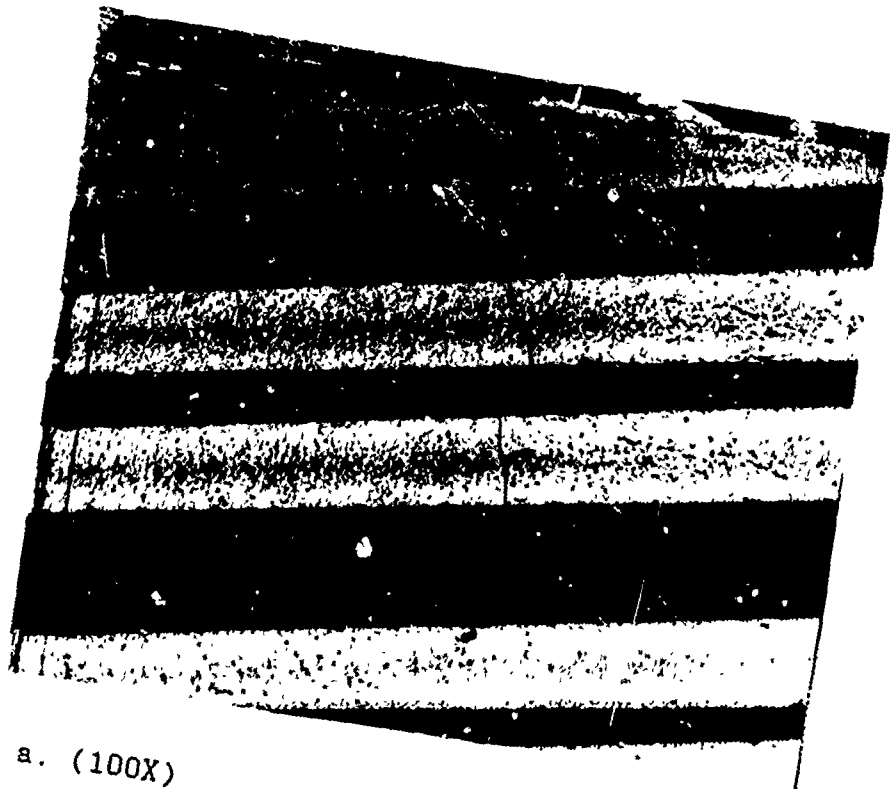


a. (50X)

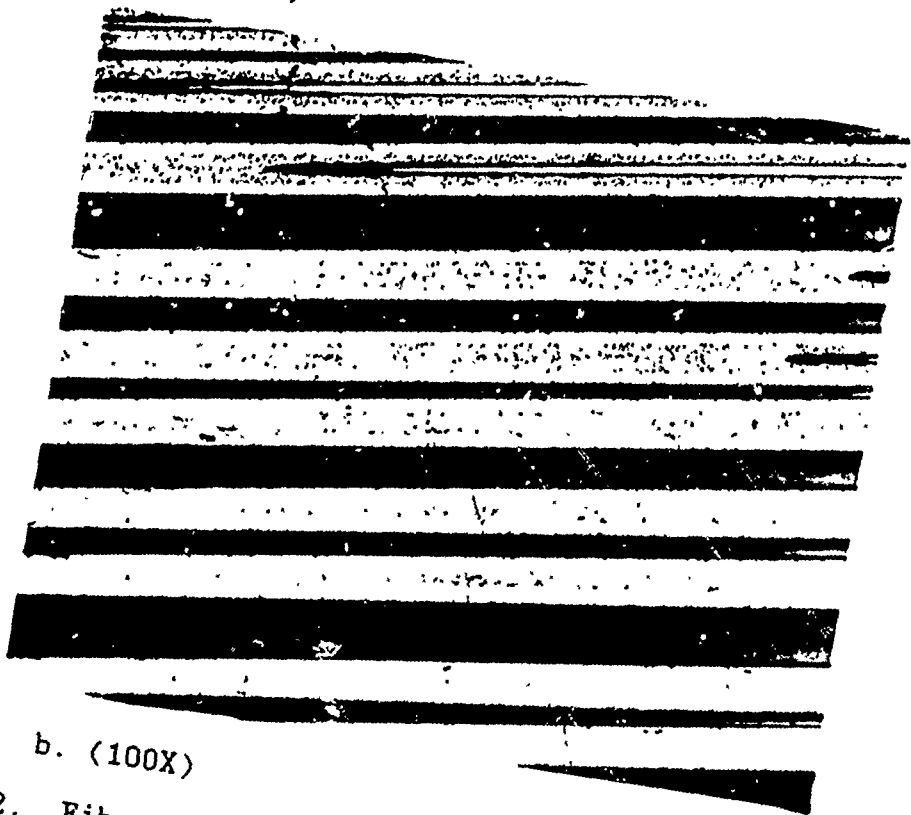


b. (50X)

Figure 31. Multiple matrix cracking in 7052/AVCO samples prior to testing



a. (100X)



b. (100X)

Figure 32. Fiber cracks close to existing matrix cracks in 7052/AVCO composite at .06 percent strain

compressive stress field at the fiber-matrix interface is most likely responsible for the lack of debonding and excellent matrix integrity.

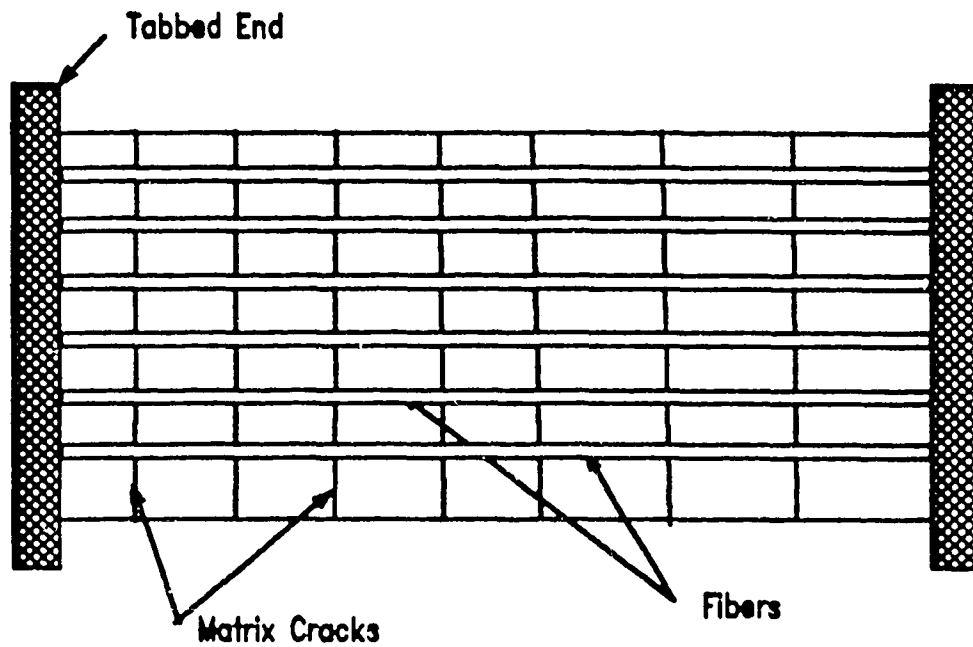
Because of matrix cracking in the 7052/AVCO composites due to the thermal expansion mismatch, two samples using CGW 9741 glass were also fabricated. The 9741 glass has a CTE of $4.9 \times 10^{-6}/^{\circ}\text{C}$ which is still greater than the fiber CTE but the overall mismatch is not as large as that in the 7052/AVCO system. It was hoped that the smaller CTE mismatch between fiber and matrix would prevent the matrix pre-cracking. Unfortunately, the cracks again were present in the samples using 9741 glass. The crack spacing in these samples was slightly greater than the spacing in the 7052/AVCO samples because of the smaller CTE mismatch. One sample of the 9741/AVCO system was tested on the straining stage. However it failed prematurely due to a large previously undetected crack between fiber layers in the sample.

In summary, for the 7052/AVCO and 9741/AVCO composites, the large CTE mismatch between the fiber and matrix caused high tensile stresses in the axial direction resulting in transverse cracks in the matrix during fabrication. The pre-cracked samples were still tested and the existing cracks opened further under tensile loading. At strains of .08 percent fiber cracks appeared near the matrix cracks. Extensive matrix cracking did not occur at

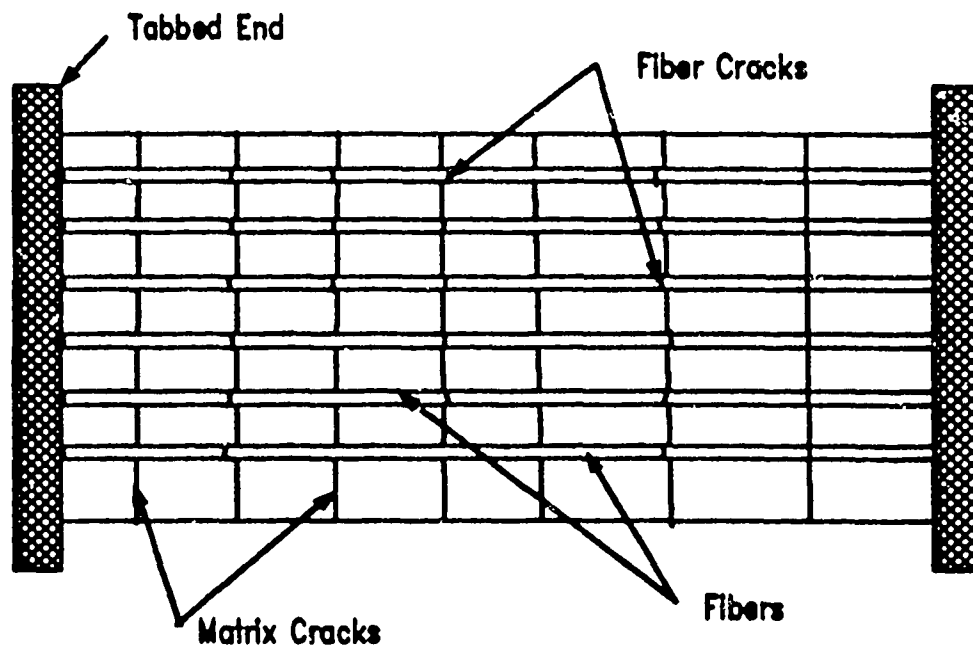
high stresses and the matrix remained intact throughout the testing. Figure 33a illustrates the matrix cracking in a sample prior to testing while 33b shows the formation of fiber cracks that occurred at strains near .06 percent.

Case III: Corning 7740 Glass with AVCO SCS-6 Fibers

The reported coefficient of thermal expansion of the 7740 glass is $3.7 \times 10^{-6}/^{\circ}\text{C}$ which is very close to that of the AVCO SCS-6 fiber. Theoretically no residual state of stress would exist at the fiber-matrix interface due to CTE mismatch. The fabrication of samples using 7740 glass proved difficult. The combination of high temperatures required for hot pressing ($1125-1175^{\circ}\text{C}$) and high pressures to reduce the formation of residual bubbles caused excessive glass leakage from the die. The heavy glass leakage produced samples with high volume fraction of fibers ($V_f \approx .5$). Also the high temperatures decreased the viscosity of the glass allowing the fibers to move more freely. Hence several samples had poor fiber alignment. All of the 7740/AVCO samples fabricated exhibited either poor fiber alignment, high porosity and bubble content, high volume fraction of fibers, or a combination of the three. One 7740/AVCO sample was tested on the straining stage. The sample had a volume fraction of fibers of .469. During testing, the onset of matrix cracking appeared approximately at .08 percent strain (Figure 34). A fiber



a. Evenly spaced matrix cracks in sample prior to testing



b. Fiber and matrix cracks at .06 percent strain

Figure 33. 7052/AVCO Sample before and after testing



Figure 34. Multiple matrix cracking in 7740/AVCO composite at .08 percent strain (50X)



Figure 35. Fiber crack in 7740/AVCO composite at .06 percent strain (100X)

crack was first observed at .06 percent strain and is shown in Figure 35. The test was not completed because the matrix under the strain gage cracked extensively so that no valid strain readings could be obtained (Figure 36). Further, extensive matrix cracking was observed at a stress of 142 MPa. No further tests were accomplished using the 7740/AVCO samples because the remaining samples all had defects as discussed earlier. Because of the poor success in fabricating suitable samples for testing using the 7740 glass, no additional samples were fabricated.

As a summary, the results from the straining fixture tests for each system will be briefly discussed here. The 7761/AVCO composite, in which the CTE of the fiber is greater than the matrix, has radial tensile stress at the fiber-matrix interface. Under tensile loading, random fiber and matrix cracking appeared. In some cases debonding at the fiber-matrix interface was present as well as fiber-core pullout. Fibers at the surface of the composite cracked at low strain values compared to the failure strain of the fiber. Possible explanations for this include degradation of the fibers from polishing and partial debonding between the fiber and matrix. At high stresses, the matrix in the samples shattered extensively and fell away from the fibers. The 7052/AVCO and 9741/AVCO systems both have radial compressive stresses at the fiber-matrix interface resulting from the CTE mismatch between



Figure 36. Extensive matrix cracking under strain gage in a 7740/AVCO composite sample

fiber and matrix. The glasses both have CTE's higher than the AVCO fiber. The high residual stresses at the fiber-matrix interface in these two systems caused transverse cracking in the matrix prior to any loading. Samples were fabricated using the 9741 glass which has a CTE closer to the fiber than the 7052 glass to reduce the high residual stresses and prevent the matrix cracking. However, the reduction in residual stress was not sufficient and cracks were, still, present in the 9741/AVCO system. Samples of both these systems were tested on the straining fixture. The pre-existing cracks opened under tensile loading and at strains near .06 percent fiber cracks appeared near the matrix cracks. The matrix did not crack extensively or debond from the fibers even at high stresses. In the 7740/AVCO system the fiber and matrix CTE's are very close and should have little residual stresses at the fiber-matrix interface. For this system, the samples fabricated exhibited high porosity, poor fiber alignment, and high volume fraction of fibers. The problems with fabrication in this system resulted in few samples suitable for testing. One sample was tested on the straining fixture but the results were inconclusive because the strain gage debonded from the sample. Overall it appears the residual stress state at the fiber-matrix interface greatly affects the composite's behavior under tensile loading. Radial tensile stresses as in the 7761/AVCO system result in heavy

matrix cracking and debonding at the fiber-matrix interface. The 7052/AVCO and 9741/AVCO systems with radial compressive stress at the fiber-matrix interface showed excellent matrix integrity under tensile loading. However the axial tensile stresses along the fiber-matrix interface caused transverse cracks throughout the matrix.

C. Theoretical Models

As a result of the increasing interest in fiber reinforced ceramic composites, much work has been done to develop models to predict the strengths of these composites. Several of the models in existence were discussed in Chapter II. These models generally predict the matrix cracking stress and residual stresses at the fiber-matrix interface. A comparison of the predicted stresses and those determined experimentally will help in the determination of the accuracy of the models. Before the designer can safely use such models as tools in design, the limitations of the models must be known. Thus empirical results are needed to further refine and validate the theoretical models.

Table VIII shows the predicted interfacial shear stresses using the model developed by Aveston, Cooper, and Kelly (2) based on the average crack spacing in the matrix (equation 6). The crack spacing was measured from samples

tested under tensile loading in the straining stage over the gage length. The experimental interfacial shear strengths were determined by fiber pullout tests conducted by Kerans and Jurewicz (8). The pullout tests were conducted on single AVCO fibers imbedded in the glasses (CGW 7761, 7740, 7052, and 9741). The samples were hot pressed in graphite dies under similar conditions to those used in fabrication of the composites for this work. The experimentally determined interfacial shear stresses agree fairly closely with the predicted values as shown in Table VIII. Some of the difference between the predicted and experimental values can also be attributed to the nature of the single fiber pullout test. It can be shown that the shear stress for a single fiber embedded in glass is higher than that for fibers in a composite. Hence the shear stress in glass and AVCO composites may be closer to the predicted values than Table VIII indicates. Of special note is that both the predicted and experimental values of shear stress increase as the coefficient of thermal expansion for the matrix increases. Specifically, for the 7761/AVCO system, $\alpha_f > \alpha_m$, and the radial stress state at the fiber-matrix interface is in tension. The values of interfacial shear stress for this system are the lowest of the four composites. On the other hand, the 7052/AVCO system ($\alpha_m > \alpha_f$) has compressive stresses in the radial direction at the fiber-matrix interface. Hence the matrix

Table VIII. Comparison of Interfacial Shear Stresses.

| <u>Glass/AVCO Fibers</u> | <u>7761</u> | <u>7740</u> | <u>9741</u> | <u>7052</u> |
|--|-------------|-------------|-------------|-------------|
| Predicted Interfacial Shear Stress from ACK model* (MPa) | 3.83 | 4.83 | 5.31 | 7.02 |
| Measured Interfacial Shear Stress** (MPa) | 4.10 | 5.75 | 8.40 | 9.95 |
| Volume fraction fiber | .400 | .469 | .230 | .300 |

* From Ref. 2

** From Ref. 8

squeezes the fiber and there is a higher interfacial shear stress.

As discussed in Chapter II, the models by Aveston, Cooper, and Kelly (ACK); Marshall, Cox, and Evans (MCE); and Budiansky, Hutchinson, and Evans (BHE) all use the same basic relation to predict the matrix cracking stress (2,3,13). However the BHE model includes the state of residual stress in the determination of the overall stress required for matrix cracking. Table IX compares the predicted matrix cracking stresses of the four composite systems studied. The stress σ_{cr} is the matrix cracking stress predicted identically by the ACK, MCE, and BHE models. The equations used by these models for matrix cracking stress were discussed in Chapter II and are repeated here.

ACK:

$$\sigma_{mu} = E_o \{12\tau K_m^2 (1-\mu^2) E_f V_f^2 / E_o E_m^3 r_f V_m\}^{1/3} \quad (17)$$

MCE:

$$\sigma_o = \{6(1-\mu^2) K_m^2 \tau E_f V_f^2 V_m (1+\Gamma)^2 / E_m r_f\}^{1/3} \quad (18)$$

where $\Gamma = E_f V_f / E_m V_m$

BHE:

$$\sigma_1/E_o = 1/E_m \{6V_f^2 E_f \tau K_m c^2 (1-\mu^2) / r_f E_m E_o V_m\}^{1/3} \quad (19)$$

The stress σ_{cr} is that predicted by the BHE model accounting for the residual matrix stress:

$$\sigma_{cr} = \sigma_1 - (E_c/E_m)\sigma^1 \quad (20)$$

$$\text{where } \sigma^1/E_m = \beta_2/\beta_1[E_f/E_c][V_f/1-\mu]\Omega \quad (21)$$

$$\beta_1 = 1 - \frac{1}{2}(1 - 2\mu/1 - \mu)(1 - E_c/E_f), \quad \beta_2 = \frac{1}{2}(1 + E_c/E_f) \quad (22)$$

$$\Omega = (\epsilon_f - \epsilon_m) \quad (23)$$

The experimental cracking stresses were determined from observations of crack formation during the straining stage tests. The 7052/AVCO samples were cracked prior to testing because of the CTE mismatch in the system. However, the stress listed in Table IX is that at which new matrix cracks occurred under tensile loading. As mentioned previously, the 9741/AVCO samples tested were cracked between fiber layers and failed prematurely and no matrix cracks were noted prior to the catastrophic sample failure. In all cases, the matrix cracking stresses predicted by the models vastly exceeds the experimental values. Thus it appears the models overestimate the matrix cracking stresses for the composites. A possible explanation for this is the effect of flaws in the glasses comprising the matrices of the composites. The glasses in the fabricated samples all have some degree of porosity and imperfections reducing their strength. The models do not account for the

Table IX. Theoretical Model Comparisons

Predicted Matrix Cracking Stress (MPa)

Glass/AVCO Fibers 7761 7740 8741 7052

ACK¹, MCE²

σ_{cr} 183.8 255.0 140.3 205.6

BHE^{3*}

σ_{cr} 297.5 268.6 70.4 74.7

Experimental Stress at First Microcrack (MPa)

σ_{cr} 116.7 142.7 - 38.6

Matrix Residual Stresses at Fiber-Matrix Interface (MPa)

BHE³

σ_z -35.0 -3.8 26.0 42.6

Oel and Frechette⁴

σ_x 14.2 1.4 -12.1 -17.8

σ_θ -33.1 -3.3 28.3 41.6

NDSANDS⁵

σ_z -37.4 -3.8 28.0 40.6

σ_x 18.5 1.8 -15.5 -22.2

σ_θ -43.2 -4.1 36.2 51.8

T (°C) for residual stress calculation

800 600 500 525

¹ Aveston, Cooper, and Kelly (2)

² Marshall, Cox, and Evans (13)

³ Budiansky, Hutchinson, and Evans (3)

⁴ Oel and Frechette (15)

⁵ Pagano and Tandon (16)

* BHE matrix cracking stress includes residual stress from fabrication

flaws thus their predictions of matrix cracking stress are high.

In an effort to isolate the effects of the physical parameters on the matrix cracking stresses predicted by the models, interfacial shear stress and volume fraction of fibers were varied over a wide range. Figures 37 thru 40 show the effect of interfacial shear stress on the matrix cracking stress predicted by the MCE model. Again the ACK, BHE, and MCE's basic equations for matrix cracking stress are the same. The interfacial shear stress τ in equation 18, was varied from 1 MPa to 10 MPa for all four composite systems. This range of shear stresses encompasses the experimentally measured shear stresses measured by Kerans and Jurewicz (8). The curves indicate that the variation of interfacial shear stress does significantly affect the matrix cracking stress. The matrix cracking stress for a shear stress of 10 MPa is roughly twice that for a shear stress of 1 MPa. As expected, the greater the interfacial shear stress, the greater the matrix cracking stress.

Figures 41 through 44 show the variation of matrix cracking stress with volume fraction of fibers. V_f in equation 18 was varied from 0.0 to 1.0 for the four composite systems. The matrix cracking stress increases dramatically with increasing V_f . However a limitation of the models becomes apparent from this parametric study. In the mid-range of values of V_f the predicted values of

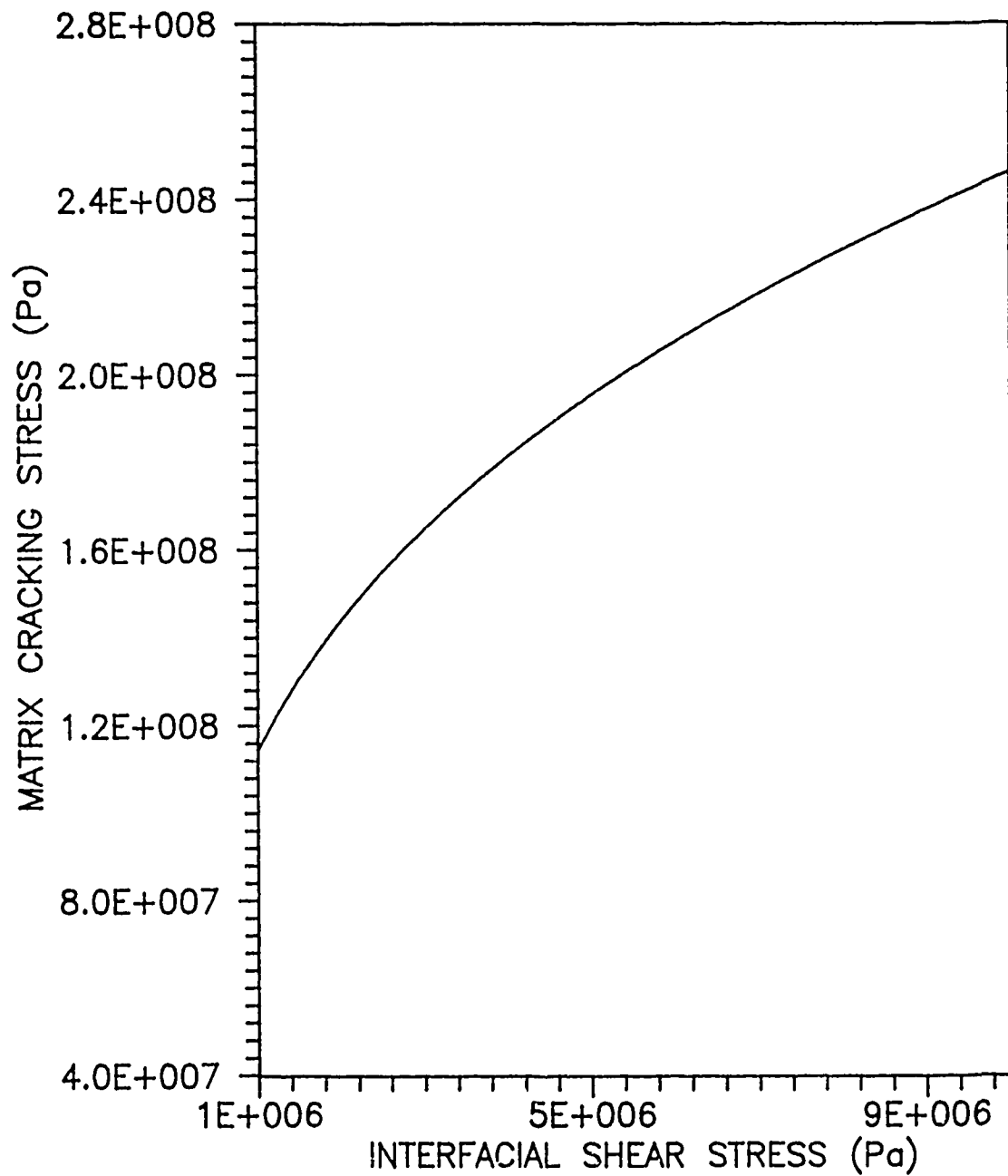


Figure 37. Matrix Cracking Stress Vs Interfacial Shear Stress
 Predicted Stress from MCE Model
 CGW 7761 Glass with AVCO Fibers

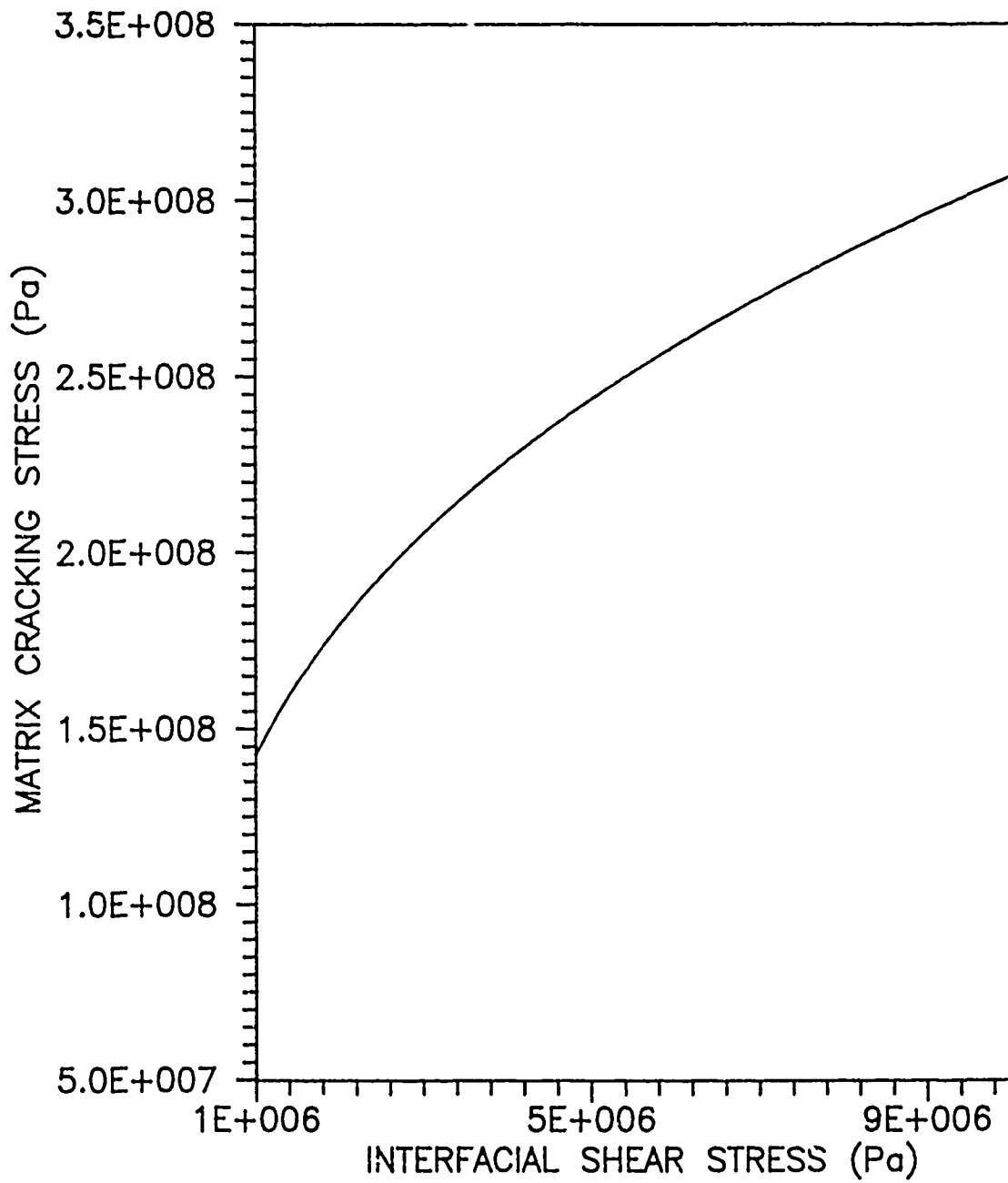


Figure 38. Matrix Cracking Stress Vs Interfacial Shear Stress
 Predicted Stress from MCE Model
 CGW 7740 Glass with AVCO Fibers

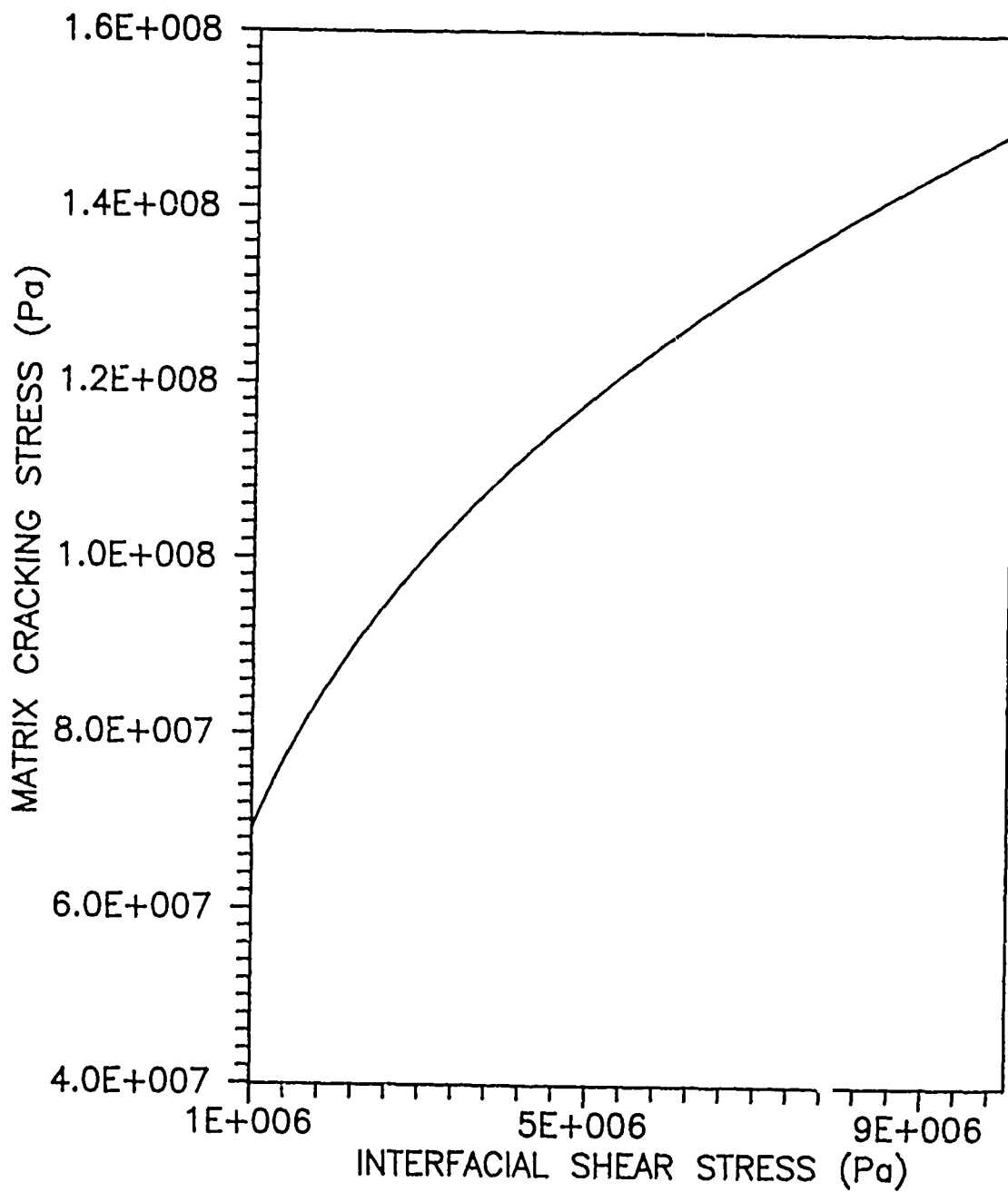


Figure 39. Matrix Cracking Stress Vs Interfacial Shear Stress
Predicted Stress from MCE Model
CGW 9741 Glass with AVCO Fibers

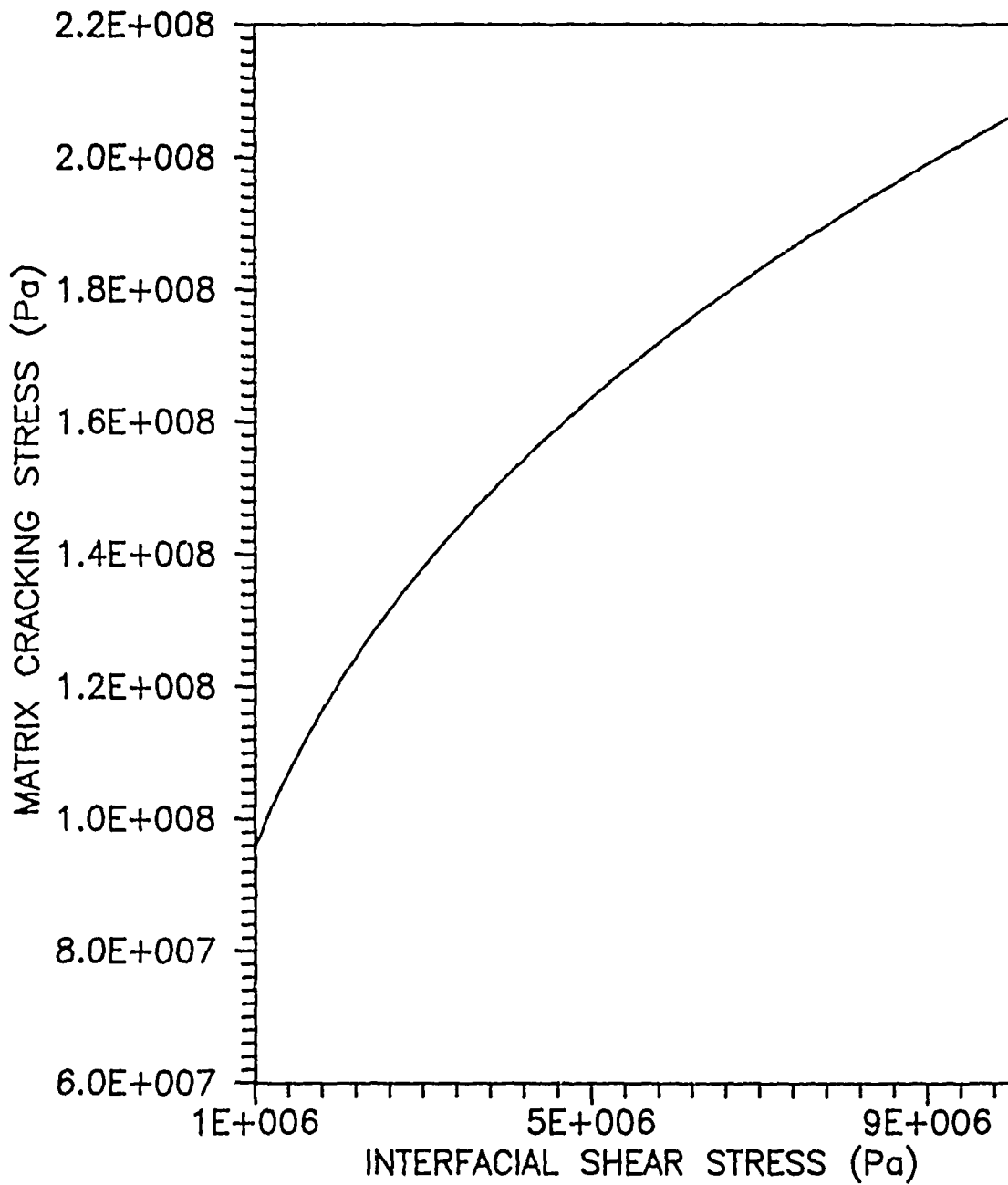


Figure 40. Matrix Cracking Stress Vs Interfacial Shear Stress
 Predicted Stress from MCE Model
 CGW 7052 Glass with AVCO Fibers

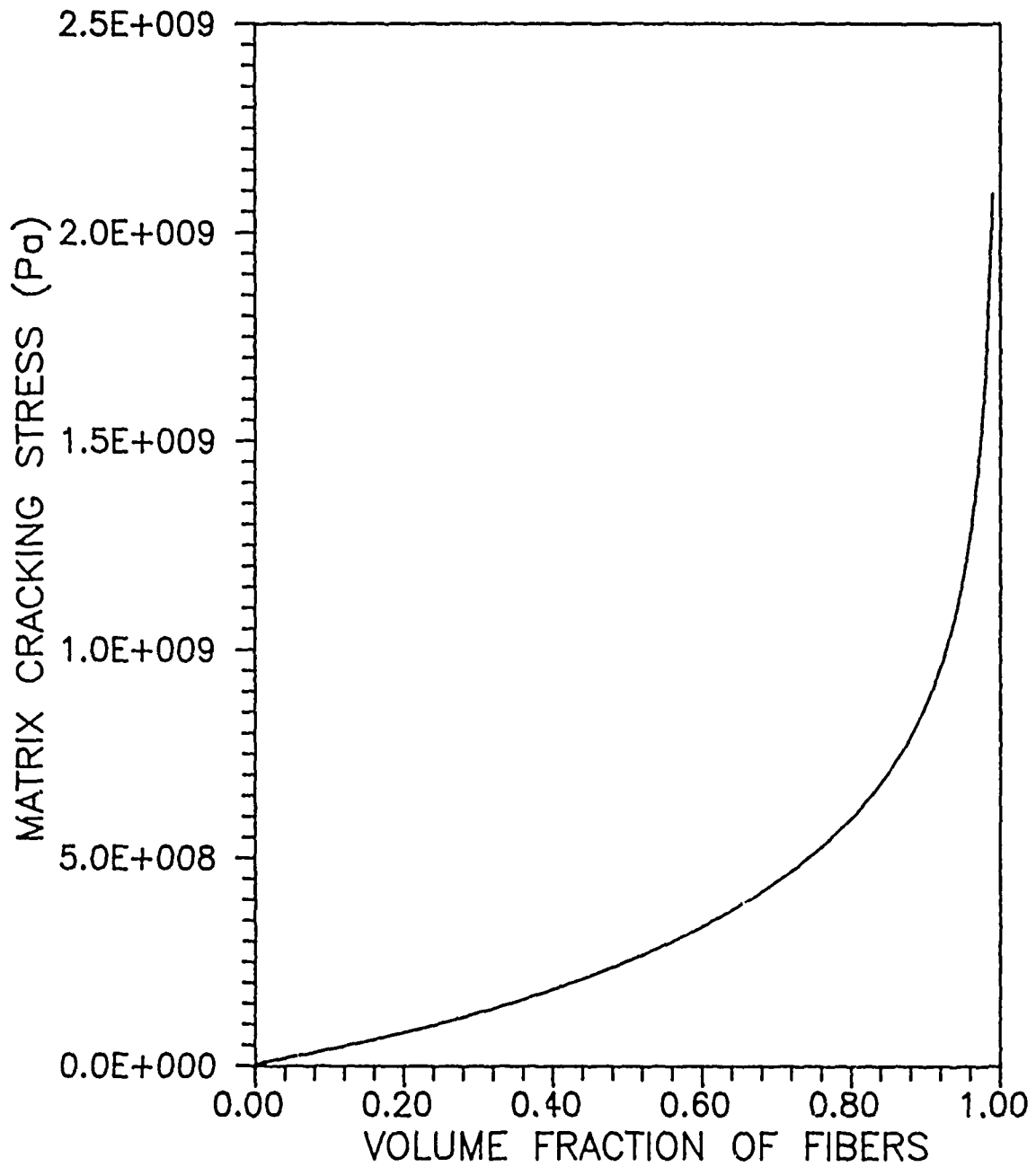


Figure 41. Matrix Cracking Stress Vs Volume Fraction Fibers
Predicted Stress from MCE Model
CGW 7761 Glass with AVCO Fibers

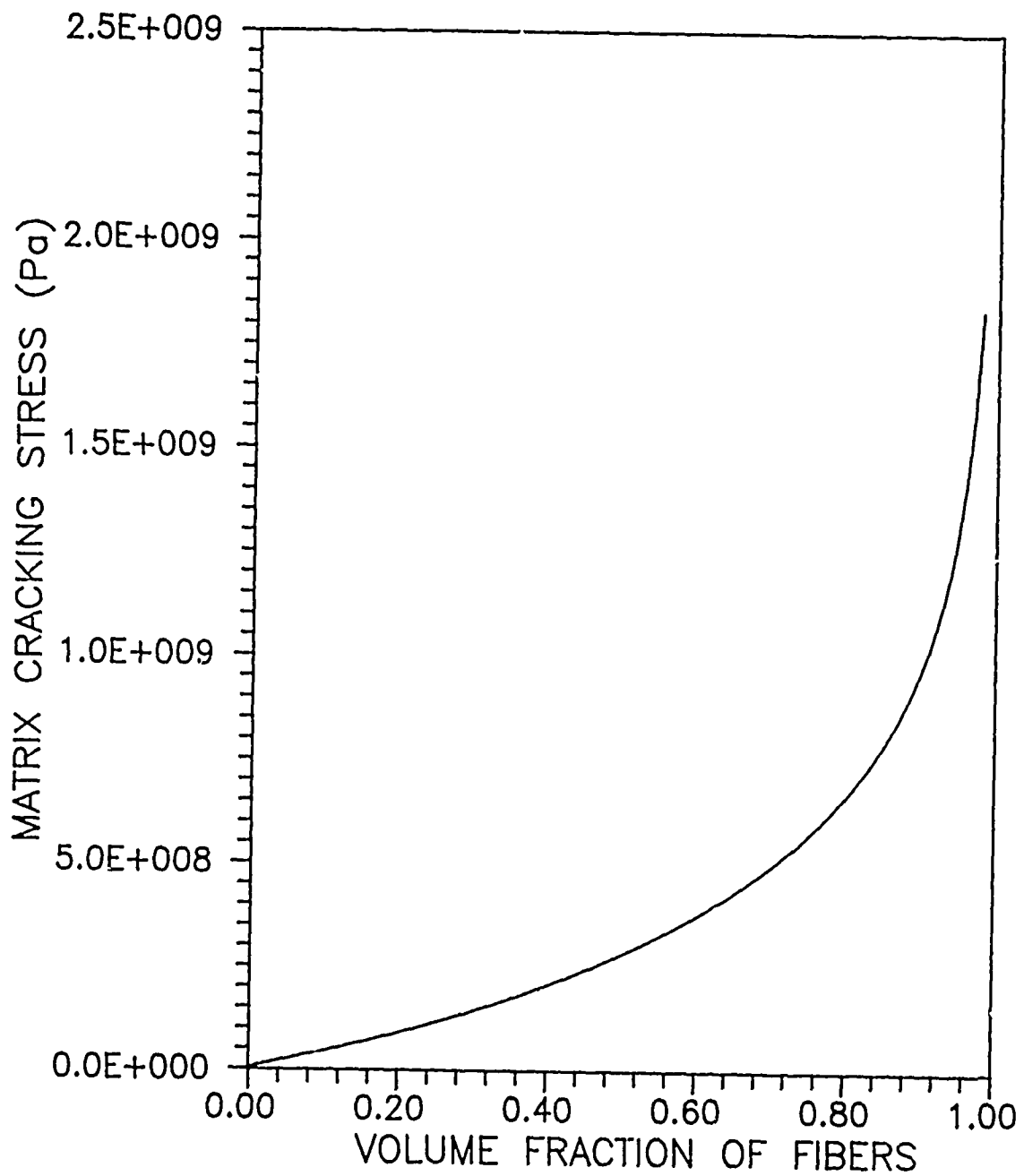


Figure 42. Matrix Cracking Stress Vs Volume Fraction Fibers
Predicted Stress from MCE Model
CGW 7740 Glass with AVCO Fibers

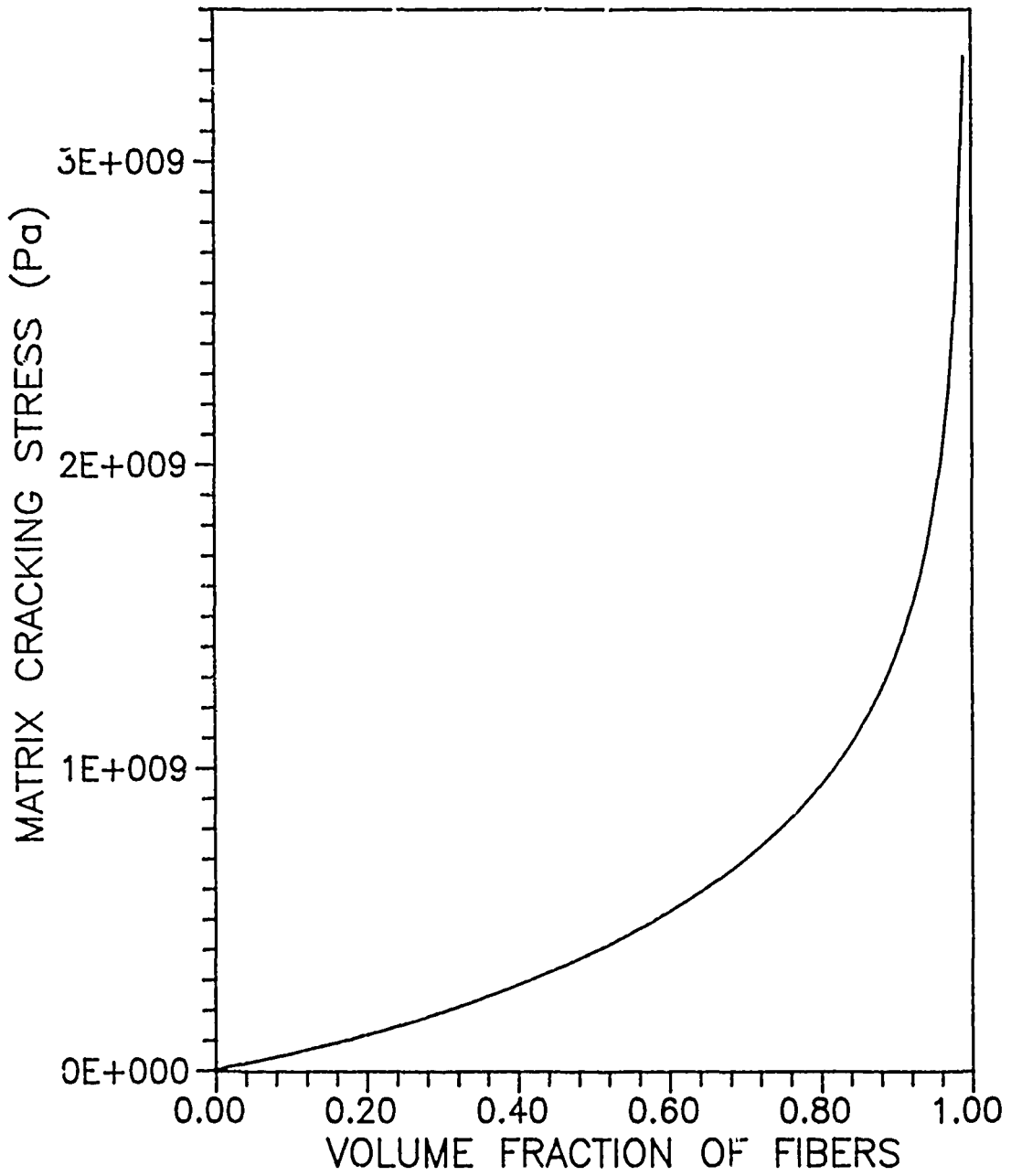


Figure 43. Matrix Cracking Stress Vs Volume Fraction Fibers
 Predicted Stress from MCE Model
 CGW 9741 Glass with AVCO Fibers

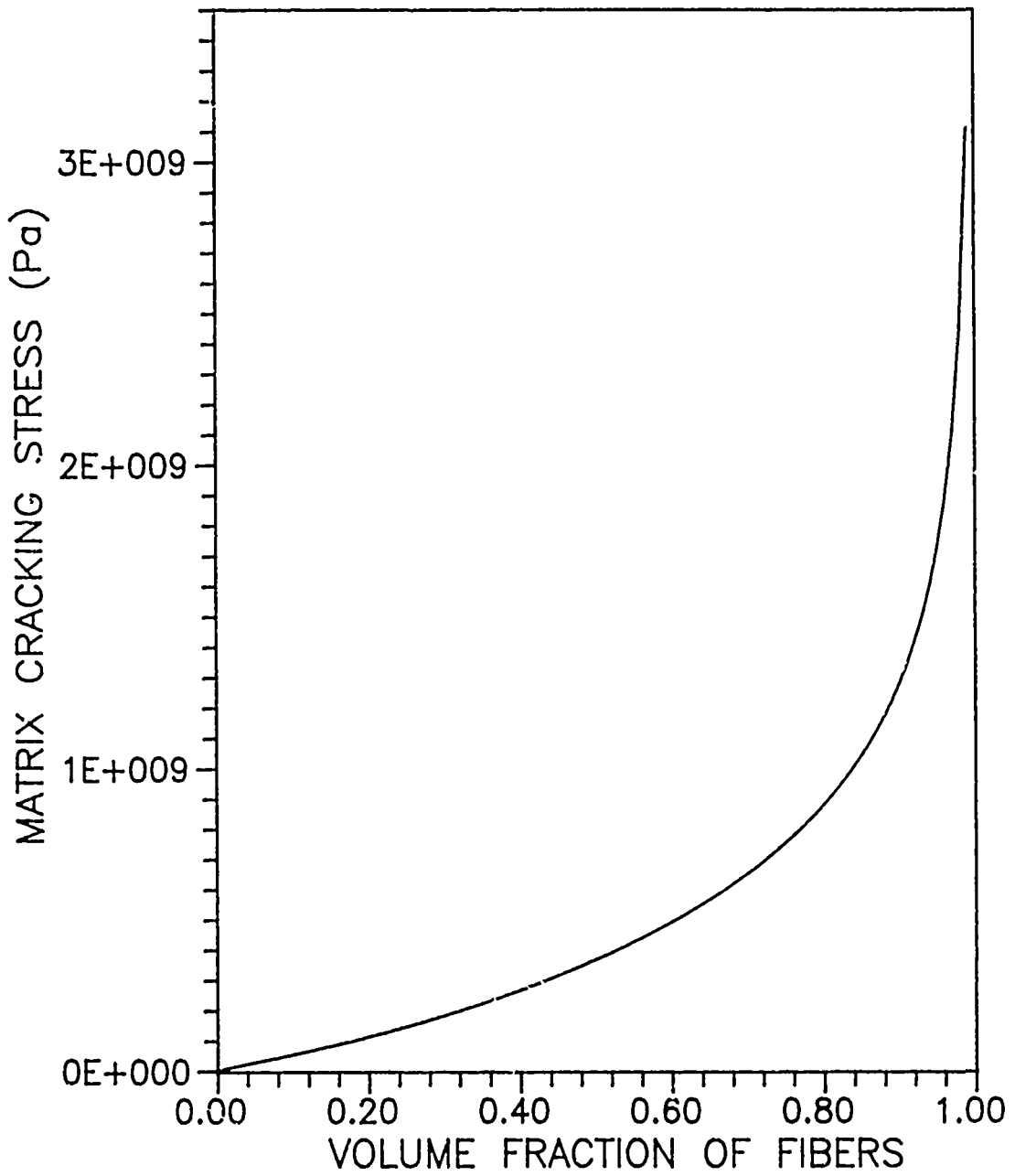


Figure 44. Matrix Cracking Stress Vs Volume Fraction Fibers
Predicted Stress from MCE Model
CGW 7052 Glass with AVCO Fibers

matrix cracking stress appear valid. However as V_f approaches zero, the predicted matrix cracking stress also goes to zero. In reality for $V_f = 0$, the matrix cracking stress should be that of the monolithic matrix. At the other end of the scale where V_f approaches one, the model predicts the matrix cracking stress goes to infinity or a singular solution. For $V_f = 1$, the matrix cracking stress should be equal to that of the fibers. Thus for the cases of very small V_f and very large V_f , the models are not satisfactory.

Table IX also includes the comparisons of the residual stresses at the fiber-matrix interface predicted by NDSANDS (16), Oel and Frechette (15), and the BHE model (3). The BHE model only predicts the residual stress in the axial direction, but its predicted values of σ_z are very close with those of the NDSANDS model. The model by Oel and Frechette was developed for thin cylindrical disks and the assumption of plane stress, so σ_z is assumed equal to zero. While the values of σ_r and σ_θ from NDSANDS and Oel and Frechette agree fairly closely, the plane stress formulation of the latter accounts for most of the differences between the two models' predictions. The calculation of the residual stresses is dependent on the change in temperature the composite system undergoes from fabrication (when the system is considered stress free) to the temperature at which the composite will be used (room

temperature for this study). To obtain accurate temperatures at which the composite would be stress free, thermal expansion data for each glass was used. An example of this type of data is shown in Figure 45. The change in temperature was measured from room temperature to the point where the curve reaches a peak which corresponds to the temperature at which the glass will not support any stress.

This chapter discussed, in detail, three main phases involved in the study of damage progression in fiber reinforced glass matrix composites. Section A covered the tensile testing of longitudinal and transverse composite

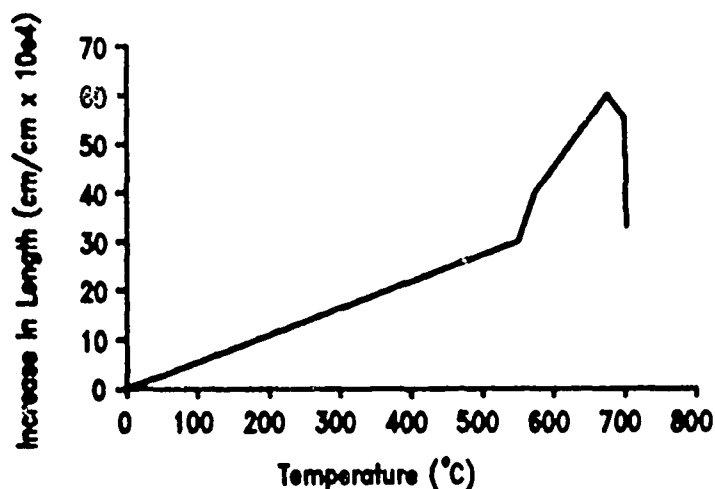


Figure 45. Example of Thermal Expansion Data for Glass from Ref. 11.

samples using a servo-hydraulic testing machine (MTS). The results of these tests are summarized in Tables V, VI, and VII. Table V lists all the samples tested and the mechanical properties measured for each. Table VI shows the average mechanical properties for the four composite systems tested. And Table VII compares the average elastic moduli determined from the MTS tests to the predicted composite moduli for each system. From the load-strain curves generated by the MTS machine tests, stress-strain curves were plotted and are shown in Figures 16-17 and Figures 46-52. Section B discussed the straining fixture testing of the four composite systems and the damage progression for each. The different states of residual stresses in the four systems is explained as well as the effect these stresses have on the damage that occurred during loading. Finally in Section C, experimentally determined stresses are compared to values predicted by theoretical models. Table VIII shows the comparison of interfacial shear stress predicted by Aveston, Cooper, and Kelly to shear stresses measured in fiber pullout tests. Table IX compares the matrix cracking stress observed experimentally to the stress predicted by the models of Aveston, Cooper, and Kelly; Marshall, Cox, and Evans; and Budiansky, Hutchinson, and Evans (2,3,13). Also compared are the residual stresses predicted by the NDSANDS model (Pagano and Tandon) and a model by Fel and Frechette. A

parametric study was conducted on the MCE equation for matrix cracking stress. In this study, volume fraction of fibers (V_f) and the interfacial shear stress were varied to see their effects on the predicted matrix cracking stress.

V. Conclusions

This study was conducted to investigate the damage progression in fiber reinforced brittle matrix composites under tensile loading. There is great potential for these composites in high temperature applications. The failure mechanisms of fiber reinforced ceramic composites are not well understood. Before these systems can be used in components subjected to high stresses, the characteristics of failure must be known so that designers can safely predict their strength and design life. Composites were fabricated using four different glasses manufactured by Corning Glass Works and AVCO SCS-6 fibers. Testing of the composites was accomplished in three phases. First, each system's mechanical properties were measured using a MTS machine. Next the initiation and progression of damage in the composites under tensile loading was observed. Finally the experimentally determined values of matrix cracking stress were compared to predicted values by three theoretical models. The conclusions drawn from this experimental study are as follows:

1. The proper fabrication conditions were essential to produce samples with the desired characteristics such as good fiber alignment, low porosity, and a specified volume fraction of fibers.

2. The fabrication conditions varied for each glass and were dependent upon the glass composition.
3. The composite elastic modulus predicted by the rule of mixtures was higher than the modulus experimentally measured for the 7761/AVCO and 7740/AVCO systems. The predicted modulus for the 9741/AVCO system was very close to the average measured value. For the 7052/AVCO system, the predicted modulus that assumed that the matrix did not contribute to the composite strength was very close to the experimental value.
4. The transverse ultimate strength and modulus for these unidirectional composites were very low compared to the longitudinal properties.
5. Transverse strain reversal was observed in the stress-strain curves for the 7761/AVCO composite. This phenomena was first reported by Kim and Katz (9).
6. Matrix cracking was observed in tensile tests prior to the onset of nonlinearity in the stress-strain curves. This is in contrast to many theoretical models and literature where the initiation of matrix cracking is assumed to coincide with the onset of nonlinearity in the stress-strain curve.
7. The residual stress state at the fiber-matrix interface in the composites tested has a large effect on the nature of damage progression under tensile loading.

8. In the 7761/AVCO system, which has tensile radial stresses at the fiber-matrix interface, damage was characterized by random fiber and matrix cracking, and extensive matrix cracking at high tensile stresses. Some debonding at the fiber-matrix interface and fiber-core pullout was also observed.

9. High residual tensile stresses along the fiber-matrix interface in the 7052/AVCO and 9741/AVCO systems caused transverse matrix cracking during fabrication. The high residual stress in the axial direction was caused by the large CTE mismatch between the fiber and matrix where $\alpha_m > \alpha_f$.

10. Compressive radial stresses at the fiber-matrix interface in 7052/AVCO and 9741/AVCO systems prevented extensive matrix cracking and fiber-matrix debonding under tensile loading.

11. Fiber cracks formed in the 7052/AVCO system at a very low strain level of .06 percent during tensile testing and were very close to the pre-existing matrix cracks.

12. The interfacial shear stresses predicted by the Aveston, Cooper, and Kelly model (2) agreed well with the experimental values from fiber pullout tests.

13. The Aveston, Cooper, and Kelly (2); Marshall, Cox and Evans (13); and Budiansky, Hutchinson, and Evans (3) predictions of matrix cracking stress were much larger than the experimental stresses observed in testing.

14. The theoretical models (2,13,3) are not valid for volume fractions of fibers near zero or one.

VI. Recommendations

Although much has been learned about the failure mechanisms in the Glass/AVCO composites used in this study, there remains much to be accomplished. Several areas are listed here that deserve further consideration:

1. More samples of the composites should be tested to verify the failure characteristics and mechanical properties determined in this study. In the mechanical properties particularly, the data had considerable scatter and in some cases no valid results were obtained.
2. The fibers and matrices to be used in composites must be carefully chosen so that the difference between the CTE's of the fiber and matrix is limited. By limiting the CTE mismatch, the residual stresses at the interface can be limited to stop matrix pre-cracking.
3. Alternate methods of fabrication should be researched. Hot pressing using graphite dies proved difficult for some glasses and the ability to control the processing conditions is limited.
4. The use of a high speed camera in conjunction with the straining fixture should be investigated. Presently, the samples being tested have to be moved across the lens of the microscope by hand which takes a great deal of time and new cracks and damage can easily be overlooked. A high speed

camera would better document the damage progression in the samples tested.

5. The analytical models considered in this study should be refined to give more accurate predictions of matrix cracking stress.

Bibliography

1. Allaire, Roger A. and others. "Glass Matrix Composites for Higher Use Temperature Applications," Proceedings of the 32nd International SAMPE Symposium. 624 - 634. 1987.
2. Aveston, J., G. A. Cooper, and A. Kelly, "Single and Multiple Fracture," Proceedings of Conference on the Properties of Fiber Composites. 15 - 26. National Physical Laboratory, IPC Science and Technology Press, 1971.
3. Budiansky, Bernard, John W. Hutchinson, and Anthony G. Evans. "Matrix Fracture in Fiber Reinforced Ceramics," Journal of Mechanical and Physical Solids, 34: 167-189 (1986).
4. Cooper, G. and A. Kelly. "Role of the Interface in the Fracture of Fiber-composite Materials," American Society of Testing and Materials, STP 452: 90 - 106 (1969).
5. Coyle, T. W., M. H. Guyot, and J. F. Janet. "Mechanical Behavior of a Microcracked Ceramic Composite," Proceedings of the 10th Annual Conference on Composites and Advanced Ceramic Materials. 947 - 956. Cocoa Beach, 1986.
6. Donald, I. W. and P. W. McMillan. "Review of Ceramic Matrix Composites," Journal of Materials Science, 11: 949 - 972 (1976).
7. Flinn, Richard A. and Paul K. Trojan. Engineering Materials and Their Applications. Boston: Houghton Mifflin Company, 1975.
8. Kerans, R. and A. Jurewicz, "The Interfacial Shear Strength and Other Properties of SiC/Glass Interfaces," Unpublished work, 1988.
9. Kim, Ran Y. and Allen P. Katz. Mechanical Behavior of Unidirectional SiC/BMAS Ceramic Composites. Contract F33615-87-C-5239. Wright-Patterson Air Force Base, OH: Air Force Wright Aeronautical Laboratories/Materials Laboratory, 1988.
10. Kimber, A. C. and J. G. Keer. "On the Theoretical Average Crack Spacing in Brittle Matrix Composites Containing Continuous Aligned Fibers," Journal of Material Science Letters, 7: 353 - 354 (1982).

11. Kingery, W. D. and others. Introduction to Ceramics. New York: John Wiley and Sons, 1976.
12. Lynch, Charles T., ed. Handbook of Materials Science. Volume II: Metals, Composites, and Refractory Materials. Cleveland: CRC Press, Inc., 1975.
13. Marshall, D. B., B. N. Cox and A. G. Evans. "The Mechanics of Matrix Cracking in Brittle Matrix Composites," Acta Metall., 33: 2013 - 2021 (1985).
14. McColm, I. J. Ceramic Science for Materials Technologists. New York: Chapman and Hall, 1983.
15. Oel, H. J. and V. D. Frechette. "Stress Distribution in Multiphase Systems: II, Composite Disks with Cylindrical Interfaces," Journal of the American Ceramic Society, 69: 342 - 346 (1986).
16. Pagano, N. J. and G. P. Tandon. "Elastic Response of Multidirectional Coated-Fiber Composites," Composites Science and Technology, 31: 273 - 293 (1988).
17. Prewo, K. M. and D. C. Jarmon. Characterization of SiC Monofilament Reinforced Glass and Glass-Ceramic Composites. Contract N00014-81-C-0571. Arlington, VA: Department of the Navy, Office of Naval Research, November, 1986.
18. Van Vlack, Lawrence H. Materials Science for Engineers. Reading: Addison-Wesley Publishing Company, 1970.

Appendix: Stress-strain Curves

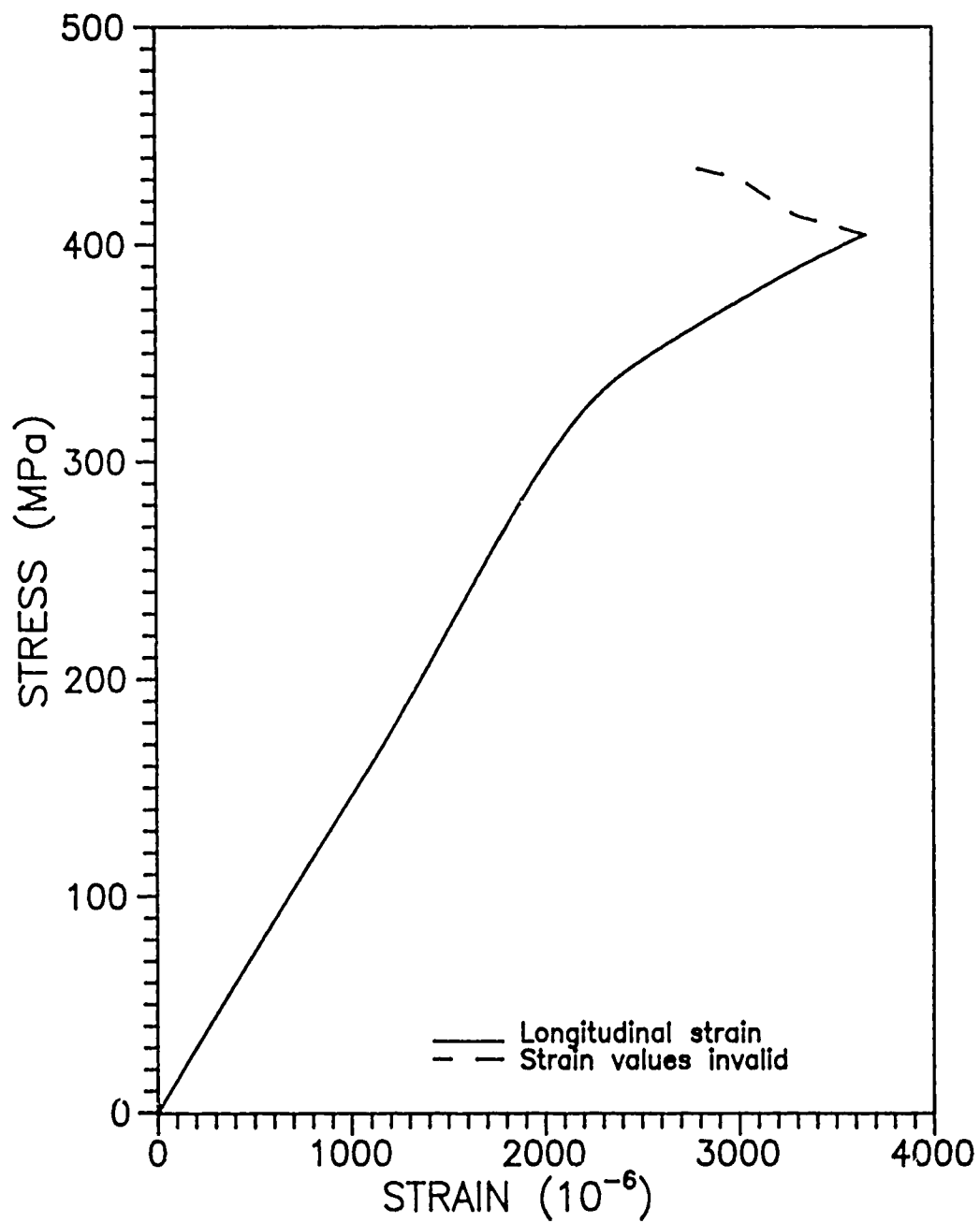


Figure 46. Stress-Strain Curve for AVCO/7761
Sample 28-X

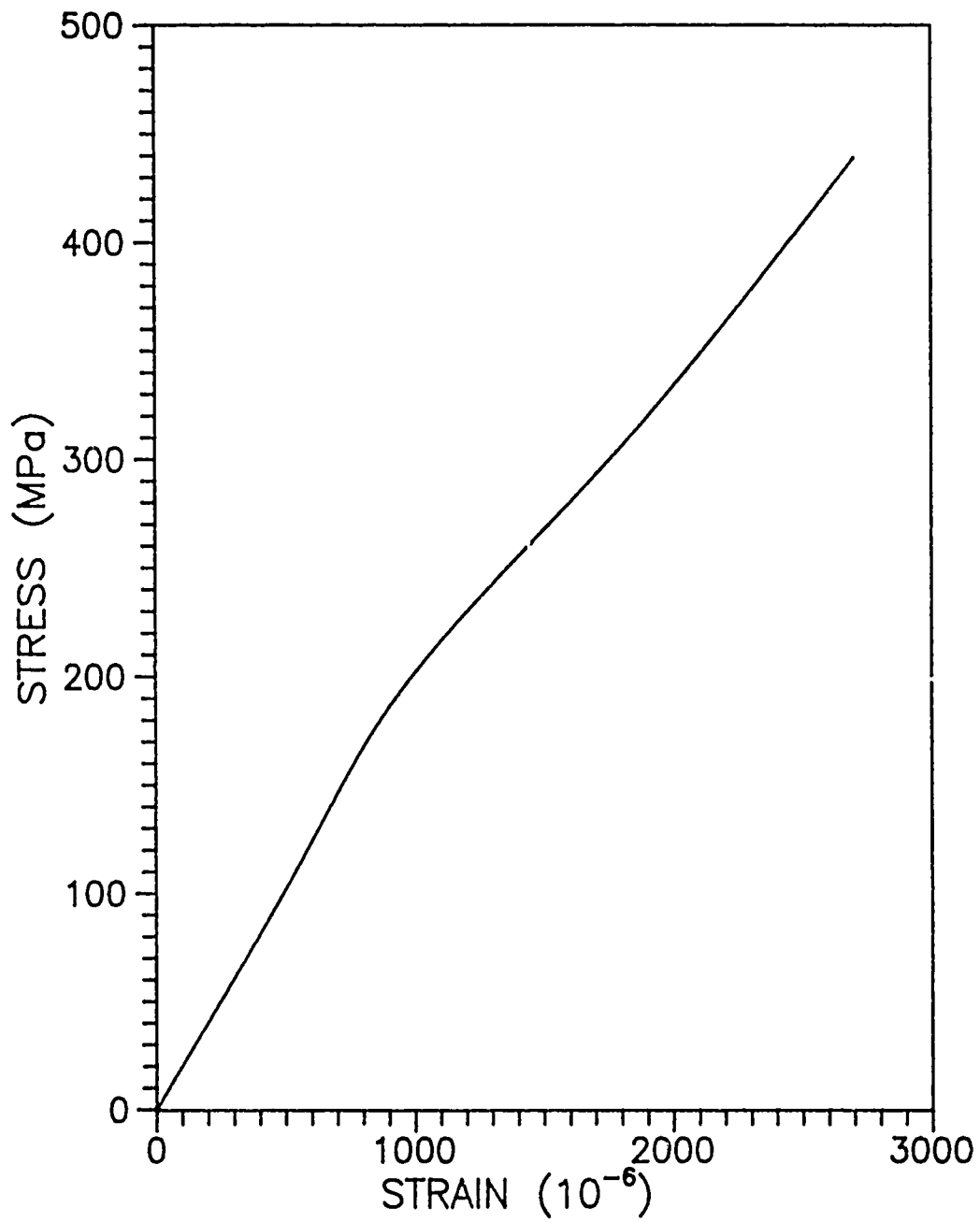


Figure 47. Stress-Strain Curve for AVCO/7761
Sample 24-B

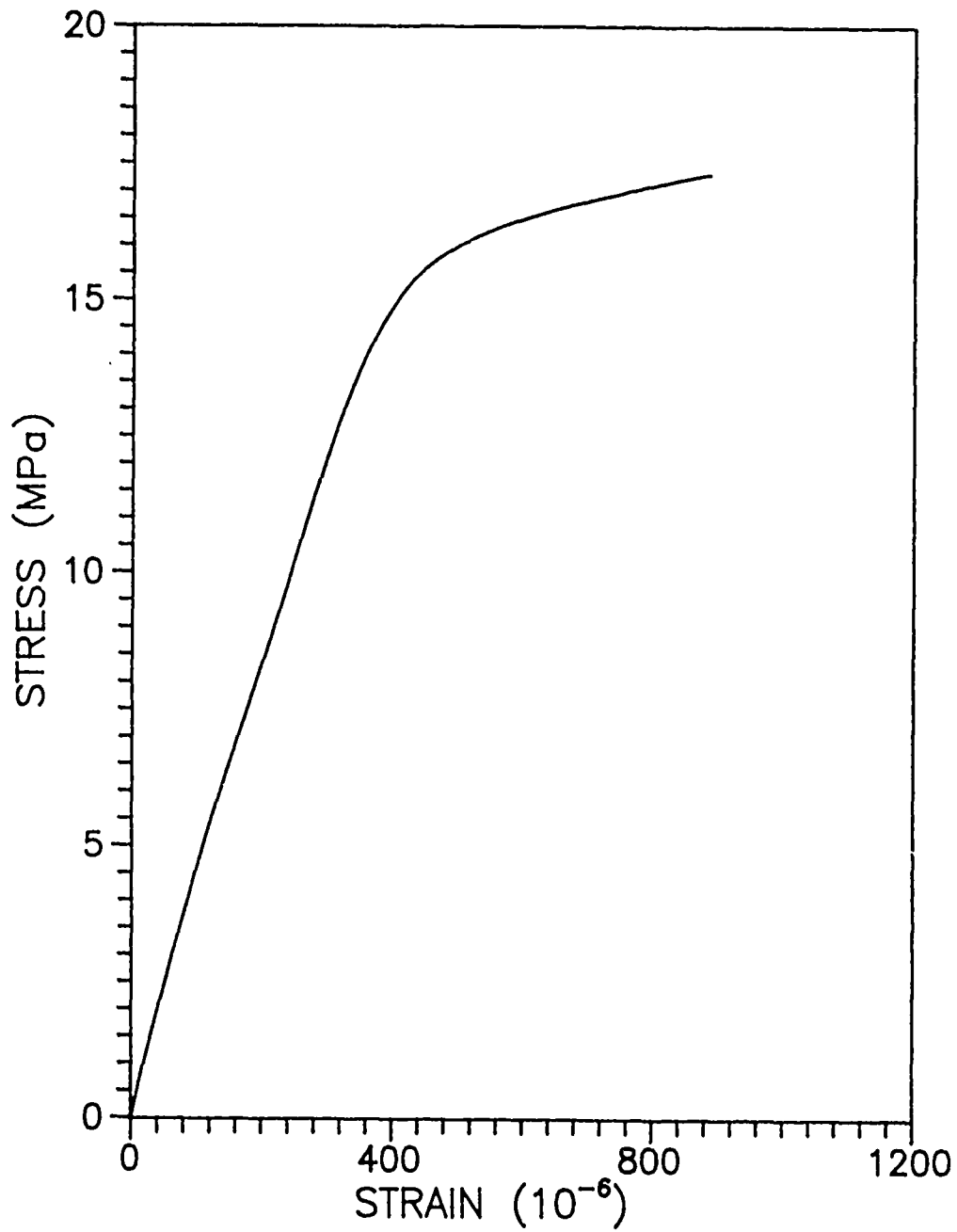


Figure 48. Stress-Strain Curve for AVCO/7761
Sample 27-C (Transverse)

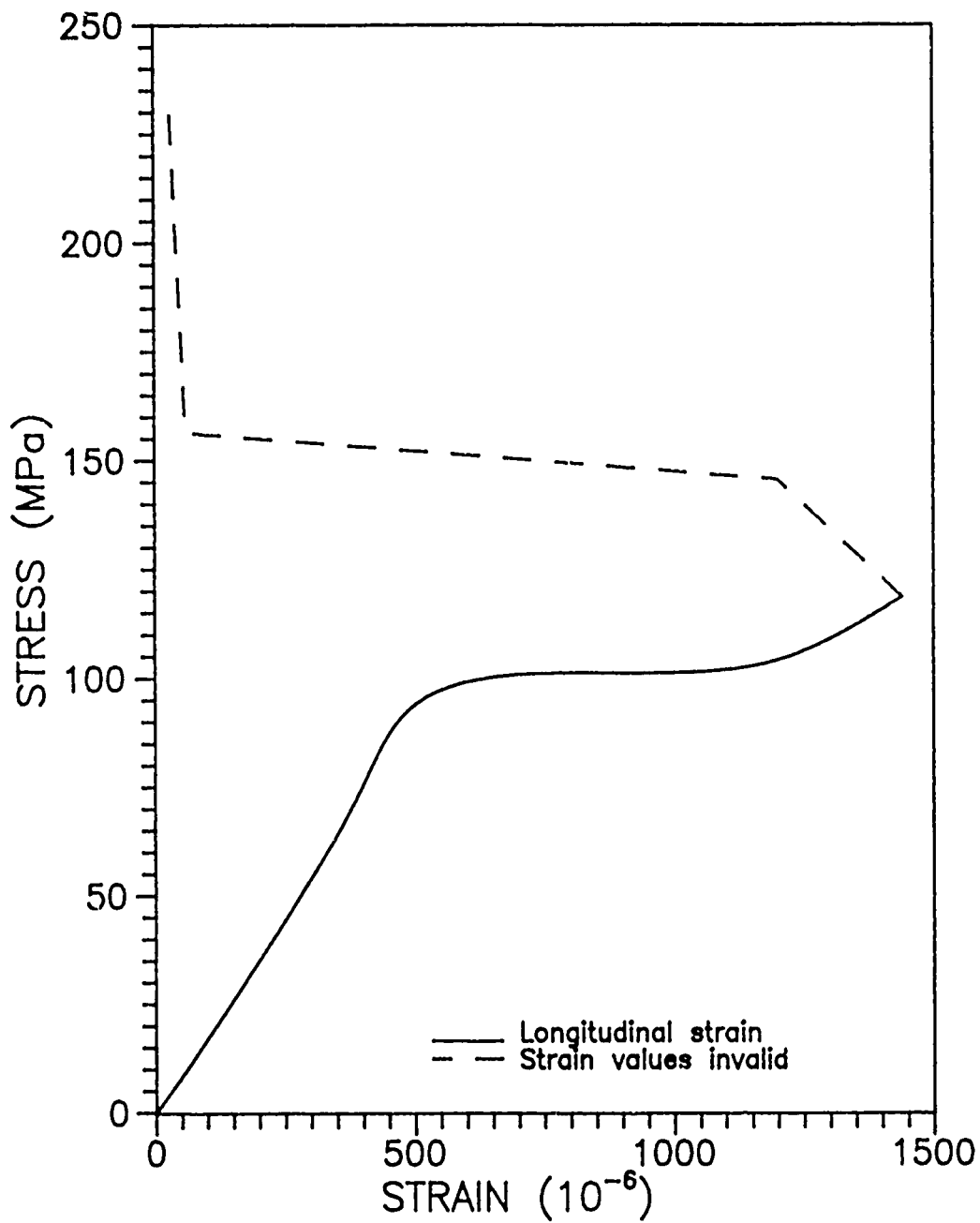


Figure 49. Stress-Strain Curve for AVCO/7740
Sample 32-A

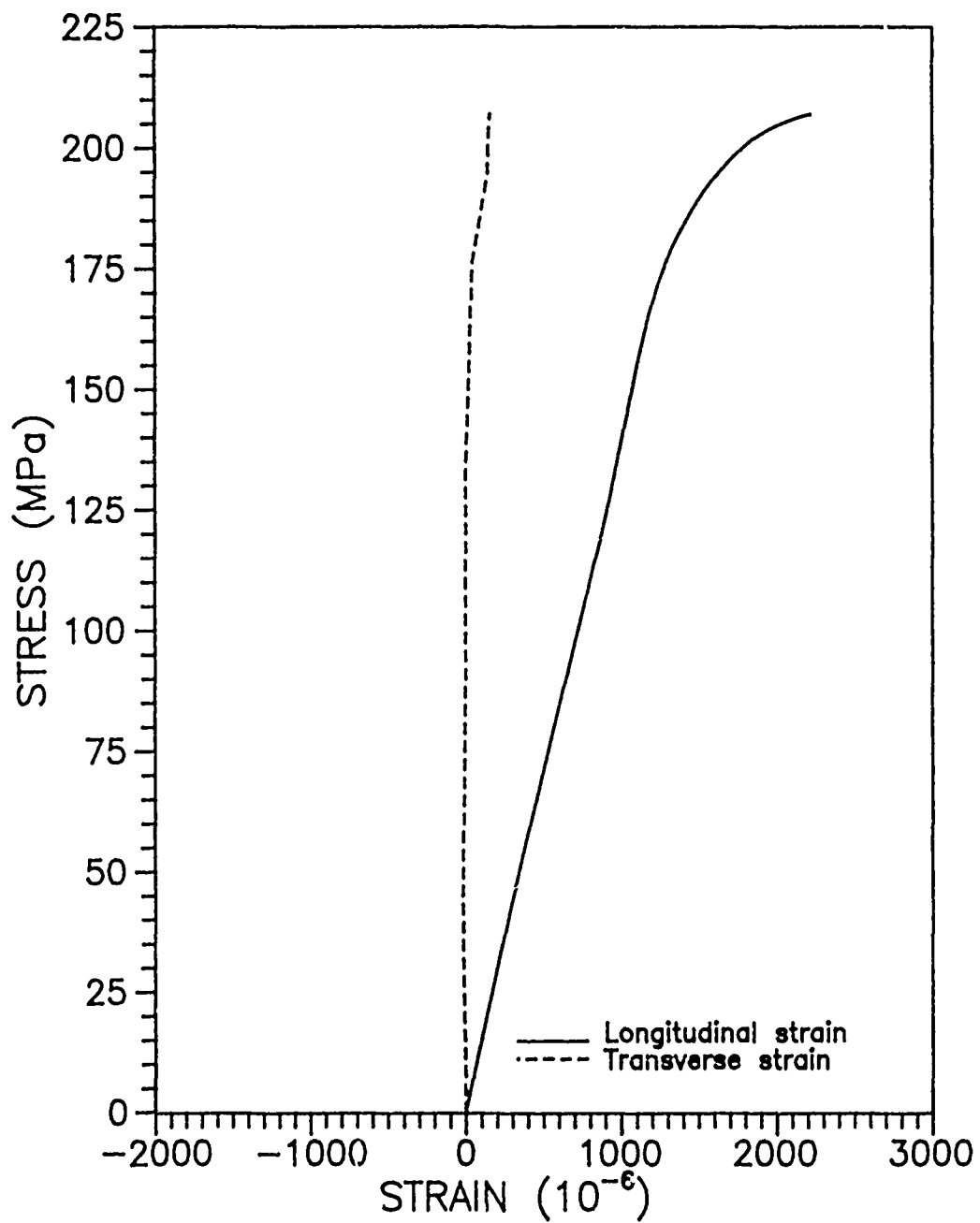


Figure 50. Stress-Strain Curve for AVCC/7052
Sample 39-C

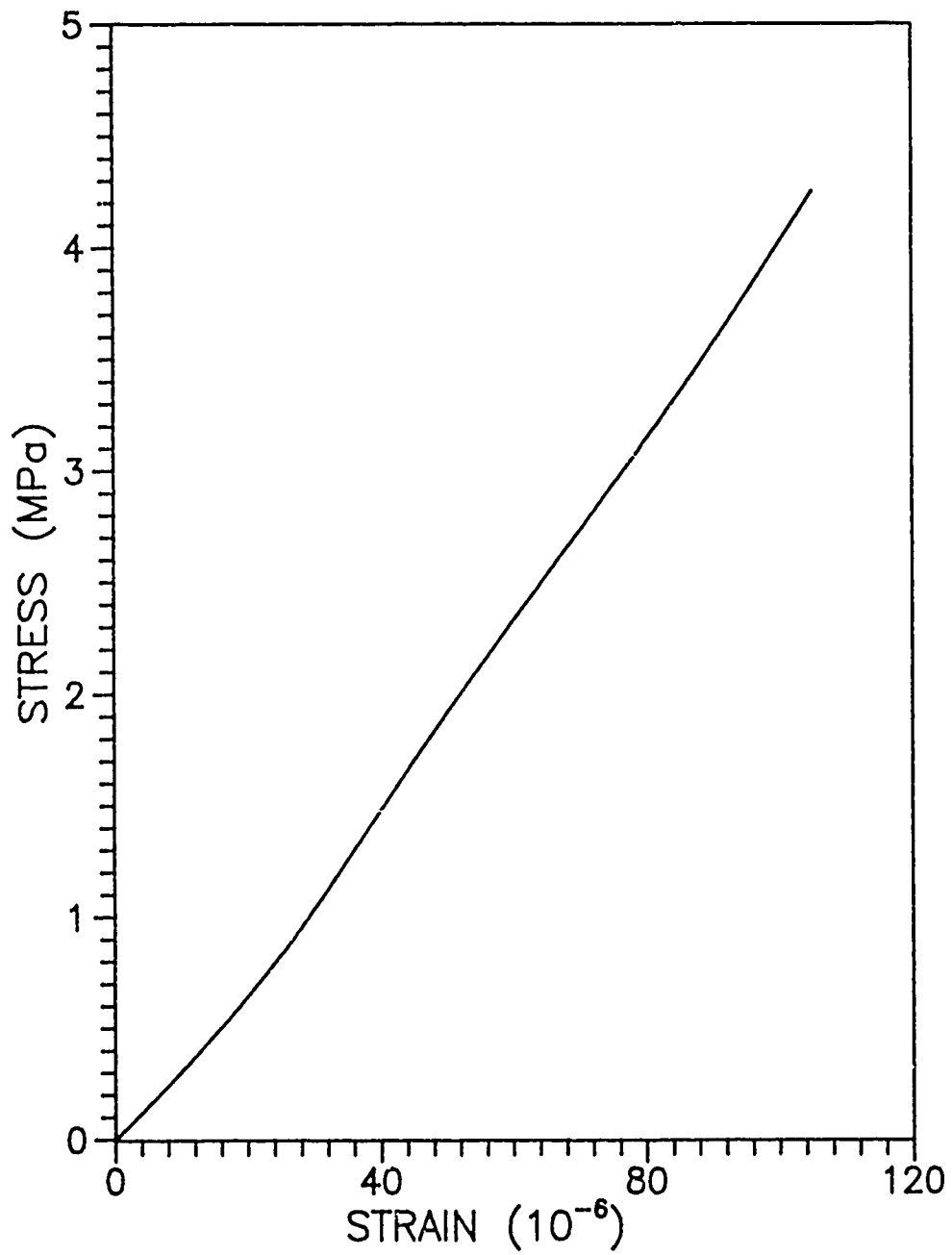


Figure 51. Stress-Strain Curve for AVCO/7052
Sample 40-B (Transverse)

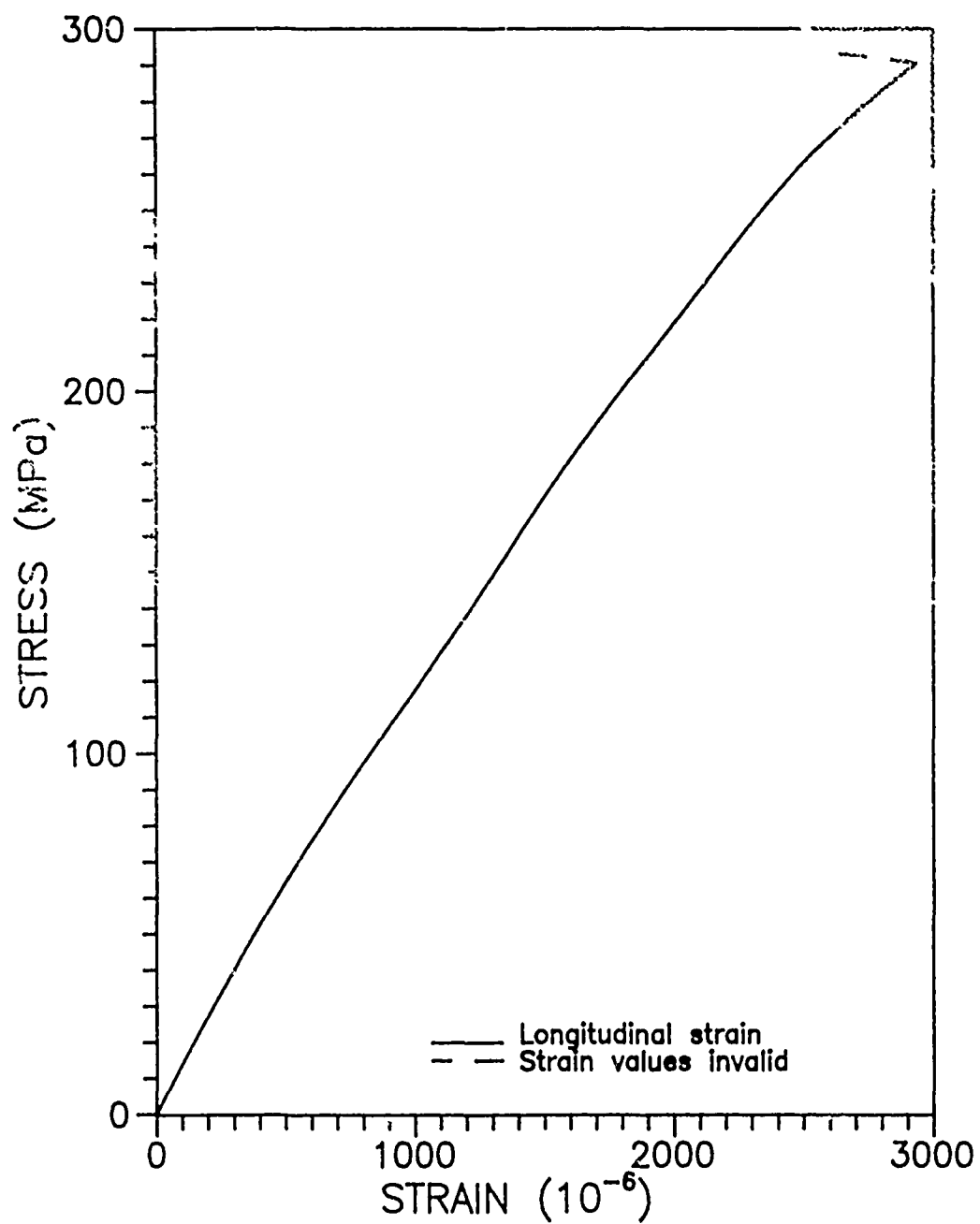


Figure 52. Stress-Strain Curve for AVCO/9741
Sample 42-C

Vita

Captain Joseph W. Moschler, Jr. [REDACTED]

[REDACTED] [REDACTED]
[REDACTED] 1976 [REDACTED] attended the United States Air Force Academy from which he received a Bachelor of Science in Engineering Sciences in May 1980. Upon graduation, he received a commission in the USAF and entered navigator training at Mather AFB, California. After completion of training in March 1981, he served as a weapon systems officer and instructor weapon system officer in the RF-4C at RAF Alconbury, United Kingdom and at Shaw AFB, South Carolina. He then entered the School of Engineering, Air Force Institute of Technology in May 1987.

[REDACTED] [REDACTED]
[REDACTED]

UNCLASSIFIED

SECURITY CLASSIFICATION OF THIS PAGE

ADA202705

REPORT DOCUMENTATION PAGE

Form Approved OMB No. 0704-0188

| | | | |
|--|--|--|--------------------------------|
| 1a. REPORT SECURITY CLASSIFICATION UNCLASSIFIED | | 1b. RESTRICTIVE MARKINGS | |
| 2a. SECURITY CLASSIFICATION AUTHORITY | | 3. DISTRIBUTION / AVAILABILITY OF REPORT Approved for public release; distribution unlimited | |
| 2b. DECLASSIFICATION / DOWNGRADING SCHEDULE | | 5. MONITORING ORGANIZATION REPORT NUMBER(S) | |
| 4. PERFORMING ORGANIZATION REPORT NUMBER(S) AFIT/GAE/AA/88D-28 | | 7a. NAME OF MONITORING ORGANIZATION | |
| 6a. NAME OF PERFORMING ORGANIZATION School of Engineering | 6b. OFFICE SYMBOL (if applicable) AFIT/ENY | 7b. ADDRESS (City, State, and ZIP Code) | |
| 6c. ADDRESS (City, State, and ZIP Code) Air Force Institute of Technology Wright-Patterson AFB OH 45433-6583 | | 9. PROCUREMENT INSTRUMENT IDENTIFICATION NUMBER | |
| 8a. NAME OF FUNDING / SPONSORING ORGANIZATION Air Force Wright Aero Lab | 8b. OFFICE SYMBOL (if applicable) MLEM | 10. SOURCE OF FUNDING NUMBERS | |
| 8c. ADDRESS (City, State, and ZIP Code) AFWAL/MLEM Wright-Patterson AFB OH 45433-6583 | | PROGRAM ELEMENT NO. | PROJECT NO. |
| | | TASK NO. | WORK UNIT ACCESSION NO. |
| 11. TITLE (Include Security Classification) INVESTIGATION OF FAILURE MODES IN FIBER REINFORCED CERAMIC MATRIX COMPOSITES | | | |
| 12. PERSONAL AUTHOR(S) Joseph W. Moschler, Jr., B.S., Capt, USAF | | | |
| 13a. TYPE OF REPORT MS Thesis | 13b. TIME COVERED FROM _____ TO _____ | 14. DATE OF REPORT (Year, Month, Day) 1988 December | 15. PAGE COUNT 133 |
| 16. SUPPLEMENTARY NOTATION | | | |
| 17. COSATI CODES | | 18. SUBJECT TERMS (Continue on reverse if necessary and identify by block number) | |
| FIELD | GROUP | Fiber reinforced composites Debonding Glass | |
| 11 | 02 | Interfacial shear stress Tensile properties | |
| 19. ABSTRACT (Continue on reverse if necessary and identify by block number) | | | |
| Thesis Advisor: Dr. Shankar Mall Professor Department of Aeronautics and Astronautics | | | |
| Abstract on Reverse | | | |
| 20. DISTRIBUTION / AVAILABILITY OF ABSTRACT <input checked="" type="checkbox"/> UNCLASSIFIED/UNLIMITED <input type="checkbox"/> SAME AS RPT <input type="checkbox"/> DTIC USERS | | 21. ABSTRACT SECURITY CLASSIFICATION UNCLASSIFIED | |
| 22a. NAME OF RESPONSIBLE INDIVIDUAL Dr. Shankar Mall, Professor | | 22b. TELEPHONE (Include Area Code) (513) 255-2998 | 22c. OFFICE SYMBOL AFIT/ENY |

Shankar Mall
12 Jan 1989

UNCLASSIFIED

→ This experimental study was conducted to investigate the damage progression in fiber reinforced ceramic matrix composites under tensile loading. As part of this study, the effect of the residual stresses at the fiber-matrix interface on damage progression was evaluated.

Composite samples were fabricated from silicon carbide fibers and borosilicate glass matrices. Each glass had a different coefficient of thermal expansion than the fiber and through the variation of this mismatch, the residual stresses at the fiber-matrix interface were varied resulting in different bonding conditions at the fiber-matrix interface.

The mechanical properties of the composites were measured using a servo-hydraulic mechanical testing machine. During these tests, transverse strain reversal was observed which is believed to be caused by axial matrix cracks and fiber-matrix debonding. Matrix cracking occurred in the composites tested before the onset of nonlinearity in the stress-strain curves. Tensile tests were conducted on the composites using a constant load straining device in which damage progression was observed using an optical microscope. The residual stress state at the fiber-matrix interface showed a significant role in the damage progression. Composite samples with tensile radial stresses at the interface failed by random fiber and matrix cracks under tensile loading and in some cases fiber-matrix debonding was observed. At high stresses, extensive matrix damage took place. Samples tested with compressive radial stresses at the fiber-matrix interface did not exhibit random cracking or heavy matrix damage even at high stresses. Composite systems in which the coefficient of thermal expansion of the matrix is much greater than that of the fiber had high axial tensile stresses from fabrication. These residual stresses caused uniformly spaced transverse cracks to form in the matrix. The experimental stresses when matrix cracks occurred were compared to predicted stress values from analytical models. The models vastly overestimated the stresses at which matrix cracking would occur in these composites.

*liquids: also fibers military uses;
fiber reinforcement; (KTES) →*

UNCLASSIFIED